rMMs - 2023

5th Rocky Mountain Muscle Symposium

Canmore Nordic Centre, Alberta, Canada
June 19 -21, 2023

Acknowledgements

We would like to acknowledge the following for their generous contributions to the muscle symposium

UNIVERSITY OF CALGARY
FACULTY OF KINESIOLOGY

UNIVERSITY OF CALGARY
Biomedical Engineering

DELSYS

aurora SCIENTIFIC
Performance. Precision. Progress.
www.AuroraScientific.com

McCAIG INSTITUTE
FOR BONE AND JOINT HEALTH

UNIVERSITY OF CALGARY
Research

ASB American Society of Biomechanics
FOUNDED IN 1977

Canadian Society for Biomechanics
Société canadienn de biomécanique

Welcome to Canmore

The symposium on skeletal muscles in Canmore is the fifth Rocky Mountain Symposium of its kind. The first was held in 1999 in Canmore, the second and third in 2002 and 2006 in Banff, and the fourth in 2019 in Canmore again. The goal of this fifth symposium is the same as that of the previous meetings: we would like to promote a scientific exchange of ideas on the highest level in a small setting with ample time for discussion and informal interaction.

Scientifically, skeletal muscle contraction and function will be addressed at all structural levels, varying from single actin-myosin interactions to the function and control of muscles during voluntary contractions in humans. This program will require some tolerance, as biophysicists working on the molecular level have a different view of muscles than physiologists working on the single fibre level, or biomechanists working in a clinical rehabilitation setting with human patients. Nevertheless, the success of the first three symposia instills confidence that there is a desire, and maybe even a need, to discuss muscle contraction and function at all scales and all structural levels.

Socially, the Canmore Nordic Centre is a fantastic and unique facility for small scale symposia. Built for the 1988 Winter Olympics and set in a Provincial Park just at the eastern edge of the Rocky Mountains, it is a destination for thousands of tourists each year and hosts world-class competitions for cross-country skiing, biathlon and Nordic combined. In the summer, you can enjoy, hiking, mountain biking and Frisbee Golf – a perfect location to discuss and use muscles!

The program shows that we have organized sessions in such a way that you can enjoy the outdoors each day and socialize in an informal way.

We have tried very hard to make this 5th Rocky Mountain Muscle Symposium an unforgettable scientific and social experience. We hope that you take the opportunity to present, discuss, interact, and explore in the scientific sessions, and that you will make new friendships and renew old ones.

Walter Herzog
Scientific Organizer and Program Chair
5th Rocky Mountain Muscle Symposium

Maps

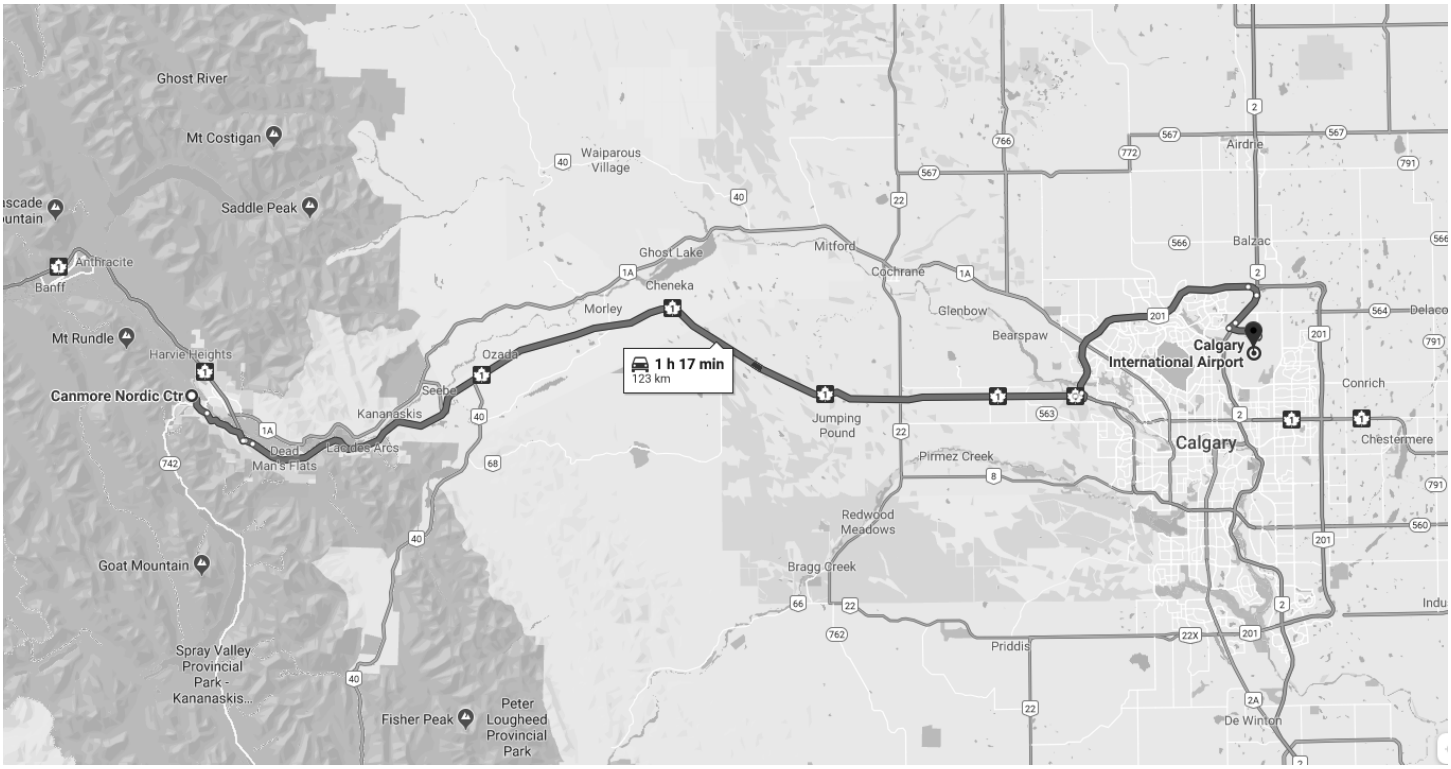
Ghost River
Mt Costigan
Waiparous Village
Saddle Peak
Anthracite
Banff
Ghost Lake
Mitford
Cochrane
Cheneka
Morley
Glenbow
Bearspaw
Airdrie
Balzac
Mt Rundle
Harvie Heights
Ozada
1 h 17 min
123 km
Canmore Nordic Ctr
Seebe
Kananaskis
Dead Man's Flats
Lac des Arcs
Jumping Pound
Calgary International Airport
Conrich
Calgary
Chestermere
Pirmez Creek
Redwood Meadows
Bragg Creek
Goat Mountain
Priddis
Spray Valley Provincial Park - Kananaskis...
Fisher Peak
Peter Lougheed Provincial Park
De Winton


Canmore Golf & Curling Club
Canmore Rocky Mountain Inn
Shell
Trans-Canada Hwy
Pallister Trail
Bow River
Larch Ave
Larch Island Walking Path
Lions Park
Crazyweed Kitchen
Safeway Canmore
Holiday Inn Canmore
Canadian Tire - Canmore, AB
Tim Hortons
Canadian Rockies Earth Science Resource Centre
Canmore Museum and Geoscience Centre
Rocky Mountain Bagel
Canmore
Three Sisters Gallery
A&W Canada
Canmore Nordic Ctr
Rundle Forebay
Riverside Park
Centennial Park
Coast Canmore Hotel & Conference Centre
Cornerstone Theatre
TR3
Bridge Rd
Benchlands Trail
Blackstone Mountain Lodge by CLIQUE

Muscle Symposium - Program		
Saturday, July 27		
14:00 - 14:30	Registration Pre-function Area 14:00 - 20:00	Disc Golf at Canmore Nordic Centre / Free Time
14:30 - 15:00		
15:00 - 15:30		
15:30 - 16:00		
16:00 - 16:30		
16:30 - 17:00		
17:00 - 17:30		Welcome Reception - Pre-Function Area
17:30 - 18:00		Keynote Lecture 1 - Rick Lieber: The mystery of human skeletal muscle contracture
18:00 - 18:30		
18:30 - 19:00		Social - Pre-Function Area
19:00 - 19:30		
19:30 - 20:00		
20:00 - 20:30	Shuttle bus leaves at 20:00 return Canmore loop	
20:30 - 21:00		

Muscle Symposium - Program			
	Sunday, July 28		
8:00 - 8:24	8:00-8:24 Coffee - Prefunction Area		
8:24 - 8:48	Molecular Muscle Mechanics / Physiology Banquet Room	Invited 1	***Venus Joumaa:*** **Towards a better understanding of muscle contraction**
8:48 - 9:00		Oral 1.1	*Anthony Hessel:* X-ray diffraction analysis before and after active and passive stretch in skinned muscle fiber bundles from wild type and mdm mice
9:00 - 9:12		Oral 1.2	*Kiisa Nishikawa:* Calcium-dependent titin – thin filament interactions in muscle: observations and theory
9:12 - 9:24		Oral 1.3	*Matthew Millard:* A three filament muscle model based on a titin-myosin interaction
9:24 - 9:36		Oral 1.4	*Seong-won Han: Residual force enhancement in cardiac myofibrils on the ascending limb of the force-length relationship*
9:36 - 9:48		Oral 1.5	*Kaylyn Bell:* The muscle mechanical basis of Freeman-Sheldon Syndrome
9:48 - 10:00		Oral 1.6	*Tim Leonard:* Adductor longus myofibrillar passive stiffness is reduced in cerebral palsy
10:00 - 10:30	**Coffee Break with Snacks - Prefunction Area**		
10:30 - 11:30	**Keynote Lecture 2 - Motoshi Kaya: Reverse stroke of cardiac myosin is essential for heart function: lessons from skeletal myosin**		
11:30 - 11:42	Cellular Muscle Mechanics / Physiology Banquet Room	Oral 2.1	*David Corr:* History-dependent behaviour in drosophila jump muscle: do myosin kinetics influence force-depression?
11:42 - 11:54		Oral 2.2	*Douglas Swank:* A myosin based mechanism for stretch activation and its possible purpose revealed by varying phosphate concentration in mammalian skeletal muscle fibers
11:54 - 12:06		Oral 2.3	*Marlies Corvelyn:* Skeletal muscle stem cell properties from young children with cerebral palsy
12:06 - 12:18		Oral 2.4	*Ridhi Sahani:* Collagen preferred direction relative to muscle fiber direction in three and six-month-old Mdx mice
12:18 - 12:30		Oral 2.5	*Nicole Mazara:* The effect of Ca2+ on rate of force redevelopment of single muscle fibres in young and older adults
12:30 - 12:42		Oral 2.6	*Eng Kuan Moo:* The influence of muscle architecture on sarcomere force-length relationship in intact muscle
12:42 - 14:00	**Lunch - Meeting Room B, some reserved seating/tables downstairs in main space or enjoy outdoors**		
14:00 - 14:30	**Keynote Lecture 3 - Henk Granzier, Titin determines passive stiffness and the sarcomere length working range of skeletal muscle**		
14:30 - 15:00			
15:00 - 15:30	**15:00 - 16:30 Poster Session 1**		
15:30 - 16:00			
16:00 - 16:30	**Meeting Room B**		
16:30 - 17:00	**Grassi Lakes Hike**		
17:00 - 17:30	**Shuttle bus to trail head leaves at 16:45**		
17:30 - 18:00	**Pick up after hike at 19:00 to return Canmore loop**		
18:00 - 18:30			
18:30 - 19:00			
19:00 - 19:30	Dinner for Keynote Presenters (downtown Canmore)	**Dinner on your own**	
19:30 - 20:00			
20:00 - 20:30			
20:30 - 21:00			

Poster Session 1	Poster 1.1	*Matthew Millard:* Is titin actively preloaded?
	Poster 1.2	*Ashley Oldshue:* Modeling muscle cross-bridge dynamics for movement simulations
	Poster 1.3	*Amy Adkins:* The paretic biceps brachii contains fewer sarcomeres in series than the contralateral biceps brachii following stroke
	Poster 1.4	*Amy Loya:* Characterizing shortening deactivation in drosophila and lethocerus muscle types
	Poster 1.5	*Kevin Boldt:* Residual and passive force enhancement in skinned cardiac fibre bundles
	Poster 1.6	*Kaat Desloovere:* Are pre-treatment assessments of muscle morphology related to the effects of treatment with Botulinum NeuroToxin-A and lower leg casting in children with cerebral palsy?
	Poster 1.7	*Atsuki Fukutani:* Effect of stretch-shortening cycle is prominent in the reduced force condition
	Poster 1.8	*Giovanni Martino:* Simulating the pendulum test to understand mechanisms of Parkinsonian rigidity
	Poster 1.9	*Nathalie De Beukelaer:* Relationship between spasticity phenotypes and muscle morphology is different in children with spastic cerebral palsy and children with hereditary spastic paraplegia
	Poster 1.10	*Brian Horslen:* Acto-myosin cross-bridge stretch mechanics underlie history-dependent changes in muscle spindle sensory feedback: a multi-scale experimental and simulation study
	Poster 1.11	*Anouk Agten:* Muscle fibre type characteristics of the lumbar multifidus and erector spinae in persons with non-specific chronic low back pain and healthy controls
	Poster 1.12	*Domiziana Costamagna:* IL4 counteracts cancer-induced skeletal muscle atrophy: one cytokine for multiple effects

Muscle Symposium - Program			
	Wednesday, June 21		
9:30 - 9:50	**9:30 - 9:50 Coffee and Pastries - Prefunction Area**		
9:50 - 10:15	**In vivo Animal Muscle Function Banquet Room**	**Invited 2**	***Doug Swank: The myosin essential light chain is not essential for muscle function***
10:15 - 10:30		Oral 3.1	**E. Wold:** A model of asynchronous flight muscle explains emergent dynamics of flapping insects
10:30 - 10:45		Oral 3.2	**E-K Moo:** The dependence of force depression on the timing of active shortening
10:45 - 11:00		Oral 3.3	**S. Dalle:** The CB1 antagonist rimonabant improves skeletal muscle regeneration via anti-apoptitic mechanisms in mice
11:00 - 11:15		Oral 3.4	**N. Khaledi:** Maternal high-intensity exercise and EDL muscle metabolic gene expression in male offspring
11:15 - 11: 30		Oral 3.5	**S. Ross:** Aponeurosis, tendon, and muscle belly length changes during in situ cyclic contractions
11:30 -12:15	**Keynote Lecture 4 - Natalie Holt: Variation, constraints, and adaptation in skeletal muscle**		
12:15 - 13:15	**Lunch - Meeting Room B, some reserved seating/tables downstairs in main space or enjoy outdoors**		
13:15 - 13:30	**In vivo Human Muscle Function Banquet Room**	Oral 4.1	**R. Lieber:** Direct intraoperative length-tension measurements of human gracilis muscle
13:30 - 13:45		Oral 4.2	**S. Muralidhar:** Metabolic cost for isometric force scales nonlinearly with force and predicts bilateral limb force sharing
13:45 - 14:00		Oral 4.3	**T. van der Zee:** Muscle force development dynamics are explained by neither Hill-type nor cross-bridge models
14:00 - 14:15		Oral 4.4	**S. Bohm:** Determination of the activation-dependent force-length relationship of the human soleus muscle in vivo
14:15 - 14:30		Oral 4.5	**J. Fletcher:** Relative muscle fascicle length and the energy cost of cyclic contractions
14:30 - 15:15	**Keynote Lecture 5 - Kaat Desloovere: Contributing factors to altered muscle growth in children with cerebral palsy**		
15:15 - 16:30	**15:15 - 16:30 Poster Session 1 - with Aurora Presentation at 15:15 - Meeting Room B**		
16:30 - 17:00	**Free Time / Outdoor Opportunities (Bike Ride) at Canmore Nordic Centre**		
17:00 - 17:30			
17:30 - 18:00			
18:00 - 18:30			
18:30 - 19:00			
19:00 - 19:30	**Social - Prefunction Area**		
19:30 - 20:00	**Banquet Dinner - Banquet Room**		
20:00 - 20:30	**Shuttle bus leaves at 21:00 return Canmore loop**		
20:30 - 21:00			

Poster Session 2	Poster 2.1	**B. Yu:** In vivo vastus lateralis fascicle excursion during speed skating imitation
	Poster 2.2	**B. Yu:** In vivo vastus lateralis fascicle length shortening during maximal isometric contractions
	Poster 2.3	**C. Svane:** Temporal relation between muscle growth and contracture development in children with cerebral palsy: implications for early intervention
	Poster 2.4	**A. Rajan:** Using EMG recordings to predict muscle forces through an artificial neural network approach
	Poster 2.5	**J. Aeles:** 3D whole muscle shape changes - exploring a novel approach
	Poster 2.6	**A. Sawers**: Hip muscle function explains a larger proportion of the variance in walking and balance performance among transtibial than transfemoral prothesis users
	Poster 2.7	**M. Baggaley:** Torque loss during simultaneous activation of agonistic muscles
	Poster 2.8	**H. de Brito Fontana:** Fascicle and muscle tendon unit shortening velocity in isokinetic contractions
	Poster 2.9	**L. Foley:** Reliability of countermovement jump force-velocity vs. velocity-load testing in athletes
	Poster 2.10	**G. Privett:** Acute skeletal muscle fatigue reduces cellular passive and active stiffness
	Poster 2:11	**E. Machado:** Muscle length change associated with fascicle shortening and fascicle rotation in the sheep medial gastrocnemius

Instructions for Presenters

Oral Presentations:

- Oral presentations are assigned a 15-minute time slot (divided into a 1-minute introduction, an **10-minute presentation**, and 4 minutes for questions)
    - The 10-minute **presentation length** will be **strictly enforced**, so we ask that you please stay within your allotted time.
- The exact date and time for your presentation is in the schedule on pages 5-7 and the event website.
- We have a speaker ready area in the foyer / pre-function area at the symposium where speakers **must** upload their presenations from a USB **on the day before** their presentation. As an alternative you can upload your presentation and ancillary files up to 24 h ahead on the event website. A link has been provided via email.

Poster Presentations:

- Posters must be **no more than 0.9 m wide (3') and 1.1 m high (3' 7")**
- Poster sessions will be held June on 20 and 21 from 15:15 to 16:30
    - The exact date and poster number for your specific poster is in the schedule on pages 5-7 and the event website.
- Pins will be provided for attaching posters to the boards.
- Posters may be **mounted between 12:15 and 13:15** (during lunch break) on the day of your session. Please **remove** your poster **promptly after** the session.

Keynote and Invited Speakers

Kaat Desloovere

Dario Farina

Samantha (Sam) Harris

Natalie Holt

Venus Joumaa

Douglas Swank

Sam Walcott

KAAT DESLOOVERE

Kaat Desloovere is full professor at the KU Leuven and research manager of the Clinical Motion Analysis Laboratory of the University Hospitals of Leuven, in Belgium. She has been focusing her research on clinical motion analysis, mainly in children with cerebral palsy. Her research is built on close collaboration and solid integration of several medical, paramedical and engineering disciplines. The clear link to the clinical field is a unique aspect of her multidisciplinary research and creates a strong translational dimension. Her specific research ambition is to unravel the relation between clinical motion data (mainly gait) and underlying neuromuscular impairments. The current research pathways are strongly focused on the alterations in macroscopic and microscopic muscle structure, defined by medical imaging and analyses of micro-biopsy of muscles and on advanced analysis of muscle behavior using instrumented assessments (spasticity and strength assessment and gait analysis) in patients with neurological and neuromuscular diseases. She guides a multidisciplinary group of > 15 researchers (with technical as well as clinical backgrounds) and a clinical team of 5 to 8 co-workers at the Clinical Motion Analysis Laboratory. Several past and ongoing research projects resulted in a continuously growing scientific output.

DARIO FARINA

Dario Farina (Fellow IEEE) received Ph.D. degrees in automatic control and computer science and in electronics and communications engineering from the Ecole Centrale de Nantes and Politecnico di Torino, respectively, and an Honorary Doctorate degree in Medicine from Aalborg University. He is currently Full Professor and Chair in Neurorehabilitation Engineering at the Department of Bioengineering of Imperial College London. He also currently holds the roles of Director of Research of the Department of Bioengineering of Imperial College London, Director of the Imperial-Meta Wearable Neural Interfaces Research Centre, and Director of the Imperial Network of Excellence in Rehabilitation Technologies. He has previously been Full Professor at Aalborg University and at the University Medical Center Göttingen, Georg-August University, where he founded and directed the Department of Neurorehabilitation Systems, acting as the Chair in Neuroinformatics of the Bernstein Focus Neurotechnology Göttingen. His research focuses on biomedical signal processing, neurorehabilitation technology, and neural control of movement. Within these areas, he has (co)-authored more than 500 papers in peer-reviewed Journals (h-index 115) and has been the Editor of the books Introduction to Neural Engineering for Motor Rehabilitation (Wiley-IEEE Press, 2013), Surface Electromyography: Physiology, Engineering and Applications (Wiley-IEEE Press, 2016), and Bionic Limb Reconstruction (Springer, 2021). Among other awards, he has been the recipient of the 2021 Engineering in Medicine and Biology Society Technical Achievement Award, the 2010 IEEE Engineering in Medicine and Biology Society Early Career Achievement Award and the Royal Society Wolfson Research Merit Award. Professor Farina has been the President of the International Society of Electrophysiology and Kinesiology (ISEK) and is currently the Editor-in-Chief of the official Journal of this Society, the Journal of Electromyography and Kinesiology. He is also currently an Editor for Science Advances, IEEE Transactions on Biomedical Engineering, IEEE Transactions on Medical Robotics and Bionics, IEEE Reviews in Biomedical Engineering, and has been held past editorial roles in several other Journals. He has been elected Fellow IEEE, AIMBE, ISEK, and EAMBES.

SAMANTHA (SAM) HARRIS

Samantha (Sam) Harris is a professor in Cellular and Molecular Medicine, Biomedical Engineering, Physiologycial Sciences GIDP, Physiology and the BIO5 Institute at the University of Arizona. She holds a PhD in Physiology from the University of Michigan.

The long-term goal of research in the Harris lab is to understand the molecular mechanisms of muscle contraction, focusing on how contractile proteins of muscle sarcomeres regulate the force and speed of contraction in the heart. The question is important from both basic science and clinical perspectives because mutations in sarcomere proteins of muscle are a leading cause of hypertrophic cardiomyopathy (HCM), the most common cause of sudden cardiac death in the young and a prevalent cause of heart failure in adults. Myosin binding protein-C (MyBP-C) is a muscle regulatory protein that speeds actomyosin cycling kinetics in response to adrenaline (b-adrenergic stimuli) and is one of the two most commonly affected proteins linked to HCM. Currently, the major research focus in the Harris lab is understanding the mechanisms by which cMyBP-C regulates contractile speed and mechanisms by which mutations in cMyBP-C cause disease.

NATALIE HOLT

Natalie Holt is an Assistant Professor of Systems Physiology at UC Riverside. They received their PhD from the University of Leeds (UK) in muscle mechanics and energetics, before completing post-doctoral positions at Harvard and UC Irvine, and a short faculty position at Northern Arizona University. Their work addresses questions concerning basic muscle physiology, the interaction of muscle with elasticity elements, the determinants of performance in specialized muscles across vertebrates and invertebrates, and the effects of aging and early-life exercise on muscle structure and performance. They teach classes in human physiology, organismal biology, and the role of biology in creating systems of oppression around race and gender.

VENUS JOUMAA

Dr. Venus Joumaa is an Adjunct Assistant Professor in the Faculty of Kinesiology at the University of Calgary since 2009. She received her PhD in Biomechanics and Biomedical Engineering from the University of Technology of Compiegne, France in 2005 and has become an expert in single muscle fibre research. Currently, Dr. Joumaa's research focuses on understanding the role of titin in active force regulation and to potentially use this knowledge for diagnostic and treatment purposes. Dr. Joumaa regularly teaches classes in biomechanics, human physiology, and biomedical engineering and supervises and mentors undergraduate, summer, visiting and graduate students in the Human Performance Laboratory. She has been member of several professional societies including the Canadian Society for Biomechanics, the American Society of Biomechanics, the International Society of Biomechanics, the American Physiological Society, and the Biophysical Society.

DOUGLAS SWANK

Doug Swank holds a PhD in physiology in 1995 from the University of Pennsylvania where he investigated the roles of different muscle fiber types in powering locomotion with his mentor Dr. Larry Rome. From 1996 to 2000 he gained expertise in Drosophila genetics through a postdoctoral position at San Diego State University in Dr. Sandy Bernstein's lab. From 2000 to 2003 his postdoctoral work at the University of Vermont focussed on insect flight muscle mechanics under the supervision of Dr. David Maughan. In 2005 he started his career at the Center for Biotechnology & Interdisciplinary Studies at Rensselaer Polytechnic Institute in Troy, New York. He has been at RPI 17 years, working his way up from Assistant to full Professor of Biological Sciences and also joining the Department of Biomedical Engineering . The expertise of his multidisciplinary lab is investigating muscle's ability to power a wide variety of locomotory tasks and understanding contractile protein mutations that cause muscle and heart diseases. His lab is a world leader in performing Drosophilia muscle mechanics. A current focus of the lab is understanding the roles and mechanisms of muscle stretch activation in insects and mammalian skeletal muscle.

SAM WALCOTT

Sam Walcott received his undergraduate degree in Biology from Cornell University in 2001, and his PhD in Theoretical and Applied Mechanics, also from Cornell University, in 2006. He did postdoctoral work in Molecular Physiology and Biophysics in the Warshaw Lab at the University of Vermont from 2006-2008. He had a second postdoc position in Mechanical Engineering in the Sun Lab at Johns Hopkins University from 2008-2011. He was an Assistant Professor in the Department of Mathematics at University of California Davis from 2011-2015, and an Associate Professor there until 2019. Since 2019, he has been an Associate Professor in the Department of Mathematical Sciences at Worcester Polytechnic Institute, Massachusetts and is currently also Associate Program Director of Bioinformatics and Computational Biology.

Presentation Schedule

Monday, June 19

Keynote Lecture 1: Dario Farina 17:30-18:30

Neuromechanics of human movement: a motor neuron centric view

Molecular Muscle Mechanics / Physiology 9:50 - 11:30

History-dependent properties of muscle contraction
Venus Joumaa - Invited Lecture

A point mutation in the switch I region of myosin's active site dramatically alters the load-dependence of phosphate-induced detachment from actin
Christopher Marang

Cooperativity between skeletal myosin molecules evaluated by information theory
Motoshi Kaya

Changes in passive stresses in single myofibrils after graded titin cleavage progressively
Seong-won Han

Mechanical contribution of immunoglobulin domain refolding under tension to myofibrils
Chris Tiessen

The molecular mechanism of the phosphate-induced loss of force during muscle fatigue
Edward Debold

Keynote Lecture 2: Samantha (Sam) Harris 11:30 - 12:15

A cut and paste approach for understanding structural and functional roles of myosin binding protein-C in skeletal muscles

Cellular Muscle Mechanics / Physiology 13:15 - 14:30

Collagen fibers within hamstring muscle of children with cerebral palsy show re-alignment during dynamic stretching
Lucas Smith

Histological analysis of the gastrocnemius muscle in young children with cerebral palsy compared to age-matched typically developing children
Jorieke Deschrevel

Botulinum toxin effect on cerebral palsy muscle stem cells and hiPSC-derived NMJs
Domiziana Costamagna

Myofibril shearing in skeletal muscle at long lengths
Jarrod Petersen

Segmental elongation of titin elastic elements in fluorescently labelled sarcomeres during stretching
Armaan Sekhon

Keynote Lecture 3: Sam Walcott 14:30 - 15:15

Building mathematical models to connect molecular and cellular muscle measurements

In vivo Animal Muscle Function 9:50 - 11:30

The myosin essential light chain is not essential for muscle function
Douglas Swank - Invited Lecture

A model of asynchronous flight muscle explains emergent dynamics of flapping insects
Ethan Wold

The dependence of force depression on the timing of active shortening
Eng-Kuan Moo

The CB1 antagonist rimonabant improves skeletal muscle regeneration via anti-apoptitic mechanisms in mice
Sebastiaan Dalle

Maternal high-intensity exercise and EDL muscle metabolic gene expression in male offspring
Neda Khaledi

Aponeurosis, tendon, and muscle belly length changes during in situ cyclic contractions
Stephanie Ross

Keynote Lecture 4: Natalie Holt 11:30 - 12:15

Variation, constraints, and adaptation in skeletal muscle

In vivo Human Muscle Function 13:15 - 14:30

Direct intraoperative length-tension measurements of human gracilis muscle
Rick Lieber

Metabolic cost for isometric force scales nonlinearly with force and predicts bilateral limb force sharing
Sriram Muralidhar

Muscle force development dynamics are explained by neither Hill-type nor cross-bridge models
Tim van der Zee

Determination of the activation-dependent force-length relationship of the human soleus muscle in vivo
Sebastian Bohm

Relative muscle fascicle length and the energy cost of cyclic contractions
Jared Fletcher

Keynote Lecture 5: Kaat Desloovere 14:30 - 15:15

Contributing factors to altered muscle growth in children with cerebral palsy

Tuesday, June 20

Poster Session 1 15:15 - 16:30

Satellite cell in vitro differentiation is altered in cells extracted from young children with cerebral palsy
Domiziana Costamagna

Passive force of skinned cardiac papillary muscle in response to dietary-induced obesity during adolescence in rats
Mauricio Delgado

The molecular signature of the peripheral CB1 antagonist AM6545 in muscle, adipose and liver tissue
Katrien Koppo

Investigating the effect of activation level on residual and passive force enhancement in skinned muscle fibres
Shuyue Liu

Investigating the effect of collagenase on the passive stiffness and total protein content of muscles in children with cerebral palsy
Faizan Syed

The effects of microtubule depolymerization on muscular viscoelastic properties
Takuya Kobayashi

The effect of sex on intramuscular fat infiltration in rat soleus muscle in a diet-induced obesity model
Hannah Smith

Wedndesday, June 21

Poster Session 2 15:15 - 16:30

In vivo vastus lateralis fascicle excursion during speed skating imitation
Bryan Yu

In vivo vastus lateralis fascicle length shortening during maximal isometric contractions
Bryan Yu

Temporal relation between muscle growth and contracture development in children with cerebral palsy: implications for early intervention
Christian Svane

Using EMG recordings to predict muscle forces through an artificial neural network approach
Amsal Rajan

3D whole muscle shape changes - exploring a novel approach
Jeroen Aeles

Hip muscle function explains a larger proportion of the variance in walking and balance performance among transtibial than transfemoral prothesis users
Andrew Sawers

Torque loss during simultaneous activation of agonistic muscles
Michael Baggaley

Fascicle and muscle tendon unit shortening velocity in isokinetic contractions
Heiliane de Brito Fontana

Reliability of countermovement jump force-velocity vs. velocity-load testing in athletes
Landon Foley

Acute skeletal muscle fatigue reduces cellular passive and active stiffness
Grace Privett

Muscle length change associated with fascicle shortening and fascicle rotation in the sheep medial gastrocnemius
Esthevan Machado

Aurora Scientific Demonstration 15:15 - 16:30

Chris Rand

Keynote Presentations

Dario Farina

Samantha (Sam) Harris

Sam Walcott

Natalie Holt

Kaat Desloovere

Neuromechanics of Human Movement: A Motor Neuron Centric View

Dario Farina
Professor and Chair in Neurorehabilitation Engineering, Department of Bioengineering, Imperial College London, London, UK

Neuromechanics is a field of research that highlights how behaviour emerges as a combination of the structure of the musculoskeletal system, the external mechanical requirements, and neural control. Our main limitation and challenge in neuromechanics is our poor ability to record in vivo from a sufficiently large number of neural cells to understand population behaviours and to associate a functional meaning to the cellular mechanisms that ultimately determine a movement. This limitation can now be partly overcome, at least at the last stage of neural processing of movement, that is at the level of alpha spinal motor neurons. Motor neurons receive synaptic inputs that they convert into the neural drive to muscles. The spiking activity of motor neurons can be identified from recordings of electrical activity of muscles using either wearable (non-invasive) or minimally invasive sensors. Using these technologies, motor neurons are the only neural cells whose individual activities can be studied in humans during natural behaviour, without the need for neural implants. This provides a practical interface with the output of the spinal cord. Moreover, modern methods allow us to decode a relatively large proportion of the active motor neurons during behavioural tasks and therefore to make a direct link with function with neuro-musculoskeletal models. The talk will overview the technologies for motor neuron interfacing, and their use in the study of neural control of movement and neuromechanics.

A cut and paste approach for understanding structural and functional roles of myosin binding protein-C in skeletal muscles

[1]**Samantha P. Harris**, [1]Nichlas M. Engels, [1]Rachel L. Sadler, [2]Michel Kuehn, [3]Devin Nissen, [3]Weikang Ma, [3]Thomas Irving, [2]Wolfgang A. Linke, and [2]Anthony L. Hessel
[1]Department of Physiology, University of Arizona, Tucson, AZ USA
[2] Institute of Physiology II, University of Muenster, Muenster, Germany
[3]BioCAT, Department of Biology, Illinois Institute of Technology, Chicago, IL USA

Corresponding author: samharris@arizona.edu

INTRODUCTION

The family of proteins known as myosin binding protein-C (MyBP-C) are regulatory proteins localized to muscle sarcomeres that are encoded by 3 separate genes (*MYBPC1*, *MYBPC2*, and *MYBPC3*). The 3 genes encode distinct MyBP-C protein paralogs expressed in fast skeletal, slow skeletal, and cardiac muscles, respectively. However, due to co-expression of the two skeletal paralogs (and their related multiple splice variants) it has been challenging to describe distinct functional roles for each MyBP-C because skeletal muscles typically express a mixture of fiber types. Here, we overcome this challenge by engineering two new mouse models that selectively target *MYBPC1* and *MYBPC2* to permit removal and replacement (cut and paste) of each protein paralog in permeabilized muscle fibers *in situ*.

METHODS

We previously developed the cut and paste approach for cardiac MyBP-C (cMyBP-C) [1] by inserting a 60 nucleotide cassette encoding a tobacco etch virus protease (TEVp) consensus cut site followed by a SpyTag [2] between domains C7 and C8 of *MYBPC3*. Here we used a similar approach to insert a cassette encoding a TEVp cut site and SpyTag between domains C7 and C8 of *MYBPC1* to target the slow (s) skeletal paralog of MyBP-C in so-called "SpyC1" mice. We targeted *MYBPC2,* which encodes the fast skeletal (f) paralog of MyBP-C, by inserting a TEVp cut site followed by a SnoopTag [3] between domains C7 and C8 to create "SnoopC2" mice.

Homozygous SpyC1 and SnoopC2 mice were phenotyped with respect to body weight, grip strength, and weights of selected muscles. Western blots of dissected skeletal muscles (e.g., soleus and psoas) were used to confirm that treatment of permeabilized muscles from SpyC1 and SnoopC2 with TEVp cut sMyBP-C and fMyBP-C, respectively. Force measurements in permeabilized muscle fibers were made before and after selective cleavage of sMyBP-C and fMyBP-C to determine the effects of MyBP-C on maximal active force and Ca^{2+} sensitivity of tension. The effects of fMyBP-C on sarcomere structure were determined using small angle X-ray diffraction of permeabilized psoas muscle under relaxed conditions at sarcomere length 2.4, 2.7, and 3.0 μm pre and post TEVp cleavage.

RESULTS AND DISCUSSION

Homozygous SpyC1 and SnoopC2 mice were born in expected Mendelian inheritance ratios and all phenotypic measures appeared overtly normal. Western blots confirmed that treatment of permeabilized skeletal muscle fibers with TEVp resulted in selective cleavage of sMyBP-C or fMyBP-C (depending on mouse line) without affecting the other paralog. Force measurements in soleus (SpyC1) and psoas (SnoopC2) showed that tension-pCa relationships were right-shifted following treatment with TEVp, indicating reduced Ca^{2+} sensitivity of tension following selective loss of either sMyBP-C or fMyBP-C. Notably, spontaneous contractile oscillations (SPOC) were also frequently observed following loss of MyBP-C. Results from X-ray diffraction experiments in permeabilized psoas fibers showed significant changes in sarcomere structure including changes in lattice spacing, $I_{1,1}/I_{1,0}$ ratios, and reflections attributable to both thick and thin filament structures (e.g., M3 and M6 spacing and A6 and A7 spacing, respectively). We interpret these data in terms of a model where the skeletal muscle paralogs of MyBP-C exert both structural and functional effects at rest and in contracting muscle, potentially by binding to both thick and thin filaments simultaneously.

ACKNOWLEDGEMENTS

We gratefully acknowledge support from the American Heart Association (N.M.E. predoctoral award), the National Institutes of Health (to S.P.H. HL080367, HL140925, AR081935). This research used resources of the Advanced Photon Source, a U.S. Department of Energy (DOE) Office of Science User Facility operated for the DOE Office of Science by Argonne National Laboratory under Contract No. DE - AC02 - 06CH11357. A.L.H. received funding from German Research Foundation grant 454867250; W.A.L. received funding from German Research Foundation grant SFB1002, A08; W.A.L. received funding from IZKF Münster Li1/029/20; and T.I. received funding from National Institutes of Health P41 GM103622 and P30 GM138395.

REFERENCES

[1] Napierski et al. (2019) *Circ Res*. **126**:737-749.
[2] Zakeri et al. (2012) *PNAS* (USA). **109**: E690-697.
[3] Veggiani et al. (2016) *PNAS* (USA). **113**: 1202-1207.

Building mathematical models to connect molecular and cellular muscle measurements

Sam Walcott
Mathematical Sciences, Bioinformatics and Computational Biology, Worcester Polytechnic Institute, Worcester, MA, USA
corresponding author: swalcott@wpi.edu

INTRODUCTION

Muscle contraction is a multiscale process. During contraction, trillions of myosin molecules perform nanometer steps and generate picoNewton forces, powering muscle contraction over meters and force generation of Newtons. Relating measurements at one scale to another is challenging, since interactions occuring at one scale cause emergent behaviors at larger scales. That is, the behavior of, say, a sarcomere cannot simply be understood by studying the behavior of isolated molecules; we must also know how those molecules interact.

Mathematical modeling provides a powerful tool to bridge scales and to take account of these emergent behaviors. I will discuss some work we have done, building off both previous modeling work and recent advances in measuring muscle function at the molecular level. The combined aim of this work is to develop a mathematical model, based on differential equations, capable of describing and predicting experimental measurements from the molecular to cellular scale.

METHODS

To understand muscle function across scales, we use a combination of Monte-Carlo simulations and partial differential equations (PDEs). Monte Carlo simulations keep track of every molecule, and assign a biochemical state to each molecule. Transitions between states are determined by drawing random numbers. We use this approach to model molecular-scale experiments. Experiments at larger scales, where large quantities of myosin molecules work together, are best-modeled by PDEs as pioneered by A. F. Huxley [1]. We have updated these models in a variety of ways, first to account for recent molecular measurements [2], then to account for local interactions during thin filament activation [3], and most recently to account for thick filament activation [4].

Importantly, the parameters of the Monte Carlo models relate directly to parameters of the PDE models, so we can infer molecular parameters by fitting the PDEs to cellular data and we can infer cellular parameters by fitting the Monte Carlo models to molecular data. In all of our work, a close collaboration with experimentalists is critical to model development, validation and biological insights that the modeling might provide.

RESULTS AND DISCUSSION

We first developed a model to desribe myosin's interaction with actin. By fitting a Monte Carlo model to measurements, we showed that a single model quantitatively describes observations of one, ten, and a hundred myosin molecules interacting with actin. The model reproduced ensemble-induced acceleration, where myosin working as part of an ensemble move actin faster than would be predicted from the behavior of a single molecule. By mathematical analysis of the PDE model, we showed that this effect is due to mechanochemical coupling between molecules, where myosin molecules apply forces on each other that cause them to proceed through chemical reactions faster and move actin more than an isolated myosin molecule. Further analysis of the PDE model provided a three-parameter fit to steady-state force-velocity measurements, similar to the three-parameter Hill fits [5], but with parameters relating to molecular-scale properties of myosin. We used this model to understand how mutations in myosin can improve jumping performance in fruit flies [6].

We next developed a model to describe myosin's interaction with actin and the regulatory proteins troponin and tropomyosin (regulated thin filaments), and at variable calcium. We first developed a mechanochemical model for the local coupling between myosin molecules introduced by tropomyosin, whereby the binding of one myosin molecule induces a deformation in tropomyosin and makes it easier for neighboring myosin to bind actin. We then tested and validated the model with measurements of one, ten, and a hundred molecules interacting with regulated thin filaments at variable calcium.

Finally, we developed a model to describe step stretch and ramp shortening experiments with permeablized muscle fibers. In this model, history-dependence occurs due to 1) the extension/contraction of a parallel elastic element, which transmits force to the thick filament, and 2) thick filament activation, where force on the thick filament activates myosin by pulling it out of a self-inhibited configuration. Fitting the model to our measurements allowed us to infer molecular-scale properties. Then, adding these molecular-scale properties to our Monte-Carlo simulations, we were able to predict our measurements of one, ten or a hundred myosin molecules interacting with actin. This model therefore provides a self-consistent description of molecular to cellular measurements, including the history dependence of isometric force production.

ACKNOWLEDGEMENTS

This work is supported, in part, by NIH R01-GM141743.

REFERENCES

[1] Huxley, AF (1957). *Prog Biophys Biophys Chem*, **7**: 256-319.
[2] Walcott et al. (2012) *Biophys J,* 103: 510-510.
[3] Longyear et al. (2017) *Sci Rep*, 7: 1-12.
[4] Liu et al. (2023) *Biophys J*, 122:29a.
[5] Hill AV (1938), *Proc Royal Soc B-Biol Sci*, 126: 136-195.
[6] Newhard et al. (2019), *Am J Physiol-Cell Physiol*, 316:C844-C861.

VARIATION, CONSTRAINTS, AND ADAPTATION IN SKELETAL MUSCLE

[1]Allyn Nguyen, [1]Alberto Castro, [1]Nihav Dhawale, [2]David Labonte, [1]Theodore Garland Jr, **[1]Natalie. C. Holt**
[1]Department of Evolution, Ecology and Organismal Biology, University of California, Riverside, Riverside, CA, US
[2]Department of Bioengineering, Imperial College London, London, UK
corresponding author: natalie.holt@ucr.edu

INTRODUCTION

Skeletal muscles have a complex, molecular-to-organismal scale, structure, and contain both contractile and connective tissue components [1]. Contractile elements consume metabolic energy to generate the force, work and power required for movement, and often work with elastic connective tissues in tendons that can enhance muscle performance. The morphological, mechanical, and physiological properties of contractile and connective tissues at all scales, and their tight integration, determine muscle performance, an organism's behavioural repertoire, and fitness. Despite a common mechanism of muscle contraction across taxa, huge variation in muscle performance is observed across muscle and species, underpinned by variation in many components of muscle. Much of this variation is considered to be adaptive, but also highly constrained by trade-offs. Here we explore the potential for variation in contractile protein structure and physiology to vary trade-offs and alter work and power density across vertebrate and invertebrate muscle, examine whether an unusual form of muscle endurance known as "sustained force" used in Southern Alligator lizard mating behaviour [2] can circumvent speed-endurance trade-offs, and use a mouse experimental evolution system to examine the co-ordinated changes in contractile and connective tissue elements in the evolution of cursoriality.

METHODS

Simple modelling and *in situ* and *in vitro* muscle physiology approaches were used to determine the effect of observed variation across muscle on aspects of performance such as work density, velocity, endurance, and strain energy storage. All animal experiments were approved by UC Riverside IACUC and animal collection was done under CA specific use permits.

Simple models of sarcomeres and muscle fibers were constructed based on the sliding filament theory. Actin and myosin lengths were varied based on published vertebrate and invertebrate values [3], and predicted force-length curves constructed. Peak force, the width of the sarcomeric and muscle fiber curves, and work density were calculated.

Southern Alligator Lizards were euthanized and muscle twitch, force-velocity and endurance properties were determined in the jaw adductor complex, and the iliotibialis (thigh) muscle, a more "typical" locomotor muscle.

Mice from a long running selection experiment, in which 4 lines of mice have been selected for high levels of voluntary wheel running are compared to 4 unselected control lines [5], were terminally anesthetised and muscle force-velocity, endurance, and morphological properties were determined in the triceps surae complex

RESULTS AND DISCUSSION

Simple sarcomeric and fiber models showed the predicted increase in peak force and sarcomeric force-length curve width with increased contractile protein length. However, extrapolation of this model to muscle fibers showed that there is no effect of contractile protein length on the fiber-level force-length curve width. Hence, while increasing contractile protein lengths increases force at the expense of velocity, it retains muscle strain capacity, so increasing work density. This may allow for the greater use of power enhancing elastic mechanisms in invertebrates compare to vertebrates.

Comparison of the Southern Alligator lizard jaw muscle and thigh muscle the confirms that sustained force is restricted to the jaw muscle suggesting specialization of this muscle for mate-guarding. The jaw muscle exhibits exceptionally slow twitch kinetics and relatively slow maximum shortening velocity. This suggests that the mechanism of sustained force does not allow this muscle to circumvent speed-endurance trade-offs, and that sustained force may be due to adaptation in Ca^{2+} handling or sensitivity rather than myosin.

Comparison of muscle morphology and force-velocity and endurance properties across 4 control and 4 selected lines of mice showed that selection for high running volumes resulted in elongation of tendons and shortened muscles across all lines, accompanied by increased normalized muscle shortening velocity, compared to control mice. This may be a co-adaptation to allow for maintenance of absolute shortening velocity while increasing the use of elastic strain energy to reduce metabolic cost. Measurements of muscle speed and endurance demonstrated a clear trade-off between these parameters across the 4 selected, but not control lines. Muscle endurance decreases as velocity increases [6]. This suggests that this trade-off have not been broken by intense selection, but that there are multiple possible muscle-level solutions that underpin increased daily running distance.

ACKNOWLEDGEMENTS

The authors thank Saad Ahmed and Kyle Leong for experimental and data analysis assistance. This work was funded by NSF grant IOS-2038528 to NCH and TG and HFSP grant RGY0073/2020 to NCH and DL.

REFERENCES

[1] Williams CD and Holt NC (2018). *Int. Comp. Biol.*, **58**: 163-173.
[2] Nguyen A et al. (2020) *Proc. Roy. Soc. B*, **287**: 20201578.
[3] Shimomura T et al (2016) *Biophys. J.*, **111**: 1295-1303.
[4] Swallow JG et al (1998) *J. Appl. Physiol.* **84**: 69-76
[5] Castro AC et al., (2022) *J. Exp. Biol.* **225**: jeb244083

CONTRIBUTING FACTORS TO ALTERED MUSCLE GROWTH IN CHILDREN WITH CEREBRAL PALSY.

[1, 2]**Kaat Desloovere**
[1]Neurorehabilitation group, Dept. of Rehabilitation Sciences, KU Leuven, Leuven, Belgium;
[2]Clinical Motion Analysis Laboratory, University Hospitals Leuven, Pellenberg, Belgium
Corresponding author: kaat.desloovere@kuleuven.be

INTRODUCTION

Cerebral palsy (CP) is the largest cause of childhood physical disability. While the disorder is caused by a non-progressive lesion in the developing brain, musculoskeletal alterations progress with age, resulting in **altered motor function**, such as **disturbed gait**. The observed **neuromuscular symptoms** mainly involve spasticity and muscle weakness. Because the brain lesion in CP changes the neural drive to muscles and because the muscle is a highly plastic tissue, these children experience significant **intrinsic muscle alterations**. Impaired macro- and microscopic muscle properties in children with CP include reduced muscle volume, length, anatomical cross-sectional area (CSA), and fiber CSA, altered fiber type proportion, reduced number of satellite cells (SCs) and hypertrophic extracellular matrix. Changes in morphological muscle properties at a macroscopic level can be studied with imaging techniques, such as ultrasound. Studies combining soft-tissue imaging with microscopic measures in growing children with CP have been lacking, but are essential for understanding the relation between different muscle properties and neuromuscular symptoms. In addition, there is a need for longitudinal follow-up studies, integrating different quantification levels (macro- and microscopic muscle properties, spasticity, strength, function), in order to properly identify deterrents to CP muscle growth.

Spasticity is the most prevalent symptom, observed in ±80% of CP children. **Intramuscular Botulinum Neuro-Toxin** (BoNT) injection, which selectively and reversibly blocks acetylcholine release at the neuromuscular junction, is popular to treat **focal spasticity**. The direct **clinical effect**, i.e. decreased muscle overactivity during muscle stretch, lasts 2-3 months. Subsequent clinical beneficial effects include reduced **spasticity** (defined by clinical scales) and increased joint range of motion, combined with the unavoidable side effect of acute but temporal muscle weakness. There is also evidence of **functional effects** of BoNT in CP, i.e. improved gait and gross motor function. Yet, concerns have been raised for **harmful effects of BoNT on intrinsic muscle properties**, which were primarily based on a series of muscle studies in animals, while human studies on macro- and microscopic muscle properties post-BoNT have been scarce.

This lecture will focus on the network of contributing factors to the pathogenesis of altered muscle growth in CP, covering an extended malleable period of childhood and the entire picture of the problem defined by integrated assessments within a longitudinal design. Special focus will be on how BoNT contributes to impaired muscle growth and whether clinical benefits of BoNT counterweight potential risks at the muscular level.

METHODS

During the past years, we have performed **combined assessments** to define macroscopic and microscopic intrinsic muscle properties, spasticity, strength, and gait pathology in one cohort of ambulant children with CP, within a **longitudinal design.** These analyses create a **full picture of muscle growth and post-BoNT muscle recovery in children aged between 0.5 and 11 years.** CP data (N>100) were compared to reference data from age-matched typically developing children (N<100), as well as pre- and post-BoNT (compared untreated control groups). The target muscle was the medial gastrocnemius.

Macroscopic muscle growth was defined by means of 3D freehand ultrasound (2D ultrasound combined with 3D motion tracking) to define muscle volume, belly length, CSA and echogenicity intensity. **Microscopic muscle properties** were defined using minimally invasive needle micro-biopsy and included fiber CSA, capillary density and the amount of SCs. **BoNT injections** were combined with casting, physical therapy and orthotics, with 1-year intervals between repeated sessions. **Clinical BoNT-effects** were defined through (1) instrumented spasticity assessments, involving collection of muscle activity, joint kinematics and torque during manual passive muscle stretches, (2) strength assessments based on dynamometry, and (3) pathological gait by means of 3D gait analysis.

RESULTS AND DISCUSSION

The longitudinal evaluation of muscle growth from the first years of life to 11 years of age revealed **piecewise trajectories of morphological muscle growth** [1].

At 2 months-post-BoNT compared to baseline, we confirmed **clinical beneficial BoNT-effects**, namely successful spasticity reduction and improved ankle kinematics, while muscle strength did not significantly decrease. These functional benefits were combined with **reduced normalized muscle volume**, compared to unaltered muscle growth in the untreated control group [2]. At 6 months post-BoNT, children who received their 1st BoNT treatment compared to an untreated control group showed **reduced muscle growth for CSA, while muscle belly length was preserved** [3]. Recent (unpublished) results of ongoing studies on the BoNT-effect at the microscopic level, which confirm initial muscle alterations post-BoNT, followed by recovery, will also be presented.

Overall, these results suggest that primary and secondary factors are contributing to altered muscle growth in children with CP, as a complex and interactive network.

The results were collected and analyzed in PhD projects (N. De Beukelaer, N. Peeters, J. Deschrevel), supervised by K. Desloovere, A. Van Campenhout, E. Ortibus, G. Gayan-Ramirez and K. Maes. The research was funded by KU Leuven (C24/18/103 and FTBO 2019) and the Research Foundation Flanders (G0B4619N, T005416N and G084523N).

REFERENCES

[1] De Beukelaer N *et al.* (2023). *J. Clin. Med.*, **12**: 1564.
[2] Peeters N. *et al.* (2022). *Toxins.*, **14**: 676.
[3] De Beukelaer N *et al.* (2022). *Toxins*, **14**, 139.

Session 1:
Molecular Muscle Mechanics / Physiology

Venus Joumaa

Christopher Marang

Motoshi Kaya

Seong-won Han

Chris Tiessen

Edward Debold

Chairperson: Henk Granzier

History-Dependent Properties of Muscle Contraction

[1]**Venus Joumaa**, [1]Timothy R. Leonard, [1]Walter Herzog
[1]Faculty of Kinesiology, The University of Calgary, Calgary, AB, Canada
corresponding author: vjoumaa@ucalgary.ca

INTRODUCTION

When a skeletal muscle is actively stretched or shortened, the resulting isometric steady-state force is always greater or smaller, respectively, than the purely isometric contraction performed at the final muscle length and corresponding level of activation without prior stretching or shortening (Figure 1). These history-dependent properties of muscle contraction, termed residual force enhancement and residual force depression, respectively, have been observed consistently in muscle preparations ranging from single myofibrils to human muscles *in vivo* [for review see 1 and 2].

Residual force enhancement and residual force depression have been perplexing observations because the cross-bridge theory predicts that the steady-state isometric force depends on the final muscle length and not on how the muscle reaches this final length.

Within the framework of the cross-bridge theory, residual force enhancement and force depression could occur if active stretching and shortening were able to rearrange the nanostructure of the contractile filaments resulting in changes in the number of attached cross-bridges and/or the force produced per cross-bridge. Understanding how a muscle can increase or decrease its isometric force would provide great insight into the mechanisms of active force regulation.

PURPOSE

The purpose of our research is to investigate the mechanisms of residual force enhancement and residual force depression, and thus provide insight into active force production and regulation in skeletal muscle.

METHODS

Residual force enhancement and residual force depression have been investigated by examining the structure of the sarcomere after active stretch and shortening using small angle x-ray diffraction, and by performing mechanical testing on single skinned muscle fibres.

RESULTS AND DISCUSSION

X-ray diffraction studies have shown that i) residual force enhancement is associated with an increase in M3 spacing, no change in stiffness and the intensity ratio I1,1/I1,0, and decreased M3 intensity, and ii) residual force depression is associated with a decreased force, stiffness, I1,1/I1,0, M3 and M6 spacings, and M3 intensity [3].

These results suggest that residual force enhancement is achieved without an increase in the proportion of attached cross-bridges, and that residual force depression is accompanied by a decrease in the proportion of attached cross-bridges. Furthermore, residual force enhancement and residual force depression are accompanied by an increase in cross-bridge dispersion and/or a change in the cross-bridge conformation compared to the reference contractions.

Mechanical testing elucidating cross-bridge kinetics in actively stretched and shortened muscle fibres and their corresponding purely isometric contractions have shown i) no change in cross-bridge cycling kinetics following active stretch compared to corresponding purely isometric contractions, and ii) that the apparent rates of cross-bridge attachment and detachment, the rate of force redevelopment (f, g, and k_{TR}, respectively), the proportion of attached cross-bridges, and the force produced per cross-bridge were significantly decreased following active shortening compared to corresponding purely isometric contractions, indicating a change in cross-bridge cycling kinetics [4].

These findings suggest that residual force depression is associated with changes in cross-bridge kinetics, while residual force enhancement does not originate from altered cross-bridge kinetics but likely from passive structures [5,6].

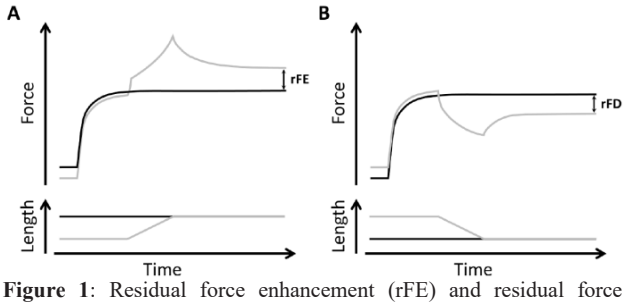

Figure 1: Residual force enhancement (rFE) and residual force depression (rFD) at steady-state following active muscle stretching (A) and shortening (B), respectively [1].

ACKNOWLEDGEMENTS

CIHR, NSERC, Canada research chair program, Benno Nigg chair in Biomechanics, Mobility and Longevity, Killam foundation.

REFERENCES

[1] Hahn D et al. (2023). *J Biomech*, 1**52**: 111579.
[2] Herzog W. (2017). *J Neuroeng Rehabil*, **14**: 98.
[3] Joumaa V et al. (2021). *Int J Mol Sci*, **22(16)**: 8526.
[4] Ames SR et al. (2022), *J Exp Biol*, **225(22)**: jeb244703.
[5] Leonard TR & Herzog W. (2010). *Am J Physiol Cell Physiol*, **299**: C14-20.
[6] Hessel AL et al. (2017). *Front. Physiol,* **8**: 70.

A point mutation in the switch I region of myosin's active site dramatically alters the load-dependence of phosphate-induced detachment from actin

[1]**Christopher P. Marang**, [1]Brent D. Scott, [2]James Chambers, [3]Laura Gunther, [3]Christopher M. Yengo, [1]Edward P. Debold
[1]Department of Kinesiology, University of Massachusetts, Amherst, MA 01003
[2]Institute for Applied Life Sciences, University of Massachusetts, Amherst, MA 01003
[3]Department of Cellular and Molecular Physiology, Penn State College of Medicine, Hershey, PA 17033
corresponding author: edebold@umass.edu

INTRODUCTION

Myosin is a molecular motor responsible for generating the force and/or motion that drive many intracellular processes, from muscle contraction to vesicular transport. It is powered by its ability to convert the chemical energy, released from the hydrolysis of ATP, into mechanical work. The key event in the transduction process is the coupling of the force-generating powerstroke with the release of phosphate (P_i) from the active site, but the mechanisms and the structural elements involved in this coupling remain unclear. Therefore, we determined the effect of elevated levels of P_i on the force-generating capacity of a mini-ensemble of myosin Va molecules (WT) in a three-bead laser trap assay.

METHODS

A three-bead optical trapping assay was used to probe the effects of Pi on actomyosin interactions under different resistive loads. A TRITC/biotin-labeled actin filament was connected to streptavidin coated 1µm silica beads. It was brought into contact with a myosin-coated pedestal bead (10µg/mL). Roughly 5 myosin heads were available to bind to the thin filament. Experimental conditions were performed at 100µM ATP, and conducted at both pH 7.0 with 0mM and 30mM Pi. Three laser trap stiffness' (0.04, 0.06, 0.10 pN/nm) were used to increase the load myosin ensembles worked against. Actin filament displacement was tracked using a quadrant photodiode (QPD) and laser trap stiffness was used to convert displacements (d) into forces: multiplying displacement (d) by the trap stiffness (i.e. Force = d * ktrap).

RESULTS AND DISCUSSION

We quantified the load-dependence of the P_i-induced detachment rate by performing the experiments at three different laser trap stiffnesses (0.04, 0.06 and 0.10pN/nm). Myosin generated higher peak forces at the higher laser trap stiffnesses, and the distance the myosin displaced the actin filament significantly increased in the presence of 30mM P_i, a finding most consistent with the powerstroke preceding P_i-release. In contrast, the duration of the binding events was significantly reduced at higher trap stiffness in the presence of P_i, indicating that the higher resistive force accelerated the rate of P_i-induced detachment from actin. A Bell approximation, was used to quantify the load-dependence of this rate ($k_1 = k_o$ x exp(F*d*/kt)), revealing a *d*-value of 0.6nm for the WT myosin (Figure 1). Repeating these experiments using a construct with a mutation (S217A) in a key region (Switch I) of the nucleotide-binding site increased myosin's sensitivity to load seven-fold (*d* = 4.1nm). Thus, these findings provide a quantitative measure of the force-dependent nature of P_i-rebinding to myosin's active site and suggest that this effect involves the switch I element of the nucleotide-binding pocket. These findings, therefore, provide important new insights into the mechanisms through which this prototypical motor enzyme couples the release of chemical energy to the generation of force and/or motion.

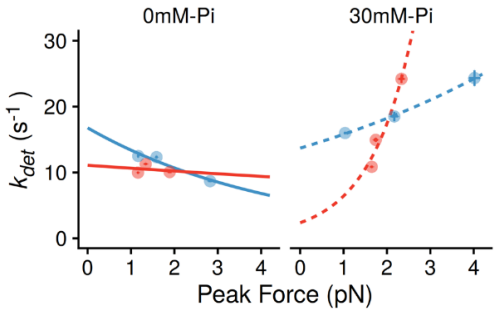

Figure 1: Load-dependence of the Pi-induced detachment rate. The durations at peak force were converted to rates (kdet) and plotted against the peak force. Values represent the mean ± SEM. Data were fit with the Bell-bond equation, which relates the effect of force on the rate of the reaction, using the form kdet = ko x exp(Fd/kT), where kdet is the observed rate of detachment (1/binding event lifetime), ko is the rate in the absence of load, F is the peak force generated, d the distance parameter that reflects the degree of load sensitivity of the rate, k is the Boltzmann constant, and T the temperature in Kelvin. For the WT construct (blue) the fit parameters ko = 16.8 ± 1.8 . s -1 (mean ± SEM) and the d value was -0.9 ± 0.3nm (mean ± SEM) in the absence of Pi and 13.7 ± 0.2 for ko and 0.6nm for d in the presence of 30 mM Pi. For the S217A construct (red) ko was 11.1 ± 0.3.0. s -1 and a d value of -0.2 ± 0.7nm in the absence of Pi, and ko was 2.5 ± 1.1 s-1 and the d-value 4.1 ± 0.9nm in the presence of Pi.

Cooperativity between skeletal myosin molecules evaluated by information theory

[1]Arun Kasimchetty, [1]Hideo Higuchi and [1]**Motoshi Kaya**
[1]Department of Physics, University of Tokyo, Tokyo, Japan
corresponding author: kaya@g.ecc.u-tokyo.ac.jp

INTRODUCTION

Information is essential for living organisms. For example, signal transduction pathways in cells sense stimuli from outside the cell as information and regulate various intracellular and extracellular activities. In particular, in muscle, satellite cells sense cytokines induced by muscle damage and are activated to differentiate and repair the damaged area. In addition, muscle cells show a large variation in response to electrical stimulation, but the response in the ensembles of muscle cells (e.g., myofibrils) is found to be more gradual, implying intercellular variation can increase the information capacity of muscle tissues [1]. On the other hand, myosin, a contractile protein of muscle, has not been investigated from the viewpoint of information, although it has been investigated how the velocity changes as an output response to an input represented by load.

In this study, we propose a method to evaluate the cooperativity among skeletal myosin molecules, which we have proposed previously [3], by calculating the amount of mutual information in myofilaments with different numbers of molecules.

METHODS

The force of filaments of myosins mixed with myosin rods in 1:1 or 1:4 molar ratios was measured using optical tweezers (Figure 1). Approximately 20 interacting molecules are estimated to interact with single actin filaments in [1:1]-myofilaments, while 10 molecules maximally interact with actin in [1:4]-myofilaments. The displacement curves of the trapped beads were multiplied by trap stiffness to obtain the load acting on the myofilaments. The velocity was obtained from the change in the load and the time variation of the displacement curve for every 1 pN. Loads were treated as an input and velocities were as an output in the calculation of mutual information.

The mutual information [2], which is calculated from the dependence of the input stimulus and output response, is used to evaluate the cell's ability to transmit information [1]. The magnitude of the mutual information is a measure of how much input information can be transmitted as output. The mutual information between probability variables x (input) and y (output) is given by

$$I(y; x)= \sum P(y|x)\log_2[P(y|x)/ P(x)/P(y)]$$

where P(x) and P(y) are an input probability distribution and output probability distribution, respectively, and P(y|x) is a conditional probability distribution of the output for a given input. These probability distributions were obtained from velocity-load data sets sorted by the adaptive portioning method [4] for each myofilaments.

RESULTS AND DISCUSSION

The sliding velocity of actin was calculated for each 1pN load from the slope of the myofilament displacement curve measured using optical tweezers (Figure 1). The mutual information of the 10 [1:1]-myofilaments at 100 μM ATP was 1.72 ± 0.22 bits compared to the input information of 2.72 ± 0.22 bits, suggesting the information transfer efficiency of 64% on average. This result implies that information capacity of individual myofilaments is remarkably higher than that of individual muscle cells [1] and that the variation between myofilaments is much smaller than that between cells.

In the future, we will calculate mutual information from force-velocity measurements of [1:4]-myofilament and compare it with the results of [1:1]-myofilament to evaluate changes in information tcapacity in response to changes in the number of molecules, and will examine whether cooperativity between myosin molecules can be discussed from information theory.

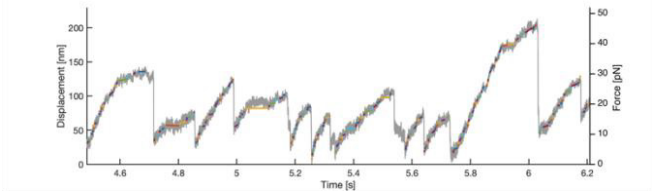

Figure 1: Example of actin displacement curve generated by [1:1]-myofilament at 100 μM ATP. The colored lines are the linear fitting curves of the displacement calculated for each 1pN, and their slopes were used as the velocity.

ACKNOWLEDGEMENTS

This work was supported by JSPS KAKENHI Grant Number JP 22H04836.

REFERENCES

[1] Wada T et al. (2020). *Cell Rep*, **32**: 108051.
[2] Shannon CE (1948). *Bell Syst.Tech. J.*, **27**: 623–656.
[3] Kaya, M et al. (2017). *Nat. Communs.*, **8**: 16036.
[4] Darbellay, GA and Vajda, I (1999) *IEEE Trans. Info. Theory*, **45** 1315-1321.

Changes in Passive Stresses in Single Myofibrils after Graded Titin Cleavage Progressively

Seong-won Han[1], Johanna K. Freundt[1], Wolfgang A. Linke[1]
[1] Institute of Physiology II, University of Münster, Germany.
Email: seongwon.han@uni-muenster.de

INTRODUCTION

Titin is a molecular ruler that connects the Z-disk and the M-band in the sarcomere, and it has been considered as the third component after actin and myosin, contributing to force generation of a sarcomere. Many attempts have been made to quantify the contribution of titin to passive and active forces, by removing titin through chemical degradation [1] or genetic impairment [2]. However, these approaches have limitations, because (i) other proteins could also be affected by the chemical degradation, and (ii) most of the genetically modified animals exhibited secondary disease phenotypes, which complicate the interpretion of the results.

Recently, the titin cleavage (TC) mouse model was established, where a cleavage site is cloned into I-band titin close to the A-band, and adding the tobacco etch virus protease to muscles allows for rapid and specific titin cleavage [3]. Using the TC model, we confirmed that titin contributes to passive and active force generation and also maintains sarcomeric structure organized [4]. Interestingly, even when all titin was cleaved, passive force did not drop to zero, but decreased by 50-55%, while titin was thought to contribute >90% of passive force previously [5]. One reason for this discrepancy could be the presence of stiff extracellular matrix proteins in the skinned muscle fibre bundles that were used [4]. Thus, we aimed at re-examining the contribution of titin to passive forces in single myofibrils, when cleaving titin progressively by 50% and 100%.

METHODS

Single myofibrils (n=3 per each; n=6 in total) were isolated from the psoas muscle of the TC mice, attached to cantilevers [e.g., 6], and set at an average sarcomere length (SL) of 2.4µm. Then, the myofibril was slowly stretched to 3.0 µm, held for 20s to measure passive force, and returned to the slack SL. The measurement was then repeated on the same myofibril, after titin was cleaved, by incubating the myofibrils with the tobacco etch virus protease.

RESULTS AND DISCUSSION

When 50% of titin was cleaved, passive stress was decreased by 32.2%, dropped from 37.9 nN/µm^2 to 25.7 nN/µm^2 on average (Fig 1).

When 100% of titin was cleaved, the reduction in the passive stress was approximately two times greater than those observed for 50% of TC, by showing 59.2% of decrease on average (changed from 30.3 nN/µm^2 to 12.4 nN/µm^2 (Fig 1)). Also, when passively stretching the myofibrils after 100% of TC, changes in myofibrillar structure were observed, including the Z-disks and the A-bands disorganized.

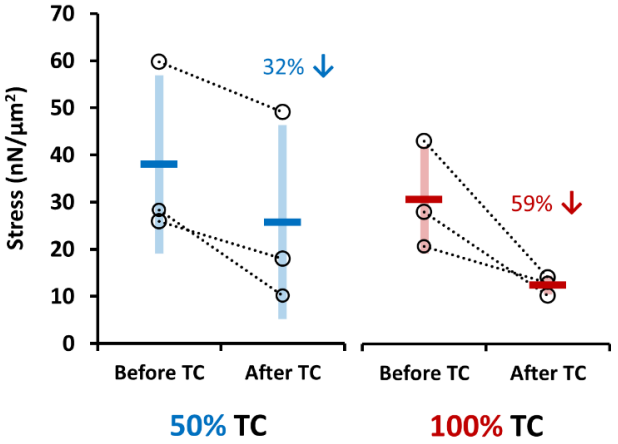

Figure 1 Changes in passive stresses (nN/µm^2) at the SL 3.0 µm, before and after TC, when titin was cleaved by 50% (left-hand side) and by 100% (right-hand side). Each open circle represents a result from a myofibril, and the horizontal bar and vertical bar represent the mean with 1SD, respectively.

Our results are aligned with the previous study that showed significant decrease in passive force in skinned muscle fibre bundles after TC [4]. However, the observed decrease in the passive stress in our study was not greater 59% on average, while titin is thought to contribute >90% of passive force in single myofibrils. Furthermore, we did not observe complete destruction of the myofibrils' structure after 100% of TC.

CONCLUSIONS

Even though we cleaved titin in single myofibrils, the changes in passive stress were not as substantial as we hypothesized. Therefore, further studies are required to determine the source of the remnant passive stress in myofibrils.

ACKNOWLEDGEMENTS

This work was supported by the German Research Foundation (SFB1002-A08; Grant to Wolfgang A. Linke).

REFERENCES

[1] Higuchi H. *J Biochem.* **111**: 291-295, 1992.
[2] Radke MH et al. *Circulation*. **139**: 1813-1827, 2019.
[3] Rivas-Pardo JA et al. *Nat Commun.* **11**:2060, 2020.
[4] Li Y et al. *eLife.* **9**:e64107, 2020.
[5] Irving T et al. *Biophys J.* **100**:1499-1508, 2011.
[6] Han et al. Biophys J. e-published, 2023.

Mechanical Contribution of Immunoglobulin Domain Refolding Under Tension to Myofibrils

[1]**Chris Tiessen**, [1]Tim Leonard, [2]Gudrun Schapper-Tilp, [1]Walter Herzog
[1]Faculty of Kinesiology, The University of Calgary, Calgary, AB, Canada
[2]Department for Mathematics and Scientific Computing, Karl-Franzens University Graz, Universitätsstr. 15 9010. Graz, Styria, Austria
corresponding author: chris.tiessen@ucalgary.ca

INTRODUCTION

In muscle, the functional unit of contraction is the sarcomere. Sarcomeres are arranged lengthwise in myofibrils, which can be mechanically tested to isolate the properties of the muscle tissue from the surrounding connective tissue. When passively stretched, mechanical properties of myofibrils can be attributed to the spring-like protein titin that runs lengthwise along the sarcomeres.[1] Mechanically, titin has two primary regions: the PEVK region and the immunoglobulin (IG) domain region. The PEVK region is generally assumed to be nearly elastic, whereas the IG domain region contains unfolding and refolding domains that tend to behave visco-elastically.[2] The IG domains are thought to contribute to stress relaxation by lengthening/unfolding under tension when stretched to lengths greater than ~3.6 um/sarcomere for rabbit psoas. When tension is released, IG domains can refold, recovering some energy, but the refolding mechanics remain largely unknown.[2]

METHODS

Previous myofibril experiments in our lab have been conducted using quick shortening rates to determine IG domain refolding kinetics under no force. Here, we seek to investigate IG domain refolding kinetics using relatively slow stretching and shortening rates to identify the mechanical contribution of IG domains and investigate their rate of refolding through comparison to the worm-like chain model.

Two protocols were performed on isolated myofibrils (n=7) on isolated myofibrils from rabbit psoas muscle. The first was a 2-4-2 second stretch, hold, and shorten cycle; the second was a 2-0-2 second stretch, hold, and shorten cycle. Stretches were performed using a piezoelectric motor from a length of 2.7 um/sarcomere to a target length of 4.5um/sarcomere. Force measurements were made using optical nano-lever force cantilevers.

RESULTS AND DISCUSSION

For both protocols, force was maintained during the entire test, and specifically for the entire myofibril shortening phase indicating that titin refolding was occurring sufficiently quick to maintain force during the shortening phase. This is a surprising result as IG domain refolding has been assumed to occur slowly under high force, and was not expected to contribute to work in a 2 s and 0.9 µm/s/sarcomere shortening event.

For both protocols, the maintenance of force did not match worm-like chain model predictions using literature values. To curve fit our experimental data, two options were tested: (i) increasing the refolding rate or (ii) decreasing the force threshold at which refolding occurs. We chose to increase the refolding rate, because stretches below ~3.6 um/sarcomere do not result in IG domain unfolding/refolding, indicating that the literature IG domain refolding force threshold is appropriate. To curve fit experimental data (figure 1), the refolding rate in the worm-like chain model was increased by a factor of 2.5 (figure 2), providing evidence that IG domain refolding may occur faster than previously thought.

In conclusion, some evidence is provided that refolding rates of IG domains in myofibrils are faster than previously thought, and that refolding may occur under tension. Notably, refolding seems to be fast enough to contribute to mechanical work if the shortening speed is below about 0.9 µm/s/sarcomere.

Figure 1: Example raw data for a 2-4-2s stretch, hold, release protocol.

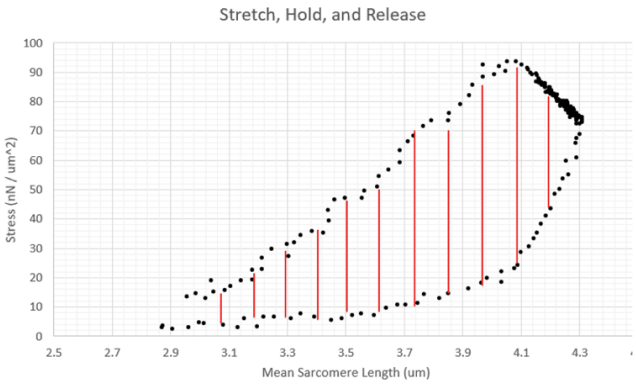

Zone of hysteresis shown in red.

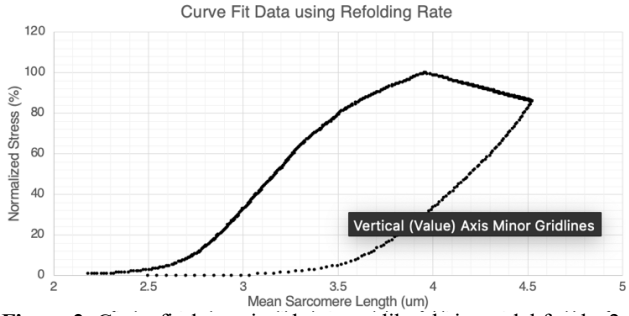

Figure 2: Curve fit data using the worm-like chain model for the 2-4-2 s protocol. The refolding rate was increased by a factor of 2.5.

REFERENCES

[1] Trombitas et al., (1998). *Journal of Cell Biology*, **140**: 853-859
[2] Linke et al., (2019). *Journal of Applied Physiology*, **126**: 1474-1482.

→

The molecular mechanism of the phosphate-induced loss of force during muscle fatigue

Christopher P. Marang, Brent Scott, Edward P. Debold
Department of Kinesiology, University of Massachusetts, Amherst, MA, USA

corresponding author: edebold@kin.umass.edu

INTRODUCTION

In response to intense contractile activity skeletal muscle fatigues, with its ability to generate force greatly diminished. A large portion of the decrease in force is thought to be due to the accumulation of high levels of inorganic phosphate (P_i), a by-product of the rapid breakdown of creatine phosphate as it acts to maintain the intracellular ATP concentration constant. The high levels of P_i are thought to reduce force by directly inhibiting the function of myosin, the molecular motor of muscle, however the exact mechanisms underlying this process are still not clear. We sought to reveal these mechanisms by directly examining the effect of P_i on the force-generating capacity of myosin in a laser trap assay.

METHODS

The force generating capacity of a mini-ensemble of myosin molecules (~8 heads) was directly determined using a three-bead laser trap assay (Figure 1). To determine the effect of an increase in resistive load on myosin's force-generating capacity the stiffness of the laser traps was systematically increased from 0.04 to 0.2 $pN \cdot nm^{-1}$. At each trap stiffness the effect of 0, 5, 10 and 30mM P_i was determined on maximum force, actomyosin binding event lifetime and the size of displacements generated by the mini-ensemble of myosin. All experiments were performed using myosin isolated from fast skeletal rabbit psoas muscle, with the ATP concentration set to 100uM. Additionally, the total ionic strength was held constant at 125mM by adjusting the amount of KCl added to buffers with less than 30mM P_i and the temperature was 25°C.

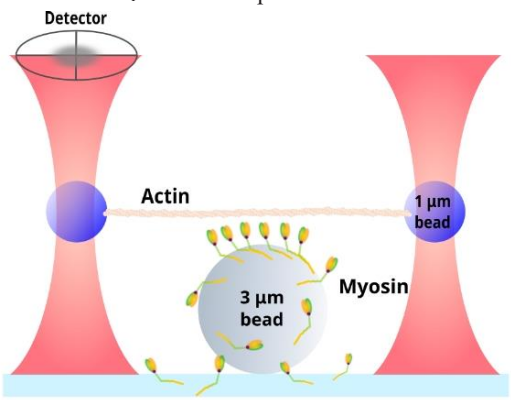

Figure 1: Schematic of the mini-ensemble laser trap assay. Red hour glass shapes indicate the laser beam.

RESULTS AND DISCUSSION

In the control condition, with 0mM added P_i increasing restive load on the myosin prolonged the lifetime of actomyosin attachments, consistent with a slowed rate of ADP-release from myosin's nucleotide-binding site. However, the opposite occurred in the presence of P_i, with increasing resistive load accelerating detachment from actin in a concentration, and load-dependent, manner. This also caused a decrease in the maximum force-generating capacity that was dependent on load and the Pi concentration as shown in Figure 2. Additional experiments performed at a lower ATP concentration (5uM) demonstrated nearly identical effects on binding event lifetimes and on the force-generating capacity. Therefore, these findings suggest that P_i rebinds to myosin's active site before ADP is release from the active site and induces detachment. We did not observe evidence of powerstroke reversals and myosin was able to generate a powerstroke even in the presence of 30mM P_i suggesting that detachment from actin occurs from a post powerstroke state.

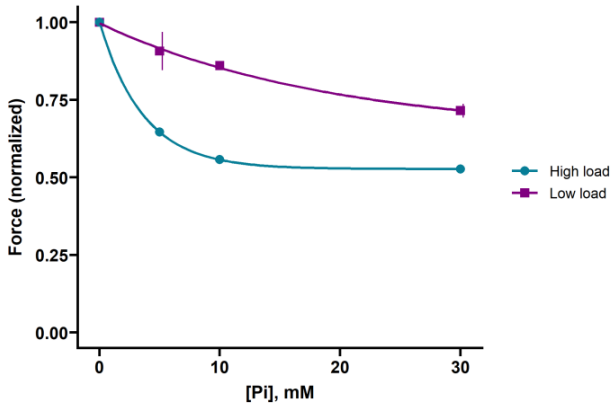

Figure 2: Effect of P_i and resistive load on myosin's force-generating capacity. Data points represent means ± SEM. Data fit to a dose response curve with EC_{50} values of 27.5mM at low load and 2.1mM at high load.

Interestingly, myosin was able to displace the actin filament even in the presence of high load and 30mM P_i. This finding is most consistent with the powerstroke occurring prior to the release of P_i from the active site.

Thus, the data suggest that elevated levels of P_i that occur during fatigue decrease muscular force, not by preventing or reversing the powerstroke, but by decreasing the number of attached cross-bridges. This provides new insight into the mechanism of force loss during fatigue

ACKNOWLEDGEMENTS

This work was supported by a grant from the NIH R01GM135923-01.

Session 2:
Cellular Muscle Mechanics / Physiology

Lucas Smith

Jorieke Deschrevel

Domiziana Costamagna

Jarrod Petersen

Armaan Sekhon

Chairperson: Rick Lieber

ALIGNMENT DURING DYNAMIC STRETCHING

[1]Ross P. Wohlgemuth, [2]Marie Villalba, [2]Vedant A. Kulkarni, [2]Jon R. Davids, [1,3]**Lucas R. Smith**
[1]Department of Neurobiology, Physiology, and Behavior, University of California, Davis, CA, USA
[2]Department of Orthopaedic Surgery, Shriners Hospital for Children – Northern California, Sacramento, CA, USA
[3]Department of Physical Medicine and Rehabilitation, University of California, Davis, CA, USA
corresponding author: lucsmith@ucdavis.edu

INTRODUCTION

The collagen fiber architecture of skeletal muscle can directly affect its mechanical properties and stiffness [1]. Muscle stiffness can be related to contracture in children with cerebral palsy [2]. However, collagen architecture is also influenced by mechanical strain [3] and children with CP have high in vivo muscle strain in contracture [4]. Thus, we investigated the collagen architecture of muscle in both typically developing (TD) children and children with CP over a range muscle strain to assess whether real-time changes in collagen fiber alignment occur during a muscle stretch and if those changes are related to muscle stiffness and function.

METHODS

Study participants were children with CP and TD children undergoing surgery at a children's surgical specialty hospital. Subjects with CP underwent gait analysis prior to surgery. Utilizing specialized clamps to maintain muscle length and architecture, gracilis muscle biopsies (N=3) were collected from patients with CP undergoing hamstring lengthening surgery. Gracilis muscle biopsies from TD patients (N=4) were collected during ACL reconstruction surgery. Multiple muscle bundles (3-5) were removed from each biopsy and were placed in a glycerol-based storage solution prior to second harmonic generation (SHG) imaging for collagen architecture. SHG imaging was performed on muscle bundles at slack length (0% strain) and up to 45% strain in 7.5% increments. Collagen deviation, an inverse measure for collagen alignment, was calculated by assigning an orientation to multiple pixel windows throughout the image (Figure 1). Collagen deviation was compared across the SHG images for each muscle bundle.

RESULTS AND DISCUSSION

In both CP and TD muscle, we found that collagen deviation was significantly decreased at 45% strain compared to 0% strain (CP 0%: 24.07°±3.729, CP 45%: 19.41°±2.716, p=0.0068; TD 0%: 28.82°±6.062, TD 45%: 22.28°±7.502, p=0.0008), indicating that muscle in both groups has increasing alignment with stretch (Figure 2A). The magnitude of difference between the collagen deviation at 0% and 45% strain was not significantly different between TD and CP muscles (TD: 6.546°±1.816; CP: 4.664°±1.013) (Figure 2B).

CP muscle has similar dynamic collagen alignment properties as TD muscle when subjected to physiologic stretch. This finding may have positive implications for dynamic stretching programs in children with CP. Additional samples are being collected to provide the ability to relate the collagen architectural changes to important gait parameters and the degree of contracture.

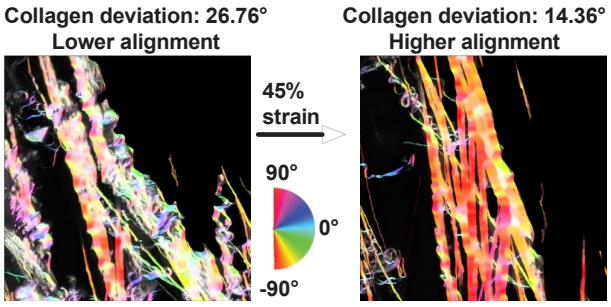

Figure 1: Representative sample of hamstring muscle biopsy imaged with second harmonic generation microscopy with sarcomeric signal removed to reveal collagen fibers. Left shows tissue as slack length with relatively low collagen alignment (ie high collagen deviation). Right is the same region imaged at 30% strain showing an increase in collagen alignment (ie low collagen deviation).

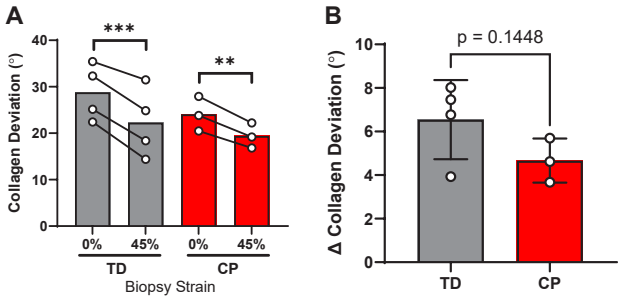

Figure 2: Quantification of changes in collagen alignment with biopsy tissue strain. **A)** both in CP and in TD there is a significant decrease in collagen deviation (ie increase in alignment) when tissue undergoes strain to 45%. **B)** The change in collagen deviation from slack length to 45% is not significantly different in CP compared to TD but tends to be less altered. ** p < .01, *** p < .001.

ACKNOWLEDGEMENTS

This research was funded by the Hartwell Foundation. Second harmonic generation imaging was performed at the UC Davis Advanced Imaging Facility.

REFERENCES

[1] Brashear SE et al. (2021). *J Physiol*, **3**: 943-962.
[2] Smith LR et al. (2011). *J Physiol*, **10**: 2625-39.
[3] Purslow PP. (1989). *J Biomech*, **1**: 21-31.
[4] Lieber RL and Friden J. (2002). *Muscle Nerve*, **2**: 265-70.

Histological analysis of the gastrocnemius muscle in young children with cerebral palsy compared to age-matched typically developing children.

[1]**Jorieke Deschrevel**, [1]Anke Andries, [1]Karen Maes, [2]Nathalie De Beukelaer, [3]Marlies Corvelyn, [2]Ester Huyghe, [2]Lauraine Staut [4]Anja Van Campenhout, [4]Hannah De Houwer, [2,5]Domiziana Costamagna, [2]Kaat Desloovere, [1]Ghislaine Gayan-Ramirez

[1] Laboratory of Respiratory Diseases and Thoracic surgery, Department of Chronic Diseases and Metabolism, KU Leuven, Leuven, Belgium, [2] Neurorehabilitation group, Department of Rehabilitation Sciences, KU Leuven, Leuven, Belgium, [3] Stem Cell Biology and Embryology, Department of Development and Regeneration, KU Leuven, Leuven, Belgium, [4] Pediatric Orthopedics, Department of Development and Regeneration, KU Leuven, Leuven, Belgium, [5] Exercise Physiology Research group, Department of Movement Sciences, KU Leuven, Leuven, Belgium. Corresponding author: ghislaine.gayan-ramirez@kuleuven.be

INTRODUCTION

Alterations in muscle microscopic properties have been reported in adolescent with cerebral palsy (CP). Whether such alterations are already present in very young CP children is not yet known [1]. This study aimed to quantify histological alterations in the medial gastrocnemius (MG) of ambulant children with CP compared to age-matched typically developed (TD) children.

METHODS

MG microbiopsies were collected in 24 children with CP with GMFCS level I - III and in 13 age-matched TD children (Table 1). Sections were stained with 1) myosin heavy chain-I, -IIa and -IIx to analyze fiber cross-sectional area (fCSA) and proportion; 2) CD31 to determine capillary to fiber ratio (C/F) and capillary density for fiber type I and II (CFD); 3) PAX7 to determine the number of satellite cells (SC)/100 fibers. fCSA was normalized to fibula length. fCSA intrasubject variation was presented as the coefficient of variation (CV).

Table 1: Population characteristics. Data shown as median (IQR). TD: typically developing children; GMFCS: gross motor classification system level I – III. * P < 0.05 compared to TD

	TD	GMFCS I	GMFCS II	GMFCS III
N	13	8	8	8
Boys/Girls	7/6	5/3	6/2	4/4
Age (years)	4.2 (1.4)	4.2 (1.3)	3.7 (1.8)	4.2 (1.4)
Age range	2.8 - 5.2	2.9 - 5.2	2.5 - 5.4	2.8 - 5.1
Body mass (kg)	16.0 (3.5)	15.5 (3.5)	15.3 (4.8)	13.4 (2.9)*
Body length (cm)	103.5 (6.5)	104.8 (11.9)	99.3 (11.1)	92.0 (7.8)*
Fibula length (cm)	21.0 (3.5)	21.3 (4.5)	19.3 (5.0)	18.0 (3.0)

RESULTS AND DISCUSSION

Absolute and normalised fCSA did not differ between CP and TD children, but CV was significantly higher for all fibers grouped together, in the total-CP-group and GMFCS-I and -II, compared to TD. The increased CV was most obvious for type I fibers (Table 2). Distribution frequency showed a significantly higher frequency of smaller fibers between 0-750 μm^2 in the total-CP-group and GMFCS-II and III (Table 2). Type IIx proportion was higher and type I proportion lower in the total-CP-group and GMFCS-III (Table 2). C/F was reduced in the total-CP-group and with GMFCS-II and III compared to TD, as was CFD for type I fibers and type II fibers (Table 2). The amount of SC/100 fibers did not differ.

	Fiber type	CP	GMFCS I	GMFCS II	GMFCS III
CV	All	+21%§	+23%*	+29%#	ns
	I	+23%§	ns	+23%$	ns
fCSA 0-750μm^2	All	+69%§	ns	+65%§	+67%§
fiber proportion	I	- 30%§	ns	ns	-39%§
	IIx	+69%§	ns	ns	+81%§
C/F		- 49%§	ns	-51%*	-64%$
CFD	I	- 27%#	ns	ns	ns
	II	- 22%#	ns	ns	ns

Table 2: Data on fiber size, fiber proportion and capillaries in children with CP and GMFCS level I – III compared to TD children. TD: typical developing children; CP: children with Cerebral palsy, GMFCS: gross motor classification system; CV: coefficient of variation, fCSA: fiber cross-sectional area, C/F: capillary to fiber ratio, CFD: capillary density, ns: not significant. Data are shown as percentage difference (Δ%) compared to TD. *p<0.05; $p<0.01; #p<0.006; §p<0.001

These results showed altered fiber size and proportion with reduced capillarization of the MG already at very young age in children with CP compared to age-matched TD children, while the SC-number was not altered.

ACKNOWLEDGEMENTS

This project was funded by an internal KU Leuven grant (C24/18/103) and by Research Foundation-Flanders (FWO; grant G0B4619N)

REFERENCES

[1] Graham HK et al. (2016). *Nat Rev Dis Primers*, **2**: 15082.

Botulinum Toxin Effect on Cerebral Palsy Muscle Stem Cells and hiPSC-derived NMJs

[1, 2]**Domiziana Costamagna**, [1]Valeria Bastianini, [1, 3]Marlies Corvelyn, [3]Maurilio Sampaolesi, [4]Ghislaine Gayan-Ramirez, [5,6]Anja Van Campenhout and [1]Kaat Desloovere

[1]Neurorehabilitation Group, Dept. of Rehabilitation Sciences, KU Leuven, Leuven, Belgium; [2]Exercise Physiology Research Group, Dept. of Movement Sciences, KU Leuven, Leuven, Belgium; [3]Translational Cardiomyology Lab., Stem Cell and Developmental Biology, Dept. of Development and Regeneration, KU Leuven, Leuven, Belgium; [4] Lab. of Respiratory Diseases and Thoracic Surgery, Dept. of Chronic Diseases and Metabolism, KU Leuven, Leuven, Belgium; [5]Department of Orthopaedic Surgery, University Hospitals Leuven, Leuven, Belgium; [6]Dept. of Development and Regeneration, University Hospital Gasthuisberg, Leuven, Belgium.

Corresponding author: domiziana.costamagna@kuleuven.be

INTRODUCTION

Spasticity in cerebral palsy (CP) and other pathologies, such as stroke, is commonly treated with intramuscular Botulinum Neurotoxin (BoNT) injections. Despite improved clinical outcomes, harmful effects, such as altered muscle morphology and loss of contractile material, have been reported in animals and healthy participants [1-4]. BoNT data on muscle stem cells are limited to transcript analyses from stroke patients, in which BoNT treatment decreased proliferation in myoblasts, affected the expression of contractile genes in myotubes and promoted the transcription of pro-inflammatory genes in muscle fibroblasts [5]. The effect of BoNT on different muscle stem cells of young CP children compared to typically developing (TD) children has not been reported yet. The aim of this study was to evaluate the effect of *in vitro* BoNT administration on satellite cell (SC) ability to differentiate, on fibroblast collagen secretion and on neuromuscular junction (NMJ) injury and recovery.

METHODS

Muscle biopsies were collected in children with CP from 2 to 9 years old, GMFCS level I-III, prior to (t0, n = 10), and 3 (t1, n = 6) and 6 months (t2, n = 9) after the first BoNT *in vivo* administration. CP were compared to age-matched TD (n = 7). By applying microbiopsy technique, ~8 mg of *medial gastrocnemius* tissue was collected and further disrupted in culture dishes. SC-derived myoblasts and fibroblasts were isolated by FACS and treated with 20 IU/ mL BoNT during 48h. Baseline and data from the different time points after BoNT *in vivo* administration were compared with TD. Furthermore, to follow BoNT effect on the neural component, coculture of lower motor neurons and myotubes, autologously derived from human induced pluripotent stem cells (hiPSCs) and allowed to form neuromuscular junctions, were treated with 20 IU/ mL BoNT during 48h (1 x BoNT) and compared to the untreated ones (1 x Untr) or to the ones recovered during 48h after BoNT treatment (1 x Rec). To mimic repetitive treatments, one serie of NMJ cocultures was treated during 48h with 20 IU/ mL BoNT for two rounds (2 x BoNT) and compared to untreated (2 x Untr) or to the cocultures recovered during 48h after twice BoNT treatment (2 x Rec).

RESULTS AND DISCUSSION

SC-derived myoblasts showed no differences in myogenic differentiation (Fusion Index, FI) or MYOD positive nuclear percentage, comparing cells at t0 to the ones extracted from age-matched TD children, with or without BoNT treatment. At t2, SC-derived myotubes showed a decrease in FI (-37%, p = 0.0476) compared to t0. Fibroblasts revealed no differences for collagen transcript and protein level for both CP compared to TD as well as for CP over time, with or without BoNT treatment. Finally, 48h BoNT treatment caused axonal swelling and fragmentation in the NMJ model (Figure 1). This was associated with a decrease in the BoNT target SNAP25 and an increase in the proteolysis marker ATROGIN1. Furthermore, hyperactivation of the autophagic-lysosomal system was induced following repetitive BoNT treatments. These results indicate that BoNT did not impair myogenic differentiation or fibroblast collagen secretion when administered on cells from young patients with CP, but it affected NMJs, by increasing axonal swelling and fragmentation. Hyperactivation of autophagic-lysosomal system after multiple BoNT administrations highlights an underestimated pathway contributing to protein degradation and affecting vesicle trafficking. Future studies are needed to determine which are the neural and muscle targets of BoNT induced impairment.

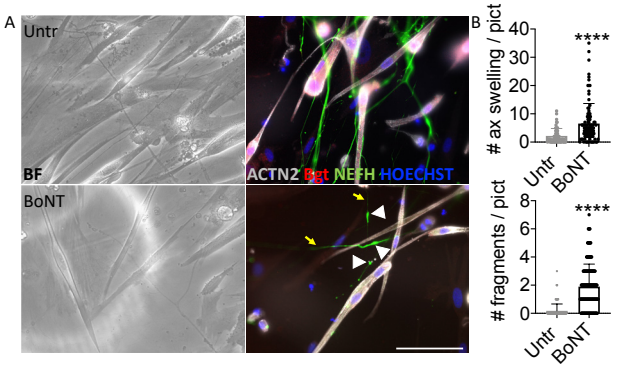

Figure 1: (**A**) Brightfield (BF) and immunostaining images of representative autologous NMJs highlighted by colocalization of α-Bgt+ areas (corresponding to Acetyl Choline Receptors; red) present on α−Sarcomeric Actinin myotubes (ACTN2+; grey) and Neurofilament H neurites (NEFH+; green) in absence (Untr) or presence of 20 IU/ mL BoNT (BoNT). Nuclei were counterstained with HOECHST (blue). Examples of axonal swelling (white arrowheads) and axonal fragmentation (yellow arrows) are reported. Scale bar = 50 µm. (**B**) Quantification of the total number of axonal swellings and NMJ fragments per picture was performed for a total of more than 60 pictures for each of the three different cell lines used. Data were representative of three independent experiments and values were expressed as mean ± SD. Significance of the differences was analyzed by t-test and expressed as ****p<0.0001 of 20 IU/ mL BoNT treated vs Untr NMJs.

ACKNOWLEDGEMENTS

DC was supported by Fund for Translational Biomedical Research (FTBO) 2019 and the project by an internal KU Leuven grant (C24/18/103) and by Scientific Research Flanders (FWO; G0B4619N).

REFERENCES

[1] Fortuna et al., 2015; *J Biochem* **48**(10): 1700-6.
[2] Valentine et al., 2016; *Muscle Nerve*; **53**(3): 407-14.
[3] Barber et al., 2013; *J Child Orthop*; **7**(5): 425-33.
[4] Schroeder et al., 2009; *Mov Disord*; **24**(10): 1494-1503.
[5] Zanotti et al., 2018; Toxicol In Vitro; **50**: 124-136.

Myofibril shearing in skeletal muscle at long lengths

Jarrod C. Petersen, John G. Capano, & Thomas J. Roberts
Department of Ecology, Evolution, and Organismal Biology, Brown University, Providence, RI, United States
corresponding author: jarrod_petersen@brown.edu

INTRODUCTION

Boa constrictor is a sit-and-wait ambush predator well adapted to large prey ingestion, a behaviour that distends the body wall extensively [1-2]. The costocutaneous inferior (CCI) muscle, a primary muscle for rectilinear locomotion that is only a single muscle fiber thick, spans the body wall and allows the snake to move to safety following prey ingestion. Recruitment of body wall muscles following their distention from a large prey bolus may be at odds with the fundamental mechanics of vertebrate skeletal muscle by acting to lengthen the CCI muscle beyond lengths where active force production should be possible [3-4].

The present study sought to (1) characterize the *in-vitro* force-length relationship of the CCI muscle with isolated muscle preparations and (2) investigate muscle ultrastructure with transmission electron microscopy (TEM). We show that the CCI muscle is capable of active force production over a 4-fold range of lengths and that adjacent myofibrils shear at the longest lengths tested. We speculate that at long lengths, myofibril shearing functions to maintain myofilament overlap.

METHODS

One to three CCI muscles were dissected out from 10 *Boa constrictor*. Muscles were placed in a bath of oxygenated physiological Ringer's solution and attached to a rigid clamp and muscle ergometer. Field stimulation was used to elicit maximal isometric contractions across a series of lengths while increasing length until the muscle tore. Notably, there was a loss in force of ~70% P_0 following the first contraction of the CCI muscle that was likely due to the difficulties associated with stimulating the dual twitch and tonic fibers of the muscle. All force measurements were taken following this decline. Samples for TEM were processed using published methods [5].

RESULTS AND DISCUSSION

Analysis of the CCI muscle *in-vitro* reveals an atypical active force-length relationship (Fig. 1A). As vertebrate skeletal muscle has a well-defined relationship between active force and sarcomere length, it is striking that our data suggests that active force only increases with increasing muscle lengths (Fig. 1A) [3-4]. It is possible that due to stimulation difficulties, this data does not represent the full shape of the active force-length relationship of the CCI muscle and primarily provides evidence of active force production over a 4-fold range of muscle lengths. This broad active force-length relationship may be further explained at shorter lengths by myosin passing through the z-disk of neighbouring sarcomeres (yellow in Fig. 1B) [6].

TEM imaging of CCI muscle ultrastructure reveals myofibril shearing at long lengths, but not short lengths, a similar result to another highly extensible muscle in snakes (Fig. 1B) [5].

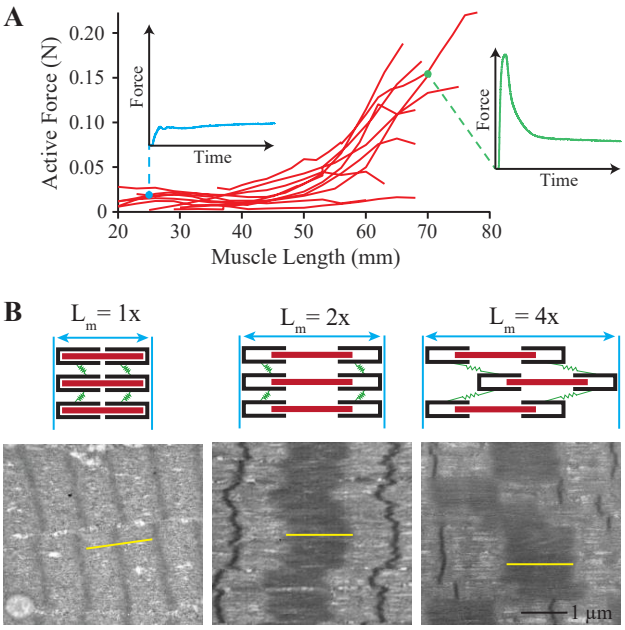

Figure 1: (**A**) Active length tension curves of CCI muscles are plotted with insets of active force profiles over time at short and long muscle lengths above (**B**) theoretical schematics of myofibril shearing placing tension on intermediate filament springs (green) with TEM images where the myosin length is represented by a yellow line (1.45µm).

Filaments between adjacent myofibrils, termed intermediate filaments (green in Fig. 2B), may allow myofibrils that do not extend the full length of a fiber to shear [7-8]. Taken together, these results lead us to speculate that CCI muscle lengthening is accommodated in part by shearing between adjacent myofibrils via elastic intermediate filaments.

ACKNOWLEDGEMENTS

We are grateful to Bruce Jayne, Richard Marsh, Alexander Wilde, Lucy Campbell, Yoshi Yajima, Christopher Anderson, and Geoff Williams for their comments and assistance with the study. This work was supported by NSF Grant (1832795).

REFERENCES

[1] Secor S et al. (1994). *Am. J. Physiol.* **266**: 695-705.
[2] Gans, C. (1961). *Am. Zool.* **1**:217-227.
[3] Ramsey R & Street S. (1940). *J. Comp. Physiol.* **15**: 11-34.
[4] Gordon A et al. (1966). *J. Physiol.* **184**: 170-192.
[5] Close M et al. (2014) *J. Exp. Biol.* **217**: 2445-2448.
[6] Tomalka A et al. (2022) *J. R. Soc. Interface* **19**: 20220642.
[7] Wagner O et al. (2007) *J. Exp. Biol.* **313**: 2228-2235.
[8] Wang K & Ramirez-Mitchell R. (1983) *J. Cell. Biol.* **96**: 562-570

Segmental Elongation of Titin Elastic Elements in Fluorescently Labelled Sarcomeres During Stretching

[1]**Armaan Sekhon**, [2]Walter Herzog
[1]Department of Biomedical Engineering, Schulich School of Engineering, University of Calgary, Calgary, AB, Canada
[2]Faculty of Kinesiology, The University of Calgary, Calgary, AB, Canada
corresponding author: armaan.sekhon@ucalgary.ca

INTRODUCTION

Myofibrils are subcellular organelles made of sarcomeres that are responsible for contraction in muscles. Contemporary sliding filament and cross bridge theories provide convincing explanations for traditional contractions, but struggle to mechanistically explain other phenomena in muscles. These include history-dependent properties like residual force enhancement, which occurs when muscles are eccentrically stretched during contraction, and counter-intuitively produce elevated tension compared to purely isometric contractions at identical lengths [1].

Titin is a filamentous protein in sarcomeres that demonstrates involvement in passive sarcomere stretching. However, titin's contribution to activated sarcomere dynamics is multifaceted. Observations indicate that titin may modulate its elastic stiffness by changing its inherent material properties, primarily through calcium binding and concurrent phosphorylation, or by shortening its extensible regions through transient electrostatic interactions with adjacent filaments. These adaptable spring properties may explain titin's involvement during eccentric contractions, and account for unusual forces encountered during residual force enhancement [2].

We propose using an immunofluorescent antibody system to delineate titin into segments and monitor displacement of segments relative to one another during micromanipulation of myofibrils in passively and actively stretched conditions. Therefore, we will investigate if certain domains have transient interactions with adjacent filaments or differential folding mechanisms.

METHODS

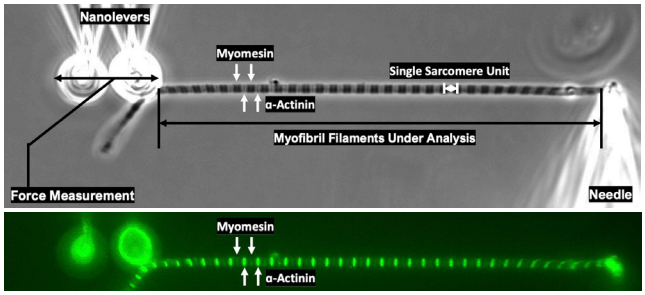

Figure 1: Myofibrils observed under phase contrast and FITC-filtered fluorescence microscopy. Optical resolution at 80x magnification is 65 nm/pixel.

Myofibrils from New Zealand White rabbits will be incubated with site-specific myomesin, α-actinin, or titin primary antibodies, followed by AlexaFluor488 secondary antibodies (Figure 1). Myofibrils will be suspended between a needle and cantilevers in relaxing solution on a chamber mounted to an Olympus IX83 microscope. They will be stretched passively or actively to monitor displacement of titin markers relative to structural bearings.

RESULTS AND DISCUSSION

Preliminary experiments indicate that timescales of maximum tension development and signal intensity for labelled myofibrils scale with concentrations of antibodies introduced. Introduction of labels at sufficiently limited concentrations do not influence passive or active stress in myofibrils to a statistically significant degree. In passively stretched conditions, stresses are 66 ± 22 and 60 ± 23 nN/μm^2 between control and labelled conditions (Figure 2). Histograms illustrating the distribution of individual sarcomere lengths during resting positions or actively and passively stretched positions are comparable although standard deviation of individual SLs decreased by 39% and 24% in relaxed positions and passively stretched positions.

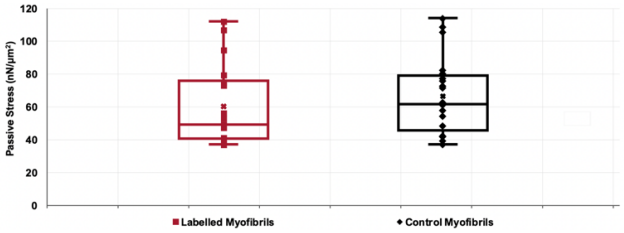

Figure 2: Passive stress produced by myofibrils in labelled and control conditions following passive stretching from average sarcomere lengths of 2.55 μm to 3.15 μm.

Following titin labelling, we expect proximal and distal lengths to behave differently in passive and actively stretched conditions. In passively stretched conditions, proximal and distal segments will linearly lengthen until 3.5 μm when Ig and PEVK domains have unfolded. In actively stretched conditions, proximal segment marker displacement will be measurably limited due to interaction with adjacent actin filaments, rendering proximal segments inextensible.

ACKNOWLEDGEMENTS

This research was funded by the Canadian Institutes of Health Research, the Natural Sciences and Engineering Research Council of Canada, the Canada Research Chairs Programme, and the Killam Trusts. This work was performed in part at the Cornell NanoScale Facility, an NNCI member supported by NSF Grant NNCI-2025233.

REFERENCES

[1] Edman KA et al. (1982). *J. Gen. Physiol.*, **80**: 769-784.
[2] Herzog W. (2018). *Biophys. Rev.*, **10(4):** 1187-1199.

Session 3:
In vivo Animal Muscle Function

Douglas Swank

Ethan Wold

Eng-Kuan Moo

Sebastiaan Dalle

Neda Khaledi

Stephanie Ross

Chairperson: Venus Joumaa

The myosin essential light chain is not essential for muscle function

[1]Bernadette Glasheen, [1]Emily Dunn, [1]**Douglas M. Swank**
[1]Departments of Biological Sciences & Biomedical Engineering
Rensselaer Polytechnic Institute, Troy, NY, USA
Corresponding Author: swankd@rpi.edu

INTRODUCTION

Myosin, the molecular motor of muscle, is composed of two identical heavy chains and two different light chains, the essential light chain (*Mlc1*) and the regulatory light chain. The light chains are part of the myosin lever arm, which is critical for generating force and motion. *Drosophila* has a single *Mlc1* gene that is alternatively spliced into two isoforms. We created a *Drosophila* null for *Mlc1* to investigate the function of these Mlc1 isoforms on muscle mechanical properties, such as stretch activation and enabling the fastest known frequency of muscle contraction.

METHODS

The CRISPR/Cas9 system was used to generate three *Mlc1* null lines, $Mlc1^{29*}$, $Mlc1^{84*}$, and $Mlc1^{85*}$. Each contains a stop codon in exon 3 of the *Mlc1* gene at amino acids 29, 84, and 85, respectively. An Mlc1 rescue line was created by transgenically expressing a 4.099 kb DNA fragment containing the genomic locus of *Mlc1* with 5' and 3' UTR and crossing this gene into the $Mlc1^{84*}$null background. All lines were assayed for percent hatched, pupariated and eclosed. Larval locomotion was assayed by filming the larvae on agar plates and computing time active and crawling velocities.

Adult flies were assays for flight and jump velocity. IFM fibres were isolated from adult flies, permeabilized, calcium activated on a muscle mechanics apparatus, and power production was measured.

RESULTS AND DISCUSSION

To our surprise, we found that *Mlc1* homozygous null animals hatched, crawled and molted. Sequencing confirmed that we had targeted *Mlc1*. *Mlc1* null larvae crawling velocity was reduced by ~50% compared to wild-type and the rescue line (Figure 1). Approximately 50% of *Mlc1* larvae pupariate, of these at least 50% progress through metamorphosis, but only 8% eclose and survive to adulthood. Fiber level IFM and TDT muscle structure appeared normal in *Mlc1* null adults, but they were unable to fly or jump. Permeabilized IFM fibers isolated from 1- or 3-day old null flies did not activate or produce power (Figure 2). The rescue line restored adult viability, crawling velocity, and IFM power production to wild-type levels. We are currently performing experiments to determine if another protein is replacing Mlc1 on the myosin lever arm in the null line. We conclude that *Mlc1* is not essential for embryonic and larval muscle development and function but is required for IFM force and power production.

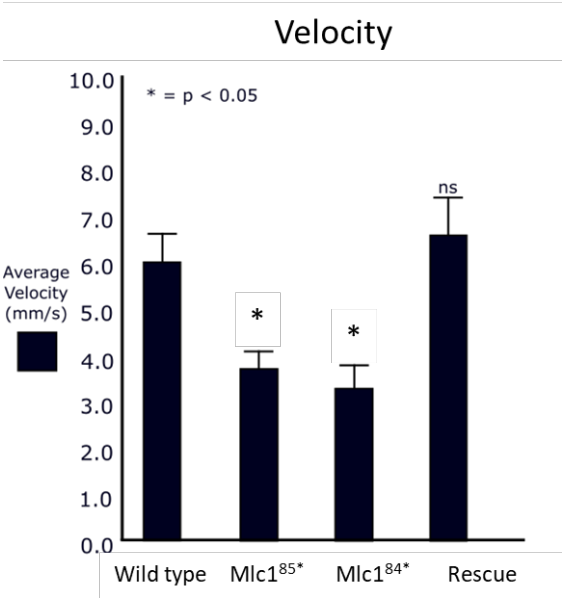

Figure 1: Mlc1 null larval crawling velocity was reduced by about 50% compared to rescue line and wild-type larvae.

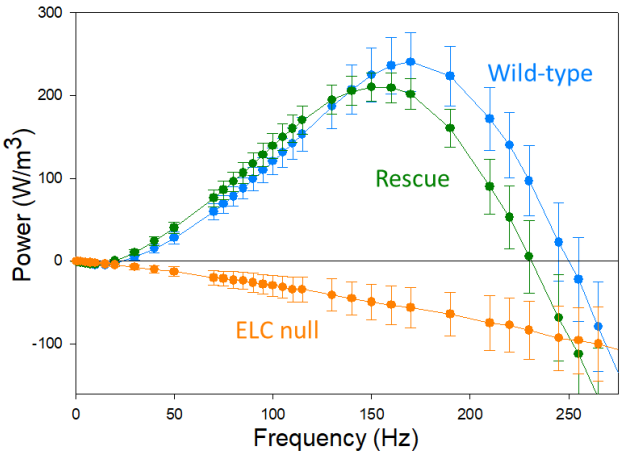

Figure 2: IFM fibres from *Mlc1* null lines were unable to generated power while the fibers from the rescue line produced similar amounts of power as wild-type fibres. Power production was measured by subjecting permeabilized IFM fibres to small muscle length amplitude sinusoidal oscillations over a range of frequencies.

ACKNOWLEDGEMENTS

This work was supported by NIAMS R01 grant AR064274 to D.M.S.

A model of asynchronous flight muscle explains emergent dynamics of flapping insects

[1]**Ethan S. Wold**, [2]James Lynch, [2]Nicholas Gravish, [1]Simon Sponberg
[1]Schools of Biological Sciences and Physics, Georgia Institute of Technology, Atlanta, GA, United States
[2]Department of Mechanical and Aerospace Engineering, University of California – San Diego, San Diego, CA, United States
corresponding author: ewold3@gatech.edu

INTRODUCTION

Many insects such as flies and bees have evolved asynchronous flight muscle, allowing them to flap at frequencies that exceed intrinsic neuromuscular speed limits. Asynchronous muscle functions by virtue of a property known as delayed stretch-activation (dSA) which causes active force to be developed in response to rapid stretch, as opposed to neural drive [1]. Since their wingbeat frequencies are not prescribed by the nervous system, it is thought that asynchronous insects must flap at their natural frequency of vibration. However, it remains unknown how stretch-activated muscles contribute to resonance when coupled to an insect's elastic body and wings. We develop a model of an asynchronous flapping insect parameterized by the time course and magnitude of the physiological dSA response. We demonstrate the model's ability to predict several emergent properties of bumblebee flight, including supra-resonant wingbeats, adaptation to modified wing inertia, and rapid collision response.

METHODS

dSA is characterized in experiment by measuring its response to a step change in length. In response to a rapid stretch, asynchronous muscle generates a force transient that is well-fit by a sum of two exponentials with rate constants r_3 and r_4 and a peak force F_a. We can generalize from a muscle's measured step-response [2], arriving at a set of coupled nonlinear differential equations that describe oscillations of the insect's wingbeat angle (ϕ) and muscle force (f_m) respectively.

$$I\ddot{\phi} + \Gamma\dot{\phi}|\dot{\phi}| + \frac{k}{T^2}\phi = \frac{\mu F_a}{T} f_m \qquad (1)$$

$$\dddot{f_m} + (r_3 - r_4)\ddot{f_m} + r_3 r_4 \dot{f_m} = -\frac{r_3 r_4 \dot{\phi}}{LT} \qquad (2)$$

Eq. 1 models the insect's body mechanics as a lumped-parameter spring-mass system with wing inertia I, thoracic stiffness k, transmission ratio T, and aerodynamic damping coefficient Γ. Eq. 2 captures the stretch dependent muscle oscillations that would be produced by two antagonistic asynchronous muscles. Eq. 2 is parameterized by the time course and magnitude of the dSA transient, as well as the rest muscle length L. The model has one free parameter, μ, which can be set by matching the amplitude of output oscillations to known *in-vivo* wing stroke amplitude in an insect of interest.

RESULTS AND DISCUSSION

Wingbeats from our model emerge at a range of frequencies that equal or exceed the natural vibration frequency of the insect. Estimates of bumblebee natural frequency and dSA parameters result in an emergent frequency close to that observed during free flight. Modification of wing inertia results in an immediate adjustment in wingbeat frequency mimicking results from classic wing-clipping experiments [3]. We demonstrate near instantaneous adaptation of wingbeats to collision in simulation, similar to observations of arrested wingbeats in freely flapping bumblebees. Finally, we build an asynchronously driven robophysical flapper and demonstrate the same emergent behaviour in a physical system.

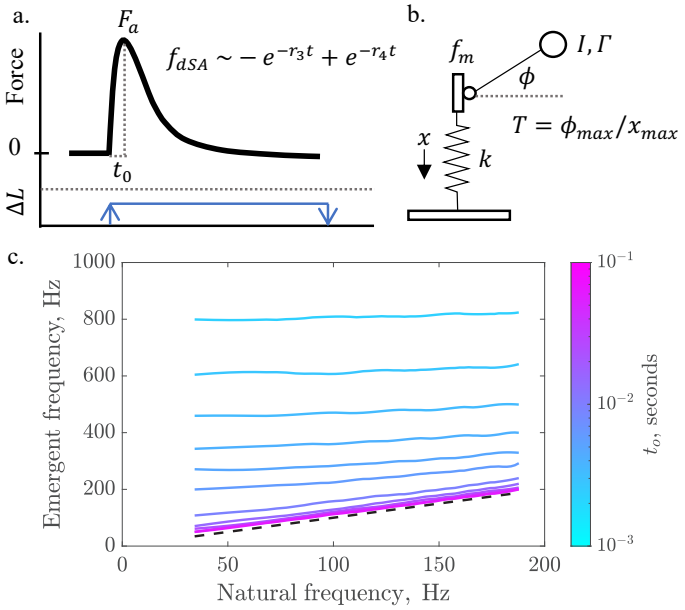

Figure 1: a. Generalized response of an activated asynchronous muscle to a length step. b. Free body diagram of body mechanical model of flapping insect. c. Emergent wingbeat frequency is supra-resonant for very fast dSA rise time and collapses onto the natural frequency equivalence line (dashed) as the dSA rise time slows down.

Our modelling framework establishes a mechanistic link between intrinsic muscle properties and emergent flapping dynamics, and highlights how interactions between muscle stretch-feedback coupled with elastic elements lead to rapid, local control of oscillatory locomotion.

ACKNOWLEDGEMENTS

US National Science Foundation RAISE grant no. IOS-2100858 and 1554790 (MPS-PoLS), the US National Science Foundation PoLS SAVI SRN (GT node grant no. 1205878).

REFERENCES

[1] Josephson et al. (2000), *J. Exp. Biol.*
[2] Lynch, J et al. (2021). *ICRA*.
[3] Greenwalt (1960), *Proc. Am. Philos. Soc*.

THE DEPENDENCE OF FORCE DEPRESSION ON THE TIMING OF ACTIVE SHORTENING

[1,2]**Eng Kuan Moo**, [2]Venus Joumaa, and [2]Walter Herzog[2]
[1] Department of Mechanical and Aerospace Engineering, Carleton University, Ottawa, ON, Canada.
[2] Human Performance Laboratory, University of Calgary, Calgary, AB Canada.
Corresponding author: engkuanmoo@cunet.carleton.ca

INTRODUCTION

Residual force depression (rFD) is the loss of force following shortening of an activated muscle compared to the corresponding isometric contraction at the same final muscle length [1, 2]. In human, muscle contraction at a fixed joint angle is typically accompanied by fascicle shortening due to the compliant nature of the muscle-tendon unit (MTU), thereby causing rFD [3]. However, active shortening of muscle fascicles during fixed-end contraction of MTU occurs instantaneously with muscle activation, which is distinctly different from the classical way of rFD measurement whereby steady-state isometric force is achieved before any active shortening. As the rFD is thought to be caused by stress-induced inhibition of cross bridge formation [4], and is strongly associated with the work done [1], the rFD resulting from activation of compliant MTU may be lower than the classical rFD for the same amount of active shortening due to the rising active force, rather than the steadily high active force, during the early phase of muscle contraction. The purpose of this study was to determine the effect of timing of active shortening on the amount of rFD. We hypothesised that rFD is lower for active shortening that occurs instantaneously with muscle activation than for shortening that occurs following the attainment of steady-state active force.

METHODS

Intact tibialis anterior MTU of 8-10 week-old male C57/BL6 mice (N = 7) was set at resting length of ~10mm, and stretched by 3 mm (L1), 3.5 mm (L2) and 4 mm (L3) by a miniature dynamometer to lengths corresponding to the descending limb of the active force-length curve [5]. The MTU was activated isometrically by electrical stimulation of the sciatic nerve for 1.13s upon reaching the target length. For trials involving active shortening, MTU was stretched by 0.15 mm longer than the target length and activated. Active shortening of 0.15 mm at 0.5 mm/s was applied either instantaneously upon activation (INST) or delayed by 500ms following activation (DELAY). The MTU was allowed to recover at the resting length for 3 min between trials. The average steady-state force following active shortening was compared with that of the reference isometric contraction (ISO, Fig. 1A). The work done during active shortening was also calculated.

RESULTS AND DISCUSSION

MTUs stretched to L1 length had active force comparable to passive force, but the active forces of MTUs stretched to L2 and L3 lengths were lower than the passive force. Under this test protocol, activation-induced muscle shortening was minimised [5]. Force depression of the DELAY group was 5–9 %, and was significantly greater than the 1–5% force depression of the INST group (Fig. 1B). However, the work done during active shortening for the DELAY group was significantly lower than for the INST group at L2 and L3 lengths (Fig. 1C), which is against the general understanding of the positive correlation between work done and rFD [1]. We speculated that the manner in which rFD developed may be altered under high passive force seen at these MTU lengths.

CONCLUSIONS

We concluded that rFD depended on the timing of active shortening. rFD was lower in the INST group than in the DELAY group. However, the driving factor for this behaviour cannot be explained by work done during active shortening.

REFERENCES

[1] Herzog et al. (2000). *J Biomech* **33**: 659-68.
[2] Chen et al. (2019). *J Appl Physiol* **126**: 1066-73.
[3] Raiteri & Hahn (2019). *Acta Physiol* **225**: e13198.
[4] Joumaa et al. (2021). *Int J Mol Sci* **22**: 8526.
[5] Moo et al. (2020). *J Exp Biol* **223**: jeb215020.

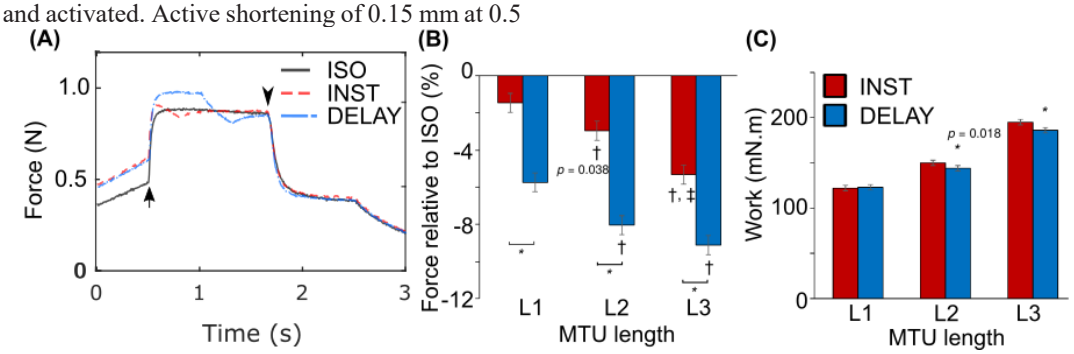

Fig 1: (A) Representative force trace, (B) magnitude of force depression, and (C) work done during active shortening for INST and DELAY conditions. The arrow and the arrowhead denote the start and end of muscle activation, respectively. * indicates statistical difference between INST and DELAY groups. † and ‡ represent statistical difference with L1 and L2, respectively.

The CB1 antagonist rimonabant improves skeletal muscle regeneration via anti-apoptitic mechanisms in mice

[1]**Sebastiaan Dalle**, [1]Moniek Schouten, [1]Monique Ramaekers, [1]Domiziana Costamagna, [1]Katrien Koppo
[1]Exercise Physiology Research Group, Department of Movement Sciences, KU Leuven, Leuven, Belgium
corresponding author: Sebastiaan.dalle@kuleuven.be

INTRODUCTION

Skeletal muscle (SkM) tissue is indispensable for energy metabolism and locomotion. Upon injury, an inflammatory and myogenic interplay is required for complete recovery. In patients and older adults, an imbalance between pro- and anti-inflammatory signaling and an impaired myogenic capacity of (stem) cells result in incomplete SkM recovery. This can result in tissue fibrosis, loss of SkM functionality and, eventually, disability. Therefore, novel targets that improve SkM regeneration are definitely required. It was shown that antagonism of cannabinoid receptor 1 (CB1) reduces fibrosis in heart tissue [1], stimulates *in vitro* myogenic capacity [2] and attenuates inflammation in dystrophic SkM [2], but it was never studied whether it can also improve *in vivo* regeneration of non-dystrophic SkM. Therefore, the present study investigates whether the CB1 antagonist rimonabant improves muscle regeneration upon injury in mice.

METHODS

Mice (n=48) were randomised into 3 conditions: controls (CON; n=16), cardiotoxin (CTX; n=16) and CTX + rimonabant (RIM; n=16). Mice received one saline (CON) or CTX injection (a 30µl injection of 10µM; CTX / RIM) in the *m. Tibialis Anterior*. Half of the CTX-injected mice were daily treated with rimonabant (10mg/kg/d; RIM), whereas the CON group and the other half of the CTX group were treated with vehicle. Within each condition, half of the mice were sacrificed 3 (n=8/condition; 3dpi) or 7 (n=8/condition; 7dpi) days post-injury. Thirty minutes prior to sacrifice, mice were injected with puromycin (0.04µmol/g) to assess muscle protein synthesis. SkM functionality was assessed via grip strength, and SkM was analysed for fibrosis, apoptosis and myogenicity via western blot analyses. A two-way ANOVA analysis (condition*time) with Bonferroni-correction was applied.

RESULTS AND DISCUSSION

The cardiotoxin injury resulted in muscle mass loss, both in CTX (3dpi: -12% & 7dpi: -30%) and RIM (3dpi: -9% & 7dpi: -31%) compared to the non-injured CON group (Fig.1A). Interestingly, the muscle strength loss (5dpi) was more pronounced in CTX than in RIM and CON conditions (Fig.1B). On a molecular level, rimonabant treatment decreased the CTX-induced upregulation of the fibrotic marker collagen (7dpi: -156%; Fig.1C) and of the apoptotic markers cleaved caspase-3 (7dpi: -174%; Fig. 1E), PARP (7dpi: -66%; Fig. 1F) and cleaved PARP (3dpi: -67% & 7dpi: -74%; Fig. 1G). Cardiotoxin increased muscle protein synthesis 7dpi compared to CON, but this was less pronounced in RIM (-19%; $p_{bonferroni}$=0.028; data not shown).

Together, these results indicate that tissue injury was attenuated due to rimonabant treatment. This might explain why lower rates of protein synthesis sufficed to restore muscle tissue in RIM. Finally, the myogenic program was also affected by rimonabant, as the proliferation marker Pax7 was more expressed (3dpi: +120%), whereas the differentiation marker MyoD1 was less expressed (7dpi: -117%) in RIM compared to CTX (Fig.1H, 1I). It remains unclear whether rimonabant treatment stimulated satellite cell proliferation and inhibited satellite cell differentiation, or whether rimonabant-induced molecular changes affected the timing of the myogenic program.

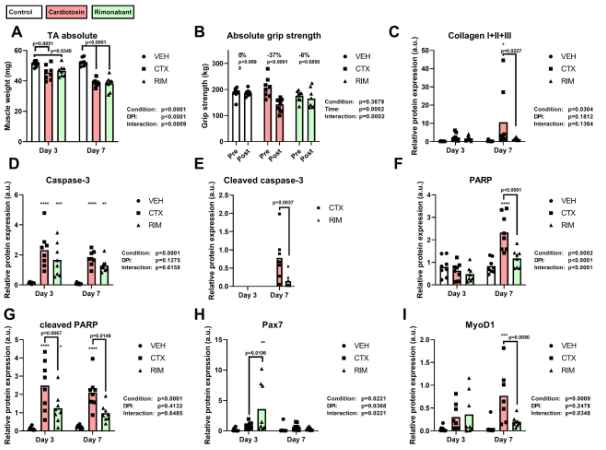

Figure 1: Treatment with the cannabinoid receptor 1 antagonist rimonabant (RIM) attenuates muscle injury-induced muscle strength loss and apoptotic markers. CTX: cardiotoxin condition; RIM: cardiotoxin + rimonabant treatment condition; VEH: non-injured, vehicle treatment condition. *p<0.05, **p<0.01, ***p<0.001, ****p<0.0001 *vs*. CON.

CONCLUSIONS

This study suggests that treatment with the CB1 antagonist rimonabant can be a novel, effective strategy to improve SkM regeneration. This is particularly relevant for older adults or patient populations suffering from impaired regenerative capacity, such as COPD, type 2 diabetes and osteoarthritis. Further (*in vitro*) work should uncover the myogenic adaptations in response to rimonabant treatment.

ACKNOWLEDGEMENTS

Sebastiaan Dalle has received a postdoctoral fellowship (12Z8622N) from Research Foundation Flanders (FWO). This study was funded by FWO (G086823N).

REFERENCES

[1] Rajesh M et al. (2012). *Diabetes*, **61**: 716-727.
[2] Iannotti F et al. (2018. *Nature Comm*, **9**: 3950.

Maternal High-Intensity Exercise and EDL Muscle Metabolic Gene Expression in Male Offspring

[1,2] Neda Khaledi, [2]Hamid Rajabi, [2]Shaghayegh Abbasi, [2]Sahar Torabi, [2]Behnaz Ghiyasi, [2]Sogand Khamse Poor
[1] Faculty of Kinesiology, The University of Calgary, Canada.
[2] Department of Exercise Physiology, Faculty of Physical Education, Kharazmi University, Tehran, Iran.
corresponding author: neda.khaledi@ucalgary.ca

INTRODUCTION

Skeletal muscle is programmable and can 'remember' early-life metabolic stimuli affecting its function in adult life. Skeletal muscle epi-memory in metabolic genes sustained for generation, and metabolic regulators will benefit from maternal exercise. Therefore, exercise during pregnancy can modify skeletal muscle gene expression and transcriptional factors in offspring metabolic genes [1,2]. Peroxisome proliferator-activated receptor gamma (PPARγ) and fibronectin type III domain containing 5(FNDC5) are regulatory metabolic genes that control glucose, lipid metabolism, mitochondrial regulation, and cardiovascular health [3,4]. HIIT-associated increases in the cellular metabolism of skeletal muscle result in fiber-specific responses since Type II fibers with higher recruited thresholds are fully active during HIIT[5].

METHODS

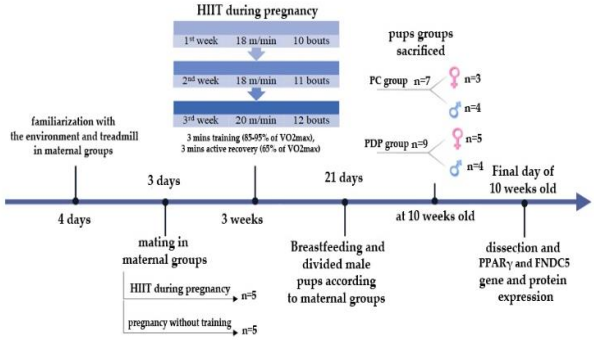

Figure 1: study methodology. Pc: pups of sedentary mother, Pdp: pups of mothers who exercise only during pregnancy.

RESULTS AND DISCUSSION

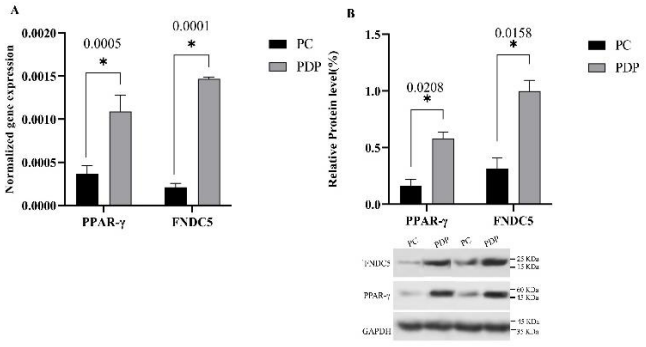

Figure 2: Effect of HIIT on protein (A) and genes (B) expression of PPARγ and FNDC5 in EDL muscle of Maternal exercise and sedentary groups. *P < 0.05.

The results show that HIIT training during pregnancy increased protein and gene expression of PPARγ and FNDC5 in the EDL muscle of the first generation of rats in the maternal exercise group (PDP) compared to the sedentary group (pc) (figure2A&2B). Previously reported that following diet and aerobic exercise interventions, the expression level of PPARγ and FNDC5 pathway elaborated in skeletal muscle and they contributed to energy expenditure-related genes that can promote the expression of genes involved in mitochondrial biogenesis, leading to an increase in the number and function of mitochondria [6]. Also, a study indicated Maternal aerobic exercise upregulated the metabolic gene expressions in fast and slow-twitch skeletal muscle and enhanced the metabolic memory in male offspring [7]. PPARγ has been shown to reduce inflammation and oxidative stress in skeletal muscle cells, following HIIT, which may contribute to improved skeletal muscle metabolic health, and expression reduced after a high-fat diet [8, 9,10]. However, several studies showed that HIIT improves the metabolic health of skeletal muscle through increasing FA oxidation, FA and Glucose uptake, and insulin sensitivity[4]. According to the results, it's likely maternal HIIT training during pregnancy can enhance metabolic regulation and it might increase the skeletal muscle health in the offspring.

ACKNOWLEDGEMENTS

This research was financially supported by Kharazmi University, Iran. We extend our deepest appreciation to Dr.Walter Herzog at the University of Calgary, for his unwavering support in enabling our participation in this conference.

REFERENCES

[1] Sharples, A.P., C.E. Stewart, and R.A. Seaborne, *Does skeletal muscle have an 'epi'-memory? The role of epigenetics in nutritional programming, metabolic disease, aging, and exercise.* Aging Cell, 2016. **15**(4): p. 603-616.
[2] Bheda, P., *Metabolic transcriptional memory.* Mol Metab, 2020. **38**: p. 100955.
[3] Maak, S., et al., *Progress and Challenges in the Biology of FNDC5 and Irisin.* Endocrine Reviews, 2021. **42**(4): p. 436-456.
[4] Ma, C., et al., *Irisin: A New Code Uncover the Relationship of Skeletal Muscle and Cardiovascular Health During Exercise.* Frontiers in Physiology, 2021. **12**.
[5] Ferenc Torma, Zoltan Gombos, Matyas Jokai, Masaki Takeda, Tatsuya Mimura, Zsolt Radak, High-intensity interval training and molecular adaptive response of skeletal muscle, Sports Medicine and Health Science, Volume 1, Issue 1, 2019 Pages 24-32,
[6] Abedpoor, N., Taghian, F., Ghaedi, K. et al. PPARγ/Pgc-1α-Fndc5 pathway up-regulation in gastrocnemius and heart muscle of exercised branched chain amino acid diet-fed mice. Nutr Metab (Lond) 15, 59 (2018). https://doi.org/10.1186/s12986-018-0298-3
[7] Beyhaghi, S., N. Khaledi, and H. Askari, *The aerobic maternal exercise increases PDK4 gene expression in slow and fast twitch muscles of rat male offspring.* Research in Sport Medicine & Technology, 2022. **20**(23): p. 13-23.
[8] Sparks, L.M., et al., *A high-fat diet coordinately downregulates genes required for mitochondrial oxidative phosphorylation in skeletal muscle.* Diabetes, 2005. **54**(7): p. 1926-33.
[9] Vidal-Puig, A., et al., *Regulation of PPAR gamma gene expression by nutrition and obesity in rodents.* J Clin Invest, 1996. **97**(11): p. 2553-61.
[10] Ferenc Torma, Zoltan Gombos, Matyas Jokai, Masaki Takeda, Tatsuya Mimura, Zsolt Radak,High intensity interval training and molecular adaptive response of skeletal muscle, Sports Medicine and Health Science,Volume 1, Issue 1, 2019, Pages 24-32, ISSN 2666-3376, https://doi.org/10.1016/j.smhs.2019.08.003.

Aponeurosis, tendon, and muscle belly length changes during in situ cyclic contractions

Stephanie A. Ross, Christine Waters-Banker, Andrew Sawatsky, Timothy R. Leonard, Walter Herzog
Faculty of Kinesiology, The University of Calgary, Calgary, AB, Canada
corresponding author: stephanie.ross1@ucalgary.ca

INTRODUCTION

Aponeuroses are thin sheet-like layers of elastic tissue that connect to and cover the surface of skeletal muscle. While aponeurosis is structurally a continuation of tendon and shares much of the same tissue properties, its role in muscle contraction and energetics is less clear. Early studies of aponeurosis behaviour considered it to be mechanically in series with both muscle and tendon [e.g. 1]. If this were true, aponeurosis would behave similarly to tendon and would act like a spring and stretch to store energy when force is applied and shorten to return energy when force is removed. However, studies examining aponeurosis behaviour *in vivo* have shown that its behaviour is likely much more complex. Most recently, measures of medial gastrocnemius aponeurosis in sheep during walking showed that aponeurosis length change is largely uncoupled from muscle forces in that it undergoes minimal stretch when force is high [2]. While this directly contrasts what would be expected of tendon, the study did not report tendon length changes, so it is not known how aponeurosis behaviour differs from that of tendon. To address this gap, in this study we examined the behaviour of intact aponeurosis and tendon of the medial gastrocnemius simultaneously in rabbits *in situ* during cyclic contractions.

METHODS

We tested 11 mature New Zealand White rabbits. While animals were deeply anaesthetized, we isolated the medial gastrocnemius and its tendon from surrounding tissue. We measured muscle belly and superficial aponeurosis length during contraction via sonomicrometry and attached a bipolar nerve cuff around the tibial nerve to stimulate the muscle. Then, we cut the calcaneus and attached it to a muscle motor which imposed length changes and measured forces of the muscle-tendon unit. We examined concentric and eccentric cyclic contractions across the plateau region of the force-length relationship. Tendon length change was calculated as the difference between the motor and muscle belly displacements.

RESULTS AND DISCUSSION

Preliminary results from three rabbits show that tendon behaviour followed an expected course, in that it was at its longest length when the force was high and then recoiled as the force decreased (Figure 1). Although there was variability in aponeurosis behaviour in the three rabbits, we found that aponeurosis did not follow the same pattern of length change as the tendon and appeared to be uncoupled from the forces, consistent with measures of aponeurosis *in vivo* in sheep [2]. These findings provide evidence that, while aponeurosis may be structurally in series with tendon, its mechanical loading and resulting behaviour is likely much more complex during contraction.

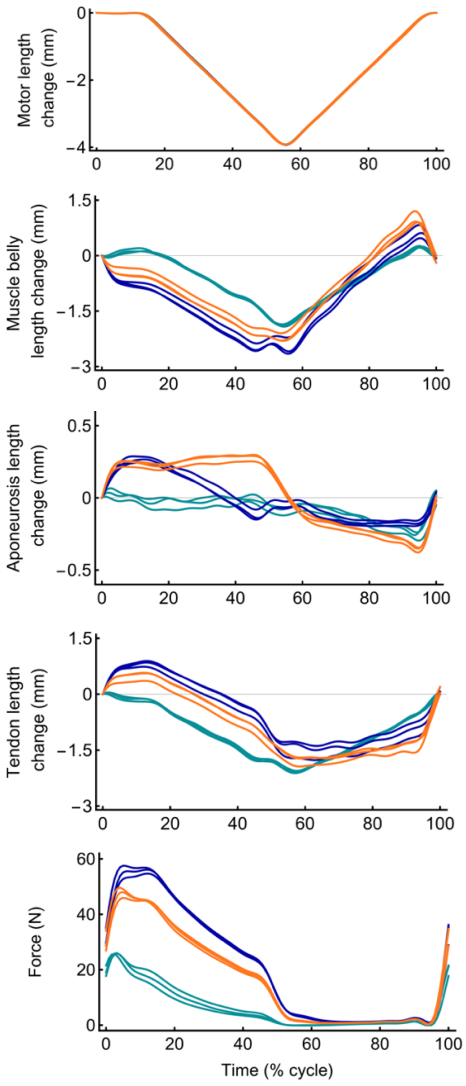

Figure 1: Muscle belly, superficial aponeurosis, and tendon length change relative to the start of shortening for cycles 2-4 of 5 repeated cyclic concentric contractions. Each colour corresponds to a different rabbit.

REFERENCES

[1] Magnusson SP et al. (2003). *Acta Physiol Scand*, **177**: 185-195.
[2] Bossuyt FM et al. (2023). *J Biomech*, **147**: 111430.

ACKNOWLEDGEMENTS

This work was supported by an NSERC Discovery Grant, the Canada Research Chair Program, and the Killam Foundation to WH, as well as a Banting Postdoctoral Fellowship to SAR.

Session 4:
In vivo Human Muscle Function

Rick Lieber

Sriram Muralidhar

Tim van der Zee

Sebastian Bohm

Jared Fletcher

Chairperson: Stephanie Ross

Direct Intraoperative Length-Tension Measurements of Human Gracilis Muscle

[1]Ben I. Binder-Markey, [2]Lomas S. Persad, [2]Alexander Y. Shin, [2]William Litchy, [2]Kenton R. Kaufman, and [3,4]**Richard L. Lieber**
[1]Drexel University, Phila., PA, [2]Mayo Clinic, Rochester, MN, [3]Shirley Ryan Ability Lab, [4]Hines VA Medical Center, Chicago, IL
Presenting Author: rlieber@sralab.org

INTRODUCTION

Understanding and quantifying human muscle structure and function relationships are critical to predicting muscle performance. Unfortunately, direct measurement of human muscle properties is extremely rare and thus relationships obtained from animal muscles are simply extrapolated to human sizes. However, human muscle is orders of magnitude larger than the animals (mice, rats, rabbits and cats) from which these relationships were established [1]. Thus, the same scaling assumptions may not apply to human muscles. To address this gap in understanding, the current study directly measured human gracilis muscle function during a free functioning gracilis muscle transfer used to restore elbow flexion (i.e., the biceps brachii) after complete avulsion of the brachial plexus. During this complex surgical procedure, muscle structural and functional properties were measured to determine the validity of using standard scaling rules obtained from small animals on human muscles.

METHODS

With IRB approval, 12 subjects were consented and completed the entire experimental protocol. Prior to gracilis muscle harvest, the lower limb was placed in one of four joint configurations (JC1 to JC4) designed to gradually lengthen the muscle through its anatomical range. At each JC, in-situ gracilis muscle-tendon unit length and passive and active tension data were measured [2,3] (Fig. 1A). To measure active tension, the anterior branch of the obturator nerve (Fig. 1A) was stimulated at 20Hz at an intensity corresponding to 50% of combined muscle action potential (CMAP). To quantify maximum muscle force, we measured spatial and temporal summation using twitch forces at 50% and 100% CMAP and tetanic forces at frequencies of 5, 10, 20, and 50 Hz. From these analyses, we determined that the tetanic force of a 20Hz tetanus at 50% CMAP was ~70% of the muscle maximum tetanic tension, all data were corrected for this [2]. Each subject's optimal fiber length was calculated from the excursion determined from their active force vs. muscle length curve's full width at half maximum force [1,2]. After the MTU was excised, it was weighed and the volume measured by photogrammetry and muscle's physiologic cross-sectional area (PCSA) calculated to determine muscle stress and specific tension. Normalized predictions of the whole muscle force-length relationship were created using our subject-specific optimal fiber length and compared to standard predictions using literature values [4]. Data are presented as mean±standard error of the mean (SEM) for 12 subjects.

RESULTS AND DISCUSSION

This is the most complete human muscle physiology data set acquired to date. The active force vs. muscle length relationship demonstrated the expected shape of the active length-tension curve, with average measured maximum active force of 150 N at JC2 and JC3 (Fig 1B). Optimal fiber length calculated from the length-tension curve was 12.9 ± 1.0 cm (Fig 1C), which was significantly shorter than the suggested literature value of ~23 cm [4]. Average specific tension calculated from subject specific PCSA of the gracilis muscle was 171 ± 25 kPa (Fig 1D) which was smaller than the current gold standard specific tension of 225kPa from small mammals [5,6]. However, based on previous animal studies suggesting that mammalian fast fibers generate ~225 kPa and slow fibers generate ~155 kPa, our value of 171 is reasonable [5,6]. This is because the gracilis, a 65% slow muscle, would be expected to generate ~180 kPa of active stress (0.65*155+0.35*225). Predicting the force-length curve based on literature values was unsuccessful with force overestimates of 70% and 65% at the shortest and longest lengths, respectively. However, using subject-specific optimal fiber lengths average error was reduced to ~14%, with a maximum error of 25% at the shortest length (Fig 1E). This novel in-situ measurement of force and length properties of a large human muscle emphasizes the critical need for subject specific values when predicting muscle function and adaptation. Further studies are needed to explore this phenomenon and to determine whether this phenomenon is unique to the gracilis or whether it applies to all large human muscles.

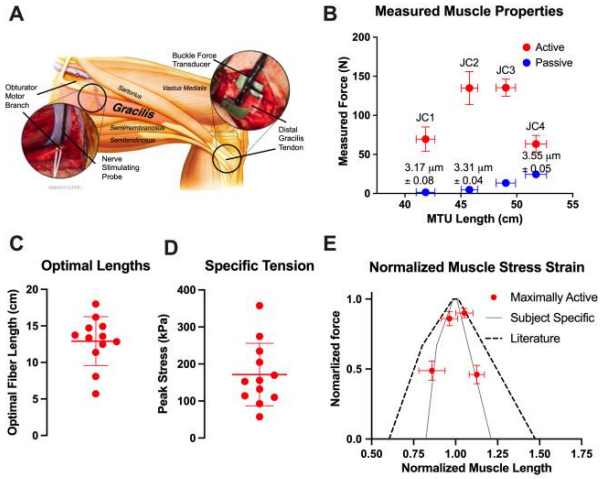

Figure 1: A) Illustration of the gracilis muscle within the thigh and insert image of the buckle force transducer on the distal tendon. B) Intraoperative data collected at each of four joint configurations (JC) in the passive state (blue) and stimulated active state (red) of actual recorded muscle force as a function of measured MTU length with measured passive sarcomere lengths. C) Individual optimal fiber lengths. D) Individual specific tensions. E) Normalized force versus muscle length relationships of the experimental active data (red), and modeled force-length curves using muscle parameters scaled from literature values (dashed black) or each subject's specific values (grey). n=12 mean±standard error for all.

ACKNOWLEDGEMENTS

Supported by VA grants: I01 RX002462 and IK6 RX003351

REFERENCES

[1] Winters *et al.* (2011) *J. Biomech* **44**:109-115; [2] Binder-Markey *et al.* (2023). *J. Phys.* **ePub** (in press); [3] Persad *et al.* (2022). *Sci Rep* **12:**6095; [4] Ward et al. (2009) *Clin. Ortho & Rel. Res.* **467**:1074-82; [5] Close (1972) *Phys. Rev* **52:**129-97; [6] Powell *et al.* (1984) *J. Applied Phys.* **57**: 1715-21

Metabolic Cost for Isometric Force Scales Nonlinearly with Force and Predicts Bilateral Limb Force Sharing

[1]**Sriram S. Muralidhar**, [1]Nadja Marin, [1]Colin Melick, [1]Zhengcan Wang, [1]Aya Alwan, [2]Sam Walcott, [1]Manoj Srinivasan
[1]Department of Mechanical and Aerospace Engineering, The Ohio State University, Columbus, Ohio, USA
[1]Department of Mathematics, Worchester Polytechnic Institute, Worcester, MA, USA
corresponding author: muralidhar.19@osu.edu

INTRODUCTION

Having a muscle metabolic cost model can inform predicting behaviour using metabolic optimization, rehabilitation, fitness interventions, and assistive device design. Previous work on metabolic cost models for isometric tasks did not explicitly seek a nonlinear relation between force level and metabolic cost [1] or only considered electrically or chemically stimulated muscles [2]. To complement such studies, here, we focus on obtaining a power law scaling for how metabolic cost changes with joint torques in a near-isometric task. Additionally, using the torque-based form of the energy rate model we performed predictive optimisation to estimate the left-right limb forces during a bilateral limb force sharing task and estimated the exponents from human experiments, showing that the cost minimized is similar to our metabolic cost model.

METHODS

Metabolic cost of isometric squats. We estimated the metabolic cost of isometric forces via experiments in which human subjects alternated between quiet standing for some time (T_{stand}) and standing with knees bent for some time (T_{bent}), each trial lasting 6-7 mins. Metabolic cost was measured using Oxycon Mobile, body movement with a Vicon T20, and ground reaction forces under each foot with a Bertec instrumented treadmill. Eight subjects (mass 77±11 kg, age 24 ±6 yr, height 1.81±0.05 m, all male) participated with informed consent. Subjects were provided visual feedback to bend their knees to lower their hip to approximately 85-95% of their standing height. Three different {T_{stand},T_{bent}} combinations, namely {15s,5s}, {10s,10s}, {5s,15s}, along with three prescribed knee-bend heights gave nine trials per subject. When the subjects have their knees bent while being still, the muscles are close to isometric. We performed inverse dynamics using a three-segment sagittal plane model to estimate the joint torques versus time for each trial, considering three joints: ankle, knee and hip [5]. We fit the metabolic rate model $\dot{E} = c_0 + c_1(\tau_{ankle}^{\gamma} + \tau_{knee}^{\gamma} + \tau_{hip}^{\gamma})$ by solving for coefficients c_0, c_1 and exponent γ. We could use the same coefficient c_1 for all joints as the torques were linearly correlated.

Bilateral limb force sharing. We performed bilateral limb force sharing experiments in which human subjects produced forces with their two hands or two legs, so as to achieve a goal force via a linear combination of the left and the right force $F_{goal} = \lambda F_{left} + (1 - \lambda) F_{right}$. See also [3,4]. We had upper and lower limb specific setups with the individual limb forces (F_{right}, F_{left}) measured using force plates (Bertec, Vernier). Thirty-three subjects (19M, 14F; height 1.71±0.85m; mass 68.4±6.5 kg; age 22±3.5 yr; all right dominant) participated and each performed 14 trials lasting 3 mins each. We had two different goal force levels and seven different left-right force contributions ($\lambda = \{0.1, 0.3, 0.4, 0.5, 0.7, 0.9, 1\}$). Subjects were told which side contributes more to the output for each trial but not the exact value of λ. We used a single segment-joint sagittal plane model of the limb and hypothesized that humans selected the forces in a manner that a torque-based form of the cost function: $\tau_{left}^{\gamma} + \tau_{right}^{\gamma}$ is minimized. These joint torques are expressed in terms of limb forces (F_{right}, F_{left}) and segment weights. We determined the value of exponent (γ) that best predicted the left and right forces across all trials.

RESULTS AND DISCUSSION

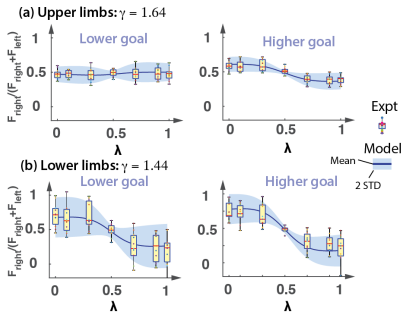

Figure 1: Bilateral force sharing optimum model prediction vs experimental data for both goal force levels and limbs.

From the metabolic measurements of isometric squats, we found that a torque exponent γ = 1.64 best fit the data. That is, metabolic cost scales nonlinearly, specifically, faster than linearly with torque or force. From the force-sharing experiments, we found that a torque γ of around 1.44 (lower limbs) and 1.64 (upper limbs) best explains the force distribution between left and right limbs (Fig 1), suggesting similarity with the metabolic cost model. Taken together, these results suggest a simple model of metabolic cost for isometric force and that this model when optimized may explain force-sharing behaviour at whole limb level. We provide evidence that the same scaling may be relevant at the muscle level: specifically, we show that if muscle cost scaled in this power-law way, the same exponent will be reflected in multi-joint isometric tasks as performed here.

ACKNOWLEDGEMENTS

This work was supported by NIH-R01GM135923-01 and NSF SCH grant 2014506.

REFERENCES

[1] Van der Zee & Kuo. (2021). *J. Exp. Biol*. 224, jeb233965
[2] Crow and Kushmerick. (1982).J.Gen.Physiol. 79, 147-166
[3] Hu et al (2011). Neuroscience letters, 490(2), 121-125.
[4] Skinner and Kuo. (2018) - US Patent 10,099,085.
[5] De Leva, *J Biomech*, 29, 1223-1230, 1996.

Muscle force development dynamics are explained by neither Hill-type nor cross-bridge models

[1]**Tim J. van der Zee**, [1]Arthur D. Kuo
[1]Biomedical Engineering Graduate Program, Faculty of Kinesiology, The University of Calgary, Calgary, AB, Canada
corresponding author: tim.vanderzee@ucalgary.ca

INTRODUCTION

Musculoskeletal simulations rely on models of muscle mechanics that attempt to reproduce the time course of force development. In Hill-type models [1], the temporal dynamics are typically modelled as first-order "activation dynamics" attributed to calcium (Ca^{2+}) transport and binding. In contrast, cross-bridge models [2] treat Ca^{2+} action as fast, and explicitly include a separate rate-limiting set of dynamics for cross-bridge cycling. These differing assumptions have not been reconciled against each other. Here we show that neither Hill-type nor cross-bridge muscle models found in the literature are sufficient to account for experimentally observed dynamics. The Hill-type Ca^{2+} dynamics have been misattributed and are much faster than typically modelled. The cross-bridge dynamics are relatively slower, but still insufficient to explain observed data. We also propose a simple set of intermediate dynamics, not included in most contemporary models, that better capture the relatively slow force development observed empirically. These dynamics integrate well with Ca^{2+} and cross-bridge cycling and may facilitate more mechanistic modelling of energetics.

METHODS

We first identify deficits in both kinds of models. Hill-type activation time constants are typically 10 – 150 ms [1, 3], but actual Ca^{2+} release and binding have long been observed several times faster, even in slow-twitch muscle [4]. In contrast, cross-bridge models classically attribute force development dynamics to cross-bridge cycling, with rate functions fitted to force-velocity. But muscle also have dynamics intermediate to Ca^{2+} and cross-bridge cycling, such as tropomyosin movement and myosin phosphorylation. If such intermediate dynamics are slow, current cross-bridge models fitted to force-velocity should be too fast.

Force development and force-velocity observations might be made compatible with a simple model of intermediate dynamics between Ca^{2+} and cross-bridge cycling. We here propose a model adapted from the distribution-moment cross-bridge model [2] to include first-order intermediate dynamics. We use an activation dynamics formulation like in Hill-type models, but with a small time constant (1 ms) in line with Ca^{2+} data. We fitted steady-state behaviour to match Hill-type force-velocity relations for human quadriceps muscle, and fitted the intermediate dynamics time constant to match force development data in humans.

We compare the proposed model against a Hill-type model, using two types of experimental data. The first is data from previous literature [5], for force development in isometric quadriceps (N = 2) from a single burst of maximal electrical nerve stimulation (8 pulses at 300 Hz). The data show brief forces about 50% of tetanus, which we expect to only be replicated by models with relatively fast activation dynamics.

The second experiment is for cyclic force production [6]. Participants (N = 9) exerted submaximal knee extension torque (~10% of max. torque) against an isometric dynamometer at cyclic frequencies 0.5 – 2.5 Hz, while quadriceps muscle excitation (EMG) and force were recorded/estimated. We expect that only muscle models with slow force development replicate the gain and phase delay of the EMG-force dynamics.

RESULTS

We found that Hill-type activation dynamics cannot simultaneously explain force data in both time- and frequency-domains (see Fig. 1). A fast time constant is needed to match force magnitude data in response to a brief pulse (dark red line, Fig. 1A). A relatively slow time constant greatly underestimates the force (light red line, Fig. 1A), but is needed to reproduce the gain and phase of cyclic force (Fig. 1B). In contrast, the cross-bridge model with intermediate dynamics (fitted time constant = 100 ms) can reproduce both types of data (blue lines, Fig. 1).

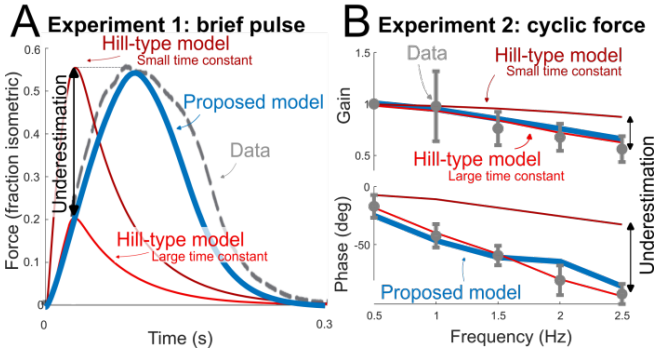

Fig 1: Hill-type model and proposed cross-bridge model predictions vs. data in two types of force development experiments. Hill-type models cannot explain both force pulses and cyclic forces. Data from [5] (panel A) and [6] (panel B).

While neither Hill-type nor traditional cross-bridge model can explain observed data, the addition of a simple set of intermediate dynamics to the cross-bridge model allows to reproduce both force-velocity and force-development data. Further studies are needed to characterize the proposed dynamics in more detail, but a single, empirically-based time constant for intermediate dynamics greatly improves the ability of muscle models to produce realistic forces.

REFERENCES

[1] Zajac FE. (1989) *Crit. Rev. Biomed. Eng.*, **17**: 359-411.
[2] Zahalak GI. (1980). *Math. Biosci.*, **55**: 89-114.
[3] Curtin NA et al. (1998). *J. Exp. Biol.* **201**: 103–114.
[4] Baylor S. (2015). *Sci. Signal.*, **8**: 2005839.
[5] de Ruiter CJ et al. (2004). *J. Appl. Physiol.*, **97**:1693-701.
[6] van der Zee TJ et al. (2021). *J. Exp. Biol.*, **224**: 233965.

Determination of the activation-dependent force-length relationship of the human soleus muscle in vivo

[1]**Sebastian Bohm**, [1]Arno Schroll, [1]Falk Mersmann, [1]Adamantios Arampatzis
[1]Department of Training and Movement Sciences, Humboldt-Universität zu Berlin, Berlin, Germany
corresponding author: sebastian.bohm@hu-berlin.de

INTRODUCTION

Skeletal muscle force-length relationships are commonly determined using maximal activation levels [1]. Yet, in vitro studies have demonstrated a shift in optimal muscle fiber length (L_0) towards longer length with decreasing activation levels [2]. This shift may influence the force generation during dynamic movements with variable activation pattern at a given muscle length [3]. In vivo investigations of the force-length relationship on humans by means of voluntary contractions, however, did not report consistently an activation-dependency for all muscles [4].

The purpose of this study was to investigate a possible activation-dependent shift of L_0 of the human soleus muscle during voluntary contractions and to consider the effect for the individual determination of the activation-dependent force-length relationship.

METHODS

Fifteen participants performed isometric plantar flexion contractions at 100%, 60% and 30% activation level (based on surface electromyography, EMG) each in ten different ankle joint angles on a dynamometer. The calculated Achilles tendon forces (ankle joint moment divided by individual Achilles tendon lever arm) during the contractions and corresponding soleus muscle fascicle length (measured by ultrasonography) were fitted by a 2nd order polynomial fit to determine soleus force-fascicle length curves specific for the three activation levels and to derive the respective L_0. The activation-dependent soleus force-length relationship was then approximated by an interpolation function on the basis of the three activation level-specific force-length curves for each individual and for the group level including all participants, respectively.

RESULTS AND DISCUSSION

The statistical ANOVA showed a main effect of activation level on L_0 ($p<0.001$). With decreasing activation level from 100% to 60% the L_0 increased by 6.5±6.0% ($p<0.001$) and from 60% to 30% by 2.4±2.7% ($p=0.014$, Figure 1). The results demonstrate a moderate, yet individually variable activation-dependent shift of L_0 of the human soleus muscle in vivo. The individual approximation of the activation-dependent force-length relationship showed a high goodness of fit ($R^2=0.913\pm0.056$, Figure 2 for a representative example). A high goodness of fit was also found for the overall approximation including all participants ($R^2=0.857$), indicating that the overall approximation may enables a sufficient representation of the individual variability of the activation-dependency of the force-length relationship.

Implementing the proposed approach and using the measurable variables fascicle length and EMG activity as inputs, allows to consider the activation-dependency of the force-length relationship during dynamic tasks with variable activation pattern.

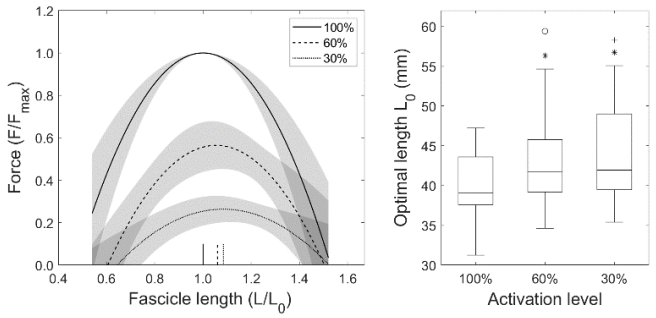

Figure 1: Experimentally-determined force-length relationships of the human soleus muscle in vivo (left, mean±standard deviation, n=15) with an increase in optimal length L_0 at 60% and 30% activation level (right), respectively (° main activation effect, post-hoc difference to *100% and to +60%, $p<0.05$).

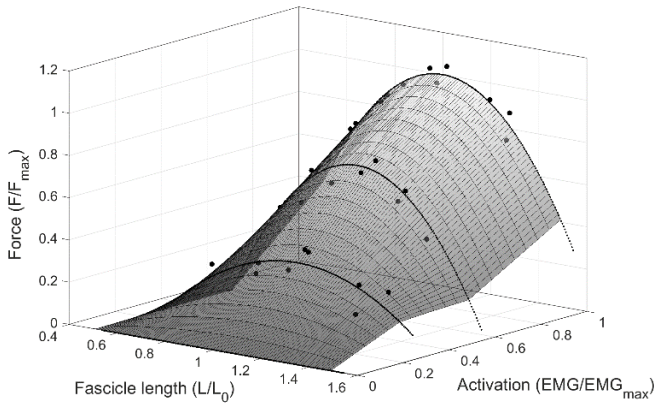

Figure 2: Approximation of the activation-dependent force-length relationship using individual experimental data of fascicle length and EMG activity of one representative participant.

ACKNOWLEDGEMENTS

Funded by the Deutsche Forschungsgemeinschaft (DFG, German Research Foundation) – 513866416.

REFERENCES

[1] Rassier DE et al. (1999). *J. Appl. Physiol.*, **86**: 1445-1457.
[2] Rack PMH & Westbury DR (1969). *J. Physiol.*, **204**: 443-460.
[3] Holt NC & Azizi E (2016). *Proc. Royal Soc. B.*, **283**: 20152832.
[4] Fontana HdB & Herzog W (2016). *Eur. J. Appl. Physiol.*, **116**: 1267-1277.

Relative muscle fascicle length and the energy cost of cyclic contractions

[1]**Jared R Fletcher**, [1]Spencer J Skaper, [1]Jack J Jin, [1]Eric C Bennett, [2]Michael J. Asmussen
[1]Department of Health and Physical Education, Mount Royal University, Calgary, AB, Canada
[2] Department of Biology, Mount Royal University, Calgary, AB, Canada
corresponding author: jfletcher@mtroyal.ca

INTRODUCTION

During locomotion, the plantarflexor muscles appear to operate on the ascending limb of the muscle's maximal force-length relationship [1], producing less force per unit activation and elevating the energy cost (EC) [2] compared to optimal length (L_o), but this has only recently been shown *in vivo* during cyclic force production [3]; EC increased by more than 2-fold at a shorter fascicle length compared to L_o. Confounding these energetic interpretations is that 'short' vs. 'optimal' vs. 'long' muscle lengths is almost exclusively based on a maximally-activated force-length relationship. This does not consider that muscles are typically not maximally activated and the shift in L_o with submaximal force production. Near-infrared spectroscopy (NIRS), during blood flow occlusion, allows the quantification of muscle EC non-invasively and without discomfort [4]. We assessed the impact of relative muscle length on the EC of submaximal cyclic contractions *in vivo*. We also evaluated the extent to which relative muscle length is captured by muscle models by comparing modelled EC to NIRS-derived EC.

METHODS

Using dynamometry and ultrasound imaging, we measured the maximal and submaximal (25,50, 75% of maximal force) force-fascicle length relationships of the right medial gastrocnemius (MG) muscle in 9 healthy male and female participants by altering ankle joint angle. We quantified muscle EC at fascicle lengths ±15% of L_o ($0.85L_o$ and $1.15\ L_o$, respectively). L_o was based on the 50% force-fascicle length relationship. Participants performed 30 submaximal cyclic contractions at $0.85L_o$, L_o, and $1.15L_o$ in a random order, targeting 50% of the maximal force achieved at $0.85L_0$ (Figure 1). EC was quantified from NIRS during blood flow occlusion and EMG quantified MG muscle activation. Model-predicted EC [5] was also estimated from EMG, muscle length, and muscle property data and compared to NIRS-derived EC.

RESULTS AND DISCUSSION

Target force was 54±5% of maximal force at $0.85L_o$, 26±6% at L_o and 28±7% at $1.15L_o$. Mean EC was 36±24% higher at $0.85L_o$ (p=0.005) compared to L_o or $1.15L_o$ (2±27% lower, p=0.81), despite lower forces at $0.85L_o$ (p=0.02), and similar fascicle shortening (p=0.10), and shortening velocity (p=0.52) across lengths. Muscle activation was ~2-fold higher at $0.85L_o$ compared to either L_o or $1.15L_o$ (p=0.001), corresponding to the lower force potential at $0.85L_o$ (r^2=0.54, p<0.0001). The EC per unit activation was similar across lengths (p=0.45), whereas the EC per unit force was significantly higher at $0.85L_o$ compared to L_o and $1.15L_o$ (p=0.008, Figure 2). The modelled EC was 32±48% higher at $0.85L_o$ and 11±27% higher at $1.15\ L_o$ relative to L_o, showing some similarity between experimentally-derived EC for short, but not long muscle lengths. These effects may in part be due to an assumed constant L_o, across activation or forces. Future muscle models should consider if/how activation- and/or force-induced changes in L_o impact EC.

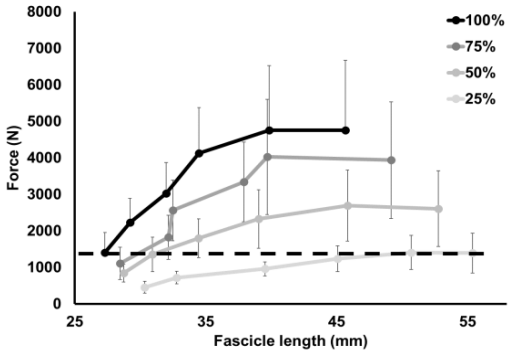

Figure 1: MG Force-fascicle length relationship at 25-50-75-100% force. The dashed line represents the target force at each length.

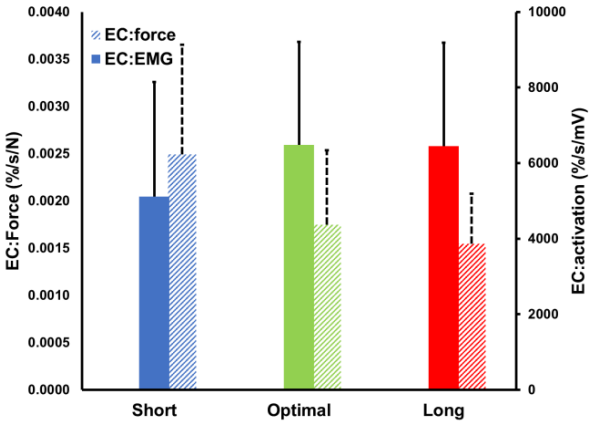

Figure 2: Energy cost per unit activation (solid bars) and energy cost per unit force (hashed bars).

CONCLUSIONS

These results suggest muscle EC is elevated at short lengths because of the need to activate a greater muscle volume and lower economy of force production rather than expending more energy per active muscle volume.

ACKNOWLEDGEMENTS

NSERC (awarded to JRF and MJA) and the Canada Research Chairs program (awarded to MJA) supported this study.

REFERENCES

[1] Bohm S et al. (2019). *Proc Biol Sci*, **286**: 20192560.
[2] Hilber K et al. (2001). *J Physiol,* **531**: 771-770.
[3] Beck ON et al. (2022). *J Appl Physiol,* **133**: 524-533.
[4] Fletcher et al. (2013). *Eur J Appl Physiol,* **113**: 2313-2322.
[5] Umberger et al. (2003). *Comput Methods Biomech Biomed Engin*, **6**: 99-111.

Poster Session 1:

Domiziana Costamagna

Mauricio Delgado

Katrien Koppo

Shuyue Liu

Faizan Syed

Takuya Kobayashi

Hannah Smith

Rana Fayazmilani

Satellite cell *in vitro* differentiation is altered in cells extracted from young children with cerebral palsy

[1, 2]Marlies Corvelyn, [1, 3]**Domiziana Costamagna,** [2]Justine Meirlevede, [4]Robin Duelen, [1]Lauraine Staut, [5, 6]Hannah De Houwer, [5, 6]Anja Van Campenhout, [1]Kaat Desloovere, [2]Maurilio Sampaolesi

[1]Neurorehabilitation Group, Dept. of Rehabilitation Sciences, KU Leuven, Leuven, Belgium; [2]Translational Cardiomyology Lab., Stem Cell and Developmental Biology, Dept. of Development and Regeneration, KU Leuven, Leuven, Belgium; [3]Exercise Physiology Research Group, Dept. of Movement Sciences, KU Leuven, Leuven, Belgium; [4] Cardiology Unit, Dept. of Cardiovascular Sciences, KU Leuven, Leuven Belgium; [5]Dept. of Development and Regeneration, KU Leuven, Leuven, Belgium; [6]Dept. of Orthopaedic Surgery, University Hospitals Leuven, Leuven, Belgium.

Corresponding author: domiziana.costamagna@kuleuven.be

INTRODUCTION

Cerebral palsy (CP) is one of the most common lifelong conditions leading to childhood physical disability, affecting approximately 2 to 3 children in 1000 live births. CP is caused by a neural lesion in the immature brain, leading to progressive musculoskeletal symptoms. Clinically, CP manifests on both neural and muscular level (spasticity, muscle weakness and decreased muscle control), resulting in decreased functional ability such as disturbed gait [1-3]. These patients can be classified following the Gross Motor Function Classification System (GMFCS), from levels I to V, based on their functional abilities [4, 5]. Literature reported muscle alterations of CP patients in comparison to typically developing (TD) children such as fibrotic tissue accumulation, reduced satellite cell (SC) numbers [6-8] and altered SC fusion capacity.

The aim of this study was to further characterise these SC-derived myoblasts in order to gain a deeper knowledge in the CP muscle pathology. The study was structured in two main objectives. The first one was to comprehensively quantify the myotube phenotype that is observed in SC-derived myotubes from young patients with CP in comparison to age-matched TD children and to associate these features with clinical parameters and with the muscle-specificity. The second objective was to exploratively assess gene expression levels to discover potentially involved actors in altered SC-derived cell functioning.

METHODS

Via muscle microbiopsies from young patients with CP (n = 16, aged 3 – 9 years, GMFCS levels I-III) and age-matched TD children (n = 12), SC-derived myoblasts were isolated and assessed for their differentiation features. Moreover, a recently developed semi-automated analysis software [9] allowed a better quantification of myotube morphology and nuclear positioning during SC-derived myoblast differentiation.

RESULTS AND DISCUSSION

Increased myotube diameter and higher number of nucleus clusters in CP- compared to TD-derived myotubes were reported. These nucleus accumulations were wider and less linear in SC-derived myoblasts from children with CP compared to TD children. No associations between these features and the clinical outcome parameters for muscle spasticity and strength were found. Furthermore, preliminary analyses of the expression levels of multiple genes associated with other muscle pathologies in literature, regarding SC differentiation (*PAX7*, *MYOG*, *MyHC1*, *MyHC3*, *ACTN1*, *ACTN2*, *CD82*), fusion (*IGF1*, *HGF*, *NOTCH1*, *ITGB1*, *MYMK*, *MYMX*) and nuclear positioning (*CDC42*, *SYNE1*, *SUN1*, *LMNA*, *MAP7*, *NINEIN*, *PARD6G*) showed no significant differences between SC-derived myotubes from TD and CP children.

In conclusion, the phenotype of SC-derived myotubes extracted from young CP children was further characterised, confirming the involvement of these cells in CP muscle pathology. No alterations of some of the main genes involved in nuclear positioning, fusion or differentiation, point at the complexity of CP. Further research is needed to better explore the heterogeneity within this cell population and elucidate pathophysiological mechanisms related to the altered SC properties observed in CP muscles.

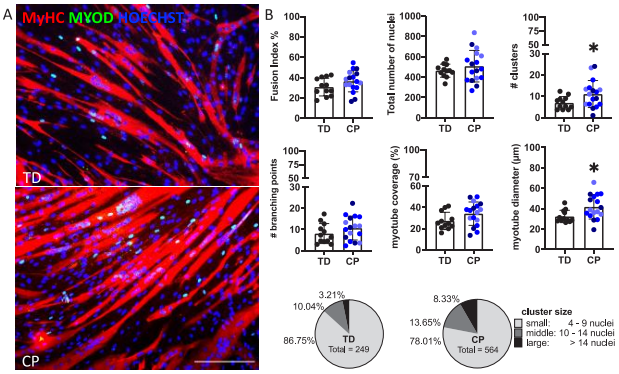

Figure 1: (**A**) Representative immunofluorescence images for SCs after six days of myogenic differentiation from typically developing (TD) children and patients with cerebral palsy (CP) stained with MYOSIN HEAVY CHAIN (MyHC; red), MYOD (green) and nuclei with HOECHST (blue). Scale bar is 200 µm. (**B**) Different parameters from the semi-automated software assessed based on IF images of SCs from TD (n = 12) and CP (n = 17), in which every dot represents an individual included subject. Patients with CP were subcategorized in different GMFCS levels (GMFCS-I: light blue, GMFCS-II: blue, GMFCS-III dark blue). Significance of the differences was calculated with t-test: *p < 0,05 while for pie diagram, representing the nucleus cluster size for TD and CP, was calculated with Chi-Square test: **p < 0,01.

AKNOWLEDGEMENTS

MC was supported by FWO-SB fellowship (1S78421N). The project was funded by a KU Leuven grant (C24/18/103) and by Fund Scientific Research Flanders (G0B4619N).

REFERENCES

[1] Mathewson et al., 2015; *Phys Med Reh Clin N Am*; **26**:57–67.
[2] Romero et al., 2021; *J Pers Med; **11**(11)*.
[3] Howard et al., 2022; *Dev Med Child Neurol*; **64**:289–95.
[4] Palisano et al., 2008; *Dev Med Child Neurol;* **39**:214–23.
[5] Palisano et al., 2008; *Dev Med Child Neurol*; **50**:744–50.
[6] Smith et al., 2013; *Dev Med Child Neurol*; **55**:264–70.
[7] Dayanidhi et al., 2015; *J Orthop Res*; **33**:1039–45.
[8] Von Walden et al., 2018; *Muscle and Nerve*; **58**:277–85.
[9] Noë et al., 2022; *Skelet Muscle*; **12**:12.

Passive force of skinned cardiac papillary muscle in response to dietary-induced obesity during adolescence in rats

[1]**Mauricio Delgado**, [1]Shuyue Liu, [1]Venus Joumaa, and [1]Walter Herzog
[1]Human Performance Laboratory, University of Calgary, Calgary, AB, Canada
corresponding author: mauricio.delgado@ucalgary.ca

INTRODUCTION

The current understanding of obesity is primarily focused on its metabolic implications, but its systemic impact is evident [1]. Obesity has been shown to significantly affect the health of the musculoskeletal system, resulting in a decrease in mobility and the adoption of a sedentary lifestyle [1,2], leading to the development of various musculoskeletal disorders [2].

Obesity is a major risk factor for developing cardiovascular disease [4]. Independent of other common co-morbidities, such as dyslipidemia and hypertension, obesity increases the risk for heart failure by a factor of two [4]. Obesity during childhood also increases the risk of cardiovascular problems in adulthood regardless of corrective behaviors adopted in adulthood [5]. Even though the effects of obesity and increased weight during childhood and adolescence on cardiac function have been frequently studied (6), little is known of the impact of obesity on the mechanical properties of the heart at the cellular level. Increased passive stiffness is an important early indicator of deterioration in cardiac health. An increase in cardiac passive force results in a reduction of diastolic filling and stroke volume, leading to cardiac dysfunction (7). The purpose of this study was to investigate the passive force of isolated skinned cardiac papillary muscle fibre bundles in normally developing hearts and those from animals with dietary-induced obesity in childhood rats.

METHODS

Three-week-old male Sprague–Dawley rats were randomized into a control group (n = 8) fed a standard chow diet, and a dietary-induced obesity group (n = 8) fed a high-fat high-sucrose (HFHS) diet during a 14-week intervention period. Rats were weighed weekly over the course of the intervention.

Following the 14-week intervention period, animals were euthanized and hearts removed and weighed. For mechanical testing, 2-3 thin strips of papillary muscle were skinned at -20°C for three weeks. On the day of experiments, approximately 100-300 µm wide and 1-2 mm long fibre bundles were isolated and attached between a length controller and a force transducer. The sample length was adjusted to an average sarcomere length of 1.8 µm using a He-Ne laser. To determine passive forces, four stress-relaxation tests were performed. The samples were stretched passively from an initial average sarcomere length of 1.8 µm to a final average sarcomere length of 2.0, 2.2, 2.4 or 2.6 µm, and held at this final length for 20 s to allow for stress relaxation. The steady-state passive force reached at the end of the stress-relaxation test was measured and converted to passive stress by normalizing force to the cross-sectional area of the sample assuming a cylindrical shape.

RESULTS AND DISCUSSION

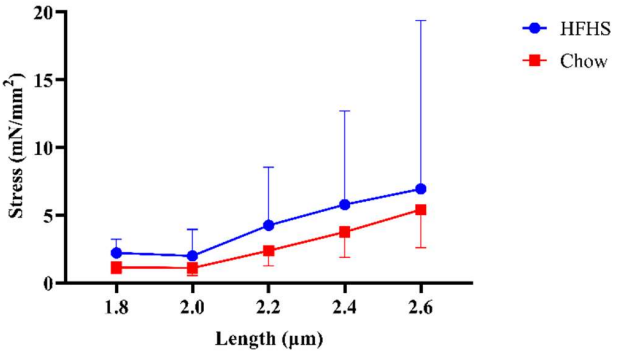

Figure 1: Passive stress of cardiac papillary bundles for control (Chow) and high-fat high sucrose (HFHS) groups. No significant differences were found between groups.

Body mass and heart mass were greater in the HFHS group rats (644 g ± 70; 1.9 g ± 0.3, $p < 0.001$) compared to the control group rats (515 g ± 26; 1.6 g ± 0.3). There was no difference in passive stress between the chow and HFHS diet group rats (Figure 1).

These results are in accordance with previous studies showing that obesity in an adolescent rat model does not affect passive force properties in isolated skinned cardiac trabecular muscle fibre bundles [8]. This result indicates that cardiac diastolic filling is likely not compromised in obese juvenile rats. However, further analysis of the contractile properties of the cardiac cells is required.

ACKNOWLEDGEMENTS

The Canadian Institutes of Health Research (CIHR), the Canada research chair programme, the Nigg Chair for Biomechanics, and the Killam Foundation.

REFERENCES

[1] Teasdale N et al. (2013). *Curr Obes Rep*. **2**: 235-240.
[2] Kortt M et al. (2002). *Aust Health Review*. **25**: 207.
[3] Houmard JA et al. (2011). *J Obes*. 250496: 1-11.
[4] Wong C et al. (2007). *Nat. Rev. Cardiol.* **4**: 436-443.
[5] Franks PW et al, (2010). *N Engl J Med.* **362**: 485-493.
[6] Rowland T. (2007). *JSSM*. **6**, 319-326.
[7] Cuijpers I et al. (2020). *J Cell Mol Med*. **25**: 729–741.
[8] Boldt K et al. (2020). *Appl Physiol Nutr Metab.* **45**: 893-901.

The molecular signature of the peripheral CB1 antagonist AM6545 in muscle, adipose and liver tissue.

Sebastiaan Dalle, Moniek Schouten, Jolien Deboutte, Elsa de Lange, **Katrien Koppo**
Exercise Physiology Research Group, Department of Movement Sciences, KU Leuven, Leuven, Belgium
corresponding author: Katrien.Koppo@kuleuven.be

INTRODUCTION

To date, most research focused on the role of cannabinoid receptor 1 (CB1) in the neural regulation. However, there is a growing interest in the role of CB1 in metabolic tissues, as it was shown in preclinical obesity models that the peripheral CB1 antagonist AM6545 improved features of metabolic health (e.g. insulin sensitivity and substrate metabolism) in muscle, adipose and liver tissue [1]. Furthermore, muscle-specific CB1 knockout prevented genetically- and diet-induced insulin resistance in murine skeletal muscle [2].

Since the signaling events and cellular adaptations upon in vivo CB1 antagonist treatment in metabolic tissues are poorly understood, the present study investigates the activation of different signaling cascades, i.e. protein kinase A (PKA), mitogen-activated protein kinases (MAPK) and Akt-mTOR, in muscle, adipose and liver tissue of mice upon acute treatment with AM6545.

METHODS

Prior to tissue sampling, 12 individually-housed C57BL/6 mice were energy-restricted overnight to standardize molecular responses to AM6545 treatment. In the morning, half of the mice were IP injected with vehicle (VEH) and the other half with AM6545 (10 mg·kg^{-1} BW; AM). Ninety minutes after AM/VEH treatment, mice were sacrificed. The Tibialis Anterior muscle (TA), the epididymal adipose tissue (white adipose tissue; WAT) and liver tissue were analysed for PKA, MAPK and Akt-mTOR signaling using western blot analyses. An unpaired t-test or a Mann–Whitney U test (in case of non-normal distribution) was used to test for significant differences ($p<0.05$).

RESULTS AND DISCUSSION

As CB1 is a G protein-coupled receptor, the adenylyl cyclase-cAMP-PKA axis is expected to be an important downstream path of CB1 inhibition. Whereas cAMP responsive element binding protein 1 (CREB1) phosphorylation remained unaffected in every tissue, a downregulation of PKA phosphorylation in WAT (-53%; p=0.02) was observed in AM vs. VEH.

Acute AM6545 treatment also induced tissue-specific changes in MAPK signaling; i.e. a (borderline) significant increase in p-ERK1 expression in TA (+56%; p=0.05), WAT (+50%; p=0.02) and liver (+51%; p=0.10) and in p-ERK2 in WAT (+67%; p=0.01). There were no differences in the phosphorylation of the MAPKs p38 and JNK between VEH and AM for any of the tissues.

Interestingly, AM6545 treatment increased phosphorylation of certain intermediates of the Akt-mTOR axis; i.e. p-Akt in TA, WAT and liver, p-mTOR in TA and liver, and p-S6rp in liver (Fig. 1). Important roles of the Akt-mTOR pathway include *de novo* lipogenesis, VLDL-triglyceride export and protein synthesis. Indeed, when assessing muscle protein synthesis (MPS) via puromycin incorporation in nascent proteins, a significantly higher (+44%) MPS was observed in AM vs. VEH (Fig. 1). Hence, CB1-induced activation of the Akt-mTOR axis can have therapeutical implications, e.g. improving metabolic health features such as glucose uptake and insulin sensitivity but can also be of interest in conditions of muscle wasting, such as ageing and disease.

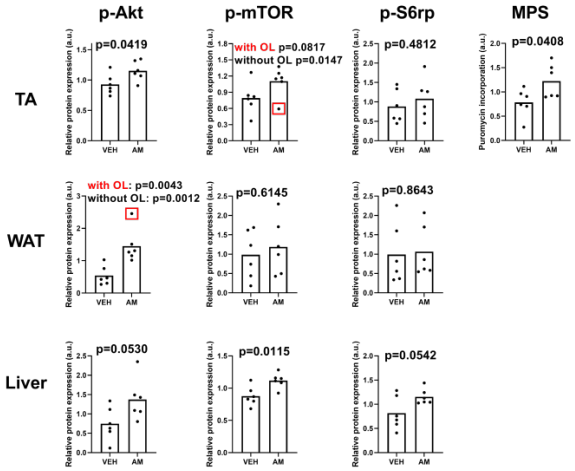

Figure 1: Effects of AM6545 treatment on Akt-mTOR activation in muscle, adipose and liver tissue and on muscle protein synthesis in the TA muscle. Anabolic signaling includes phosphorylation of Akt (p-Akt), mammalian target of rapamycin (p-mTOR), S6 ribosomal protein (p-S6rp) and muscle protein synthesis (MPS). VEH: vehicle; AM: AM6545 treatment.

ACKNOWLEDGEMENTS

Sebastiaan Dalle received a postdoctoral fellowship (12Z8622N) from Research Foundation Flanders (FWO). This study was funded by FWO (G086823N).

REFERENCES

[1] Tam et al. (2010). *J Clin Invest*, **120**: 2953-2966.
[2] Lipina et al. (2016) *Aging Cell*, **15**: 325-335.

Investigating the effect of activation level on residual and passive force enhancement in skinned muscle fibres

[1]**Shuyue Liu**, [1]Ajibola O. Anifowose, [1]Venus Joumaa, [1]Walter Herzog
[1]Faculty of Kinesiology, The University of Calgary, Calgary, AB, Canada
corresponding author: shuyue.liu@ucalgary.ca

INTRODUCTION

Residual force enhancement (rFE) is defined as the increase in steady-state isometric muscle force following active stretch compared to the purely isometric force produced at the same muscle length and level of activation [1]. When a muscle is deactivated following active stretch, the steady-state force after deactivation is often higher than the force following deactivation of the purely isometric contraction. This phenomenon is called passive force enhancement (pFE) [2]. Despite decades of study, the mechanisms underlying rFE and pFE remain unknown. It has been proposed that titin, a giant, spring-like protein in the sarcomere, might be responsible for rFE and pFE by increasing its stiffness during activation and stretch by calcium binding during activation [3], and titin-actin interactions resulting in a decrease in its characteristic length [4].

To elucidate the effect of calcium alone, without its influence on the cross-bridge-based force, on rFE and pFE, Leonard and Herzog [4] used a cross-bridge inhibitor, 2,3-butanedione 2-monoxime, to eliminate normal cross-bridge cycling and actin-myosin-based force when calcium was released during activation in myofibrils. They found that the force produced by an actively stretched myofibril was significantly lower than that obtained during rFE when cross-bridges were not inhibited. This result indicated that titin's stiffness increase through calcium binding alone cannot explain rFE, but that calcium likely influences rFE and pFE by its direct effect on the amount of active force produced by cross-bridges before active stretch.

Therefore, the purpose of this study was to investigate the relationship between the amount of active force production before active stretch and rFE and pFE in single skinned muscle fibres. We hypothesized that rFE and pFE decrease at submaximal compared to maximal activation levels.

METHODS

Single skinned fibres (n=19) from New Zealand White rabbit psoas muscle were tested at submaximal (pCa = 5.8, n = 10), and maximal (pCa = 4.2, n = 9) activation levels. Fibres were set at an average sarcomere length of 2.4 µm and then performed a reference isometric contraction, followed by an active stretch contraction. In the reference contraction, fibres were passively stretched to an average sarcomere length of 3.2 µm and then activated. The steady-state force following activation was recorded as the reference isometric force. Fibres were then deactivated, and the steady-state force following deactivation was recorded as the reference passive force. In the active stretch experiment, fibres were activated at an average sarcomere length of 2.4 µm and then actively stretched to 3.2 µm. The steady-state isometric force following the active stretching was recorded and compared to the reference isometric force to obtain rFE. After deactivation, the passive force was recorded and compared with the reference passive force to calculate pFE. Forces were normalized to the cross-sectional area of the fibres and expressed as stresses (kPa).

RESULTS AND DISCUSSION

The average increase in stress following active stretch compared to the isometric reference contraction was not different between the submaximal and maximal activation protocols (10.3 ± 1.3 kPa, or 11.5 ± 1.7%, vs. 11.7 ± 1.1 kPa or 8.7 ± 0.7 %, respectively (Figure 1). Similarly, the corresponding increase in passive stress after deactivation was not different between activation levels (10.9 ± 1.1 kPa or 24.5 ± 3.5% vs. 15.3 ± 2.6 kPa or 23.3 ± 5.8%, respectively (Figure 1). Interestingly, at the same activation level, absolute rFE and pFE were not significantly different.

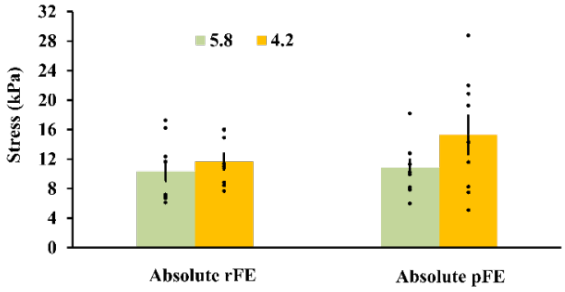

Figure 1: Absolute values of rFE and pFE at submaximal (pCa=5.8, green) and maximal (pCa=4.2, orange) activations levels for all fibres.

In contrast to our hypothesis, the activation level did not affect rFE and pFE. If titin-actin interaction is the main explanation for the rFE and pFE, this result indicates that titin-actin interaction seems independent of the active force produced before active stretch.

Furthermore, our results showed that at the same activation level, there was no difference between rFE and pFE, indicating that rFE can be fully accounted for with pFE suggesting that titin-actin interaction might be the dominant/exclusive contributor to rFE and pFE at long sarcomere lengths.

ACKNOWLEDGEMENTS

NSERC, CIHR, The Killam Foundation, CRCP, NIH.

REFERENCES

[1] Abbot BC & Aubert XM (1952). *J. Physiol.,* **1**: 77-86.
[2] Herzog W & Leonard TR (2002). *J. Exp. Biol.*, **205**: 1275–1283.
[3] Labeit D et al., (2003). *PNAS.*, **100**:23, 13716-13721.
[4] Leonard TR & Herzog W (2010). *Am. J. Physiol.,* **299**:1, C14–20.

Investigating the effect of collagenase on the passive stiffness and total protein content of muscles in children with cerebral palsy

[1]Faizan Syed, [1]Venus Joumaa, [2]Jason Howard, [1]Ruth-Anne Seerattan, [1]Tim Leonard and [1]Walter Herzog
[1]Human Performance Lab, Faculty of Kinesiology, University of Calgary
[2]Nemours Children's Health, Delaware
Faizan.syed1@ucalgary.ca

INTRODUCTION

Cerebral palsy (CP) is a group of debilitating movement and posture disorders that results in pain, muscle stiffness, and a limited range of movement[1]. This restrictive muscle stiffness is suggested to arise from a denser extracellular matrix (ECM) found in affected muscles. Current clinical interventions aim to relieve muscle stiffness and restore some range of motion. One of the two main interventions is injections of botulinum toxin which deprive nerve stimulation to the target muscle resulting in muscle relaxation and contracture relief. However, this temporary effect also results in lasting muscle atrophy, pain, and weakness. Surgical interventions such as tendon or muscle release directly relieve muscle stiffness but are temporary and invasive. Thus, it is vital to identify a long-term treatment that decreases prominent CP-associated muscle stiffness and maintains muscle properties without introducing harmful side effects.

The increased ECM which is suggested to give rise to the muscle stiffness in CP is mostly composed of collagen[1]. Collagenase, which is an enzyme that digests collagen has been previously used to decrease collagen levels in fibrotic diseases such as Dupuytren's and Peyronie's[2,3]. In both treatments, mobility of the affected structures was restored with mild to no side effects[2,3]. However, the use of collagenase to reduce collagen content and consequently muscle stiffness in CP muscles has not been systematically investigated. Thus, the aim of this study was to investigate the effect of collagenase on passive force and protein content of muscle biopsies isolated from children with CP.

METHODS

Muscle biopsies were taken from the adductor longus of 11 patients with CP undergoing tendon release surgery. Fascicles were isolated from these biopsies and subject to mechanical, biochemical and histological testing. The collagenase group consisted of fascicles incubated in collagenase for 2 hours at 37°C.

Fascicles were mounted between the length controller and force transducer of a mechanical testing system[4]. The fascicles were subject to stress-relaxation tests with stretch magnitudes of 1, 2.5, 5 and 7.5% of their initial length, this occurred at a speed of 2% of their initial length per second and was held for 2 minutes. Peak and steady state forces measured were normalized to the cross-sectional area of the fascicles.

To measure collagen content, fascicles were cut and stained using picrosirius staining. Protein content was analyzed using a bicinchoninic acid assay.

RESULTS AND DISCUSSION

After collagenase incubation, relative to control, peak and steady-state stresses decreased by an average of 49.1 ± 16.6% and 46.7 ± 15.5% respectively, across all strains. Furthermore, the Young's modulus decreased by an average of 51.1 ± 5.7%.

There was an average decrease of 12.56 ± 0.53% in collagen content after collagenase incubation, however there was notable variability ranging from 62.7% to -68.4%. There was no significant difference in the total protein content after collagenase incubation relative to control.

The passive force decreased as expected after collagenase incubation, however this was not correlated with the changes seen in collagen content after incubation. It was expected that since a notable portion of the passive force of CP muscles originates from the collagen network, a decreased passive force would have indicated a digested collagen network. However, the variable change in collagen content after collagenase incubation might indicate that the interconnections between collagen fibrils were degraded without the fibrils themselves being degraded. This would result in a decreased passive force without a notable decrease in collagen content.

Overall, the results suggest that collagenase could potentially be used to decrease the passive force and stiffness in CP muscles without impacting their protein content.

The future direction for this study includes investigating the possible impact or lack thereof of collagenase on the active force production and evaluating the effect of collagenase in a hypoxia induced CP animal model.

ACKNOWLEDGEMENTS

NEMOURS CHILDREN'S HEALTH
HPL - Calgary
CIHR IRSC Canadian Institutes of Health Research / Instituts de recherche en santé du Canada

REFERENCES

[1] Howard, J. J., Graham, K., & Shortland, A. P. (2021). *Dev Med & Child Neurol*. **64**(3), 289-295.
[2] Hurst et al., (2009). *N Engl J Med,* **361**(10), 968–979.
[3] Egui Rojo et al., (2014). *Ther Adv Urol*, **6**(5), 192–197.
[4] Joumaa et al., (2012). *J Expl Biol*, **215**(12), 2135-2140.

The effects of microtubule depolymerization on muscular viscoelastic properties.

[1]**Takuya Kobayashi**, [1]Nagomi Kurebayashi, [1]Takashi Murayama, [1]Takashi Sakurai, [2]Motoshi Kaya
[1]Department of Cellular and Molecular Pharmacology, Juntendo University, Tokyo, Japan
[2]Faculty of Physics, The University of Tokyo, Tokyo, Japan
corresponding author: tkoba@juntendo.ac.jp

INTRODUCTION

Skeletal muscles are constantly deforming, yet they retain their motor function and shock-absorbing capacity without breaking down. This special characteristic of skeletal muscle is supported by the viscoelasticity of the muscle cells, which is composed of various structures in skeletal muscle cells and their connections. In this study, we focus on microtubules, which interact with various components in skeletal muscle and are known to have high elasticity themselves [1]. We aimed to quantitatively elucidate the role of microtubules in viscoelasticity of skeletal muscle by measuring deformation stresses and performing structural imaging of skeletal muscle while applying microtubule-depolymerization agents and external loading to skeletal muscle.

METHODS

A simultaneous measurement device equipped with a stepping motor, force sensor, and fluorescence microscope was fabricated (Fig. 1) for simultaneous measurement of contractile force, deformation stress and imaging of muscle structure during external loading to muscle. Mouse extensor digitorum longus (EDL) muscles were used as the measuring samples in this study. Measurements were performed in a Krebs-Ringer solution saturated with 95% oxygen and 5% carbon dioxide, and the sample temperature was kept at 32°C. Microtubule depolymerization conditions were set by perfusion with Krebs-Ringer solution containing 10 μM colchicine. Microtubule and mitochondria imaging was performed using Tubulin Tracker™ Deep Red and MitoTracker™ Deep Red, respectively.

RESULTS AND DISCUSSION

The contractile tension of EDLs was decreased by addition of colchicine (Fig. 2). The tension decrease caused by continuous tetanus stimulation was also influenced by addition of colchicine. These findings suggest that microtubules contribute to the stable generation of tension in the muscle. We therefore focused on the role of microtubules for the viscoelasticity of skeletal muscle. We measured the deformation stress of the muscle to calculate viscoelastic modulus. Two Young's moduli were calculated from the measurement of deformation stress. One of these Young's modulus tended to increase with the addition of colchicine. The viscous modulus which was calculated from the measurement of the stress of deformation initiation point at various deformation rates was significantly decreased by the addition of colchicine. Using these calculated viscoelastic moduli, a mechanical model is being developed. In this symposium, we will discuss about the contribution of microtubules in stable tension generation using this model.

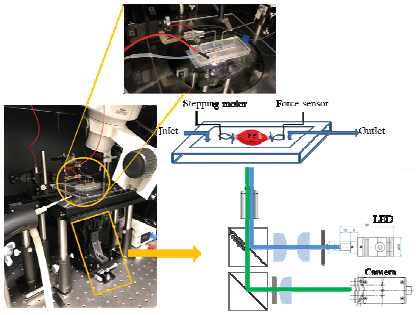

Figure 1: Simultaneous measurement device

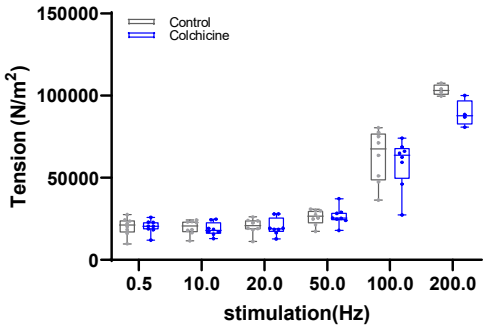

Figure 2: Measurement of muscle tension induced with electrical stimulation.

Comparison of tension in contraction induced by electrical stimulation with or without colchicine. Colchicine decreased the tension during full contraction at 200Hz, whereas there was no significant difference in twitch. Therefore, microtubules might be involved in force summation of skeletal muscle contraction.

ACKNOWLEDGEMENTS

This work was supported in part by the Japan Society for the Promotion of Science KAKENHI (grant Number 20K11368, 23K10692).

REFERENCES

[1] J.A. Tuszynski, et.al. (2005) Eur. Phys. J. E17, 29-35.

The effect of sex on intramuscular fat infiltration in rat soleus muscle in a diet-induced obesity model

[1,2]**Hannah E. Smith**, [1,2]Nada Abu Ghazaleh, [3]Ruth-Anne Seerattan, [1,2,3]Walter Herzog
[1]Department of Biomedical Engineering, University of Calgary, Calgary, AB, Canada
[2]McCaig Institute of Bone and Joint Health, University of Calgary, Calgary, AB, Canada
[3]Faculty of Kinesiology, The University of Calgary, Calgary, AB, Canada
corresponding author: Hannah.smith@ucalgary.ca

INTRODUCTION

Obesity and metabolic syndrome are risk factors in the development of sarcopenia or, muscle wasting. As muscle mass is a key indicator of long-term health [1], it is important to understand the relationship between diet and muscle integrity. In previous work, we demonstrated that a high fat/high sucrose (HFS) diet induces obesity and low level systemic and local joint, bone, and muscle inflammation in male Sprague-Dawley rats [2,3]. This led to an increase in fat infiltration in the glycolytic vastus lateralis (VL) muscle [3]. However, the oxidative capacity of the soleus muscle seemed to protect against intramuscular fat accumulation [4].

Most animal-based research still tends to over-rely on males. Up to this point, studies looking at obesity related musculoskeletal degeneration have only been done in male rats. As females can differ in the presentation and mechanism behind various diseases [5,6], it is important to understand the impact that sex has on musculoskeletal health.

Therefore, the objective of this study is to quantify the intramuscular fat (IMF) infiltration in the soleus muscle for both male and female Sprague-Dawley rats.

METHODS

Twenty-four male and twenty-four female Sprague Dawley rats at twelve weeks of age, were randomized into two different experimental groups each: 1) animals fed a chow diet (n=12); and 2) animals fed a HFS diet (n=12). The diets were maintained for twelve weeks. Rats were sacrificed and the soleus muscles were harvested at twenty-four weeks of age. The soleus muscles were then analyzed for fat content using the histological stain Oil Red O and quantified using ImageJ. The IMF percentage was determined per cross sectional area of muscle. Statistical analysis for the comparison between groups was done using a Mann Whitney U test.

RESULTS AND DISCUSSION

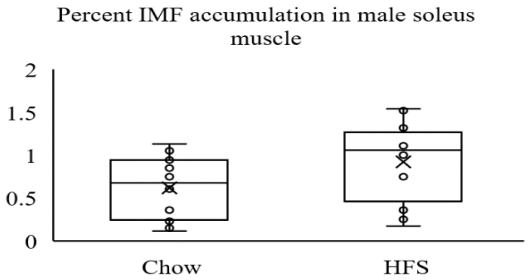

Figure 1: Percent IMF infiltration in soleus muscle male Sprague Dawley rats.

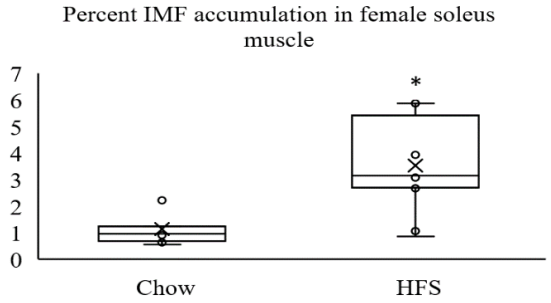

Figure 2: Percent of IMF infiltration in soleus muscle in female Sprague-Dawley rats. (*) indicates a p-value <0.005.

Based on these results (figure 1), we can conclude that male and female Sprague-Dawley rats accumulate different amounts of intramuscular fat in soleus muscle when subjected to a high fat sucrose diet. In males, no difference was found in IMF content between each of the diet groups. However, female animals who consumed the HFS diet had significantly higher IMF content than the group consuming the chow diet. These findings provide insight to how certain musculoskeletal diseases can present differently in males and females and why therapeutics may need to differ depending on sex.

REFERENCES

[1] Srikanthan & Karlamangla. (2014). *AM. J. Med.,* **127**.
[2] Collins et al. (2016). *Sci. Rep.,* **6**.
[3] Collins et at. (2016). J. Ortho. Res, 34(12).
[4] Collins et al. (2017). Phys. Rep., 5(10).
[5] De Bellis A. et al. (2020). Heart Fail. Rev., 25(2).
[6] Golden & Voskuhl. (2017). *J. Neurosci. Res.,* **95(1-2).**

Pre-Pubertal Training History Affects Satellite Cell Pool in Line with Upcoming Muscle Performance in Adult Rats: Longitudinal Study

[1*]**Rana Fayazmilani**, [1]Samira Rostami, [1]Sahar Shamloo, [1]Reyhaneh Salehizade
[1]Department of Biological Sciences in Sport, Faculty of Sport Sciences and Health, Shahid Beheshti University, Tehran, Iran
corresponding author: r_milani@sbu.ac.ir

INTRODUCTION

Postnatal skeletal muscle growth is strongly associated with a satellite cell pool [1]. Early adolescence might be a crucial period when different exercise training interventions have specific consequence on satellite cells. Nevertheless, forced and intensive physical activities may display negative effects, particularly in the pre-pubertal period [2]. The interaction of growth factors and stress parameters plays a key role in mediating effects. Pax7 and MyoD have been suggested as the leading indicators of satellite cell activation [3]. In the present study, preadolescent rats were exposed to an enriched environment and combined exercise training for three consecutive weeks to determine these interventions' effects on satellite cell pool and upcoming effect on skeletal muscle function during adulthood.

METHODS

In this study, 36 pre-adolescent male rats (28-48 postnatal days) were either subjected to an enriched environment that facilitated physical activities or combined training or control for three weeks. After three weeks, half of the rats were dissected and half were kept in the standard cages without any interventions until adulthood (48-85 postnatal days) for further functional analysis. The flexor hallucis longus muscle was removed for biochemical and histochemical analysis.

RESULTS AND DISCUSSION

Regarding performance, trained and enriched rats had significant improvement in forelimb grip strength ($P<0.01$) and load-carrying capacity ($P<0.05$). The longitudinal study showed a significant improvement in grip strength ($P<0.01$), but no differences were observed in other physical performance and general characteristics (body weight, food intake, and BMI).

Table 1. Physical and body performance parameters

	Groups	Mean Body Weight Changes (g)	Mean Food Intake (g/day/rat)	Body Weight (g)	BMI (g/cm^2)	Grip Strength (g)	Maximum Carrying Capacity (g)	Maximum Running Capacity (m)
Pre-pubertal Measurements		*PND 28- 48*		*PND 49*			*PND 50-52*	
	EE	81.24 ± 18.45	14.21 ± 0.92	149.2 ± 2.87	0.47 ± 0.01	518.6 ± 15.95**	132.1 ± 11.78*	524.3 ± 48.19
	CET	82.19 ± 18.56	14.07 ± 1.06	147.0 ± 2.81	0.47 ± 0.01	512.9 ± 17.69**	153.6 ± 12.80*	665.9 ± 84.38**
	C	83.18 ± 20.28	13.46 ± 0.94	146.9 ± 3.22	0.51 ± 0.02	435.6 ± 16.34	111.3 ± 7.79	369.4 ± 29.92
Longitudinal Measurements		*PND 28- 85*		*PND 86*			*PND 87-89*	
	EE	170.1 ± 31.22	20.41 ± 1.46	311.1 ± 9.15	0.62 ± 0.02	831.1 ± 43.95*	323 ± 15.59	531 ± 11.94
	CET	168.1 ± 29.75	18.94 ± 1.36	302 ± 4.56	0.60 ± 0.01	851.1 ± 57.89*	321.7 ± 15.02	541 ± 19.17
	C	163.7 ± 28.17	18.62 ± 1.39	296.7 ± 6.31	0.63 ± 0.01	666.7 ± 52.09	289.3 ± 6.65	492.1 ± 22.07

Data are expressed as mean ± SEM. for all groups (n= 6-8 per group). **PND,** post natal day; **EE**, enriched environment; **CET**, combined exercise training; **C**, control.
***P< 0.05, **P< 0.01 vs. control.**

Findings demonstrated that exercise trained rats displayed high levels of serum IGF-1 ($P<0.05$). There was an increase in Pax7 ($P<0.05$) and MyoD ($P<0.001$) mRNA expression. A significant increase in the mean fiber area ($P<0.01$), satellite cell ($P<0.001$), and myonuclear numbers ($P<0.01$) were also observed in both intervention groups. Importantly, enriched rats showed lower corticosterone levels ($P<0.05$) compared to training ones.

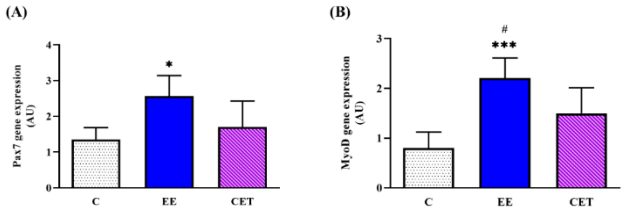

Figure 1: Enriched environment (EE) and combined exercise (CET) significantly increased Pax7 (A) and MyoD mRNA levels (B) in preadolescent rats. *P< 0.05, ***P< 0.001 vs. control group. #P< 0.05 vs. CET group.

Type of physical exercise is an essential part in changing satellite cells pool. Different and frequent physical activities in an enriched environment can be effective for muscle development.

ACKNOWLEDGEMENTS

Acknowledgments are optional and should specify research funding and resources including organisation name and reference numbers (if applicable).

REFERENCES

[1] A Bachman, J. F., Klose, A., Liu, W., Paris, N. D., Blanc, R. S., Schmalz, M., Knapp, E. & Chakkalakal, J. V. (2018). Prepubertal skeletal muscle growth requires Pax7-expressing satellite cell-derived myonuclear contribution. Development, 145.

[2] Eldomiaty, M. A., Elayat, A., Ali, S., Algaidi, S. & Elnaggar, M. (2020). Beneficial effects of voluntary over forced exercise on skeletal muscle structure and myokines' expression. Folia morphologica, 79, 350-358.

[3] Bagley, J. R., Denes, L. T., McCarthy, J. J., Wang, E. T., & Murach, K. A. (2023). The myonuclear domain in adult skeletal muscle fibres: Past, present, and future. *The Journal of Physiology*. Advance online publication.

Poster Session 2:

Bryan Yu

Christian Svane

Amsal Rajan

Jeroen Aeles

Andrew Sawers

Michael Baggaley

Heiliane de Brito Fontana

Landon Foley

Grace Privett

Esthevan Machado

In vivo vastus lateralis fascicle excursion during speed skating imitation

Bryan Yu[1] and Walter Herzog[1]
[1]*Human Performance Laboratory, University of Calgary, Calgary, Canada*
Corresponding Author Email: byu@csicalgary.ca

Introduction

Mechanical power is a key performance indicator in long-track speed skating [1]. Maximal power output in athletic performance can be achieved when mechanical properties of muscles, such as the force-length relationship, are optimized [2-3]. The purpose of this study was to determine the in vivo operating range of vastus lateralis (VL) fascicle lengths during speed skating imitation and compare the fascicle lengths to those that define the VL force-length relationship.

Methods

Sixteen sub-elite speed skaters performed nine seated maximal voluntary isometric knee extensions in a dynamometer with the left leg ranging from 20° to 120° knee flexion (0°=full extension) in a randomized order. Following the knee extension test, skaters performed three progressive trials of 50%, 75%, and 100% perceived effort of the turn-cable exercise on a treadmill.

VL forces were calculated from the knee extension torque and patellar tendon moment arm. Knee joint angle was recorded with an electrogoniometer. Surface EMG was recorded by placing bipolar electrodes on the distal portion of VL. Ultrasound images of VL were obtained using B-mode ultrasonography above the middle of the VL muscle belly. Fascicle lengths were measured using ImageJ.

Knee joint angles and VL fascicle lengths were obtained at initial-contact (IC), peak-EMG (PE), and take-off (TO) during the turn-cable test. The gliding phase of the turn-cable test was defined from initial-contact to peak-EMG, and the push-off phase from peak-EMG to take-off.

Results

Knee angle excursion during the turn-cable test covered almost the entire range of the torque-angle relationship regardless of the effort conditions (Figure 1), while the fascicle length for all three turn-cable conditions only covered the descending limb and the plateau region (Figure 2).

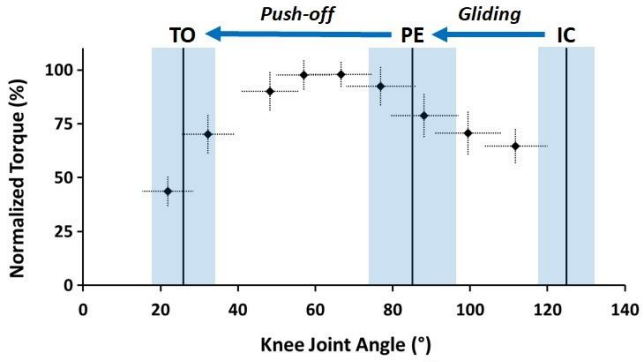

Figure 1. Knee extensor T-A relationship superimposed with turn-cable knee angle excursion.

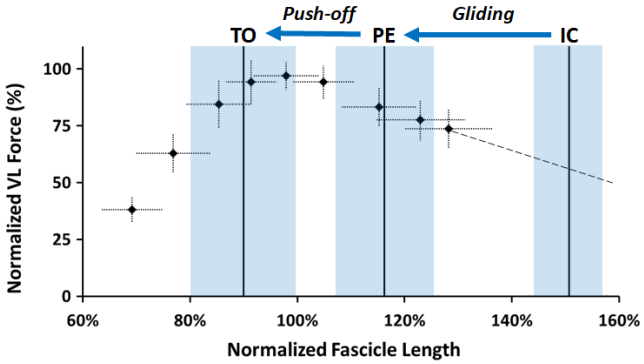

Figure 2. VL force-length relationship superimposed with normalized VL fascicle excursion during the turn-cable test at 100% effort.

Discussion

The knee angle at initial-contact in the turn-cable test (122 ± 8°) was more flexed than the knee angle (80-90°) during the gliding phase of skating the curve [4], therefore going against the commonly used training principle of specificity of movement [5].

The VL fascicle excursion for all three turn-cable conditions was contained to the descending limb of the maximal force-length relationship during the gliding phase. Fascicles then reached optimal length during the push-off phase. This result suggests that VL has a reduced force capacity in the gliding phase, which may also be energetically inefficient [6], but may work optimally in the push-off phase when skaters generate the propulsive work required to overcome air and ice friction.

Skaters can choose to optimize one stroke phase over the other based on individual gaps or competition demands. For example, sprint skaters can model the starting and pre-extension positions based on the optimal fascicle length, and long-distance skaters can choose to prioritize the gliding phase by changing the shape of the force-length relationship by performing muscle length-specific training [7-8].

Significance

Examination of the muscle fascicle lengths during the primary sport movements provides an alternative method of approaching sport-specificity in training, since fascicle length is a more sensitive metric of determining muscle force output than joint angle.

Acknowledgments

Funding: NSERC Canada

References

[1] Van Ingen Schenau (1982) *J. Biomech*, **15**: 449-458.
[2] Gordon et al. (1966) *J. Physiol,* **184**: 170-192.
[3] Lutz & Rome (1994) *Science,* **263**: 370-372.
[4] de Koning et al. (1991) *Int. J. Sport Biomech,* **7**: 344-358.
[5] Siff & Verkhoshansky (1999) *Supertraining*.
[6] Cooper et al. (2021) *J. Exp. Biology*, **224**.
[7] Herzog et al. (1991) *MSSE,* **23**: 1289-1296.
[8] Tanaka et al. (2018) *Muscle & Nerve*, **57**: 83-89.

IN VIVO VASTUS LATERALIS FASCICLE LENGTH SHORTENING DURING MAXIMAL ISOMETRIC CONTRACTIONS

Bryan Yu[1] and Walter Herzog[1]
[1]*Human Performance Laboratory, University of Calgary, Calgary, Canada*
Corresponding Author Email: byu@csicalgary.ca

Introduction

The force-length relationship describes the force generating potential of skeletal muscle during maximal, steady-state, isometric contractions, and it can be observed on all structural levels of the muscle [1]. In human testing, the force-length relationship is affected by the dissociation of fascicle (contractile element), and whole muscle-tendon unit length [2]. Fascicle lengths during isometric knee extension testing (probably the most common human muscle testing) are shortening for two reasons (i) shortening caused by the extension of the knee during contraction due to compliance of the dynamometer and human soft tissues and (ii) shortening caused by the elongation of muscle elastic tissues with increasing force [3].

The amount of fascicle shortening associated with each factor is not known but is important for accurate and reliable estimates of the *in vivo* force-length properties of human skeletal muscles. The purpose of this study was to quantify the amount of vastus lateralis (VL) fascicle shortening caused by each of these factors.

Methods

Sixteen sub-elite speed skaters participated in the study. Participants performed nine maximal voluntary isometric knee extensions with the left leg ranging from 20° to 120° knee flexion (0°=full extension) in a randomized order. They were positioned on a dynamometer (THE HUMAC NORM, Computer Sports Medicine Inc., Stoughton, MA, USA) with the back supported and the hip joint angle set at 80°.

2-D leg kinematics were recorded with two markers (medial malleolus and medial femoral epicondyle) using a high-definition camera. Knee angles were determined using Dartfish (Version 10, Dartfish, Switzerland).

Ultrasound images of VL were obtained using B-mode ultrasonography (60mm, LV8, Telemed, Lithuania). The ultrasound probe was attached to the skin above the VL (~50% of femur length). Fascicle lengths were measured using ImageJ (NIH, USA).

Knee joint angles and VL fascicle lengths were obtained for the passive and fully activated conditions. Second order polynomial approximations were used to calculate fascicle shortening from force production alone. The fascicle shortening caused by knee angle changes was then calculated as the difference between the total fascicle shortening and the shortening just caused by the increasing VL force.

Results

The greatest change in total fascicle shortening occurred between 30° to 22° knee flexion, and the lowest change occurred between 120° to 112° (Figure 1).

Fascicle shortening caused by VL force gradually decreased as the knee angle increased (85% to 40%) while, correspondingly, fascicle shortening caused by changes in knee angle increased with increasing knee angles (Figure 1).

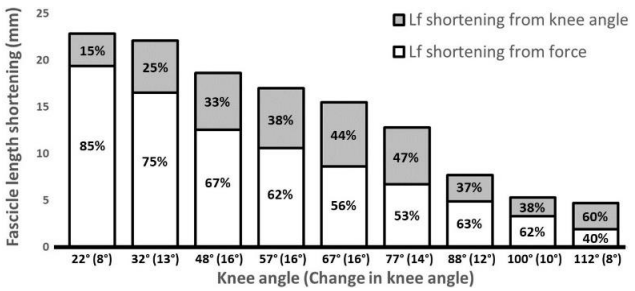

Figure 1: Total vastus lateralis fascicle length (Lf) shortening as a function of final knee angles. Angles in parenthesis indicate the knee angle change due to dynamometer and soft tissue compliance.

Discussion

In many human studies, fascicle length changes of muscles are given as the difference of fascicle lengths measured in the passive muscle and the fully activated muscle [4-6]. The implicit assumption underlying such results is that fascicle shortening occurred at the expense of elongations of elastic structures in the muscle [4-6]. Here, we demonstrate that this assumption is likely not correct for the human knee extensor muscles, as even careful strapping of subjects into the dynamometer allows for extension of the knee with force production due to the compliance of the dynamometer-human leg system. Furthermore, the contribution of muscle elastic elements and dynamometer compliance to fascicle shortening depends crucially on the knee joint angle at which the testing is performed. Fascicle shortening during "isometric" muscle testing will not only affect the force-length properties of muscles due to the changed length of fascicles but also due to the residual force depression associated with the mechanical work produced by fascicle shortening [7].

Significance

Knowing the change in fascicle length during "isometric" human muscle testing is crucial in understanding the true force-length properties of the tested muscles.

Acknowledgments

Funding: NSERC Canada

References

[1] Gordon et al. (1966) *J. Physiol,* **184**: 170-192.
[2] Kulig et al. (1984) *E. S. S. Reviews,* **12**: 417-466.
[3] Arampatzis et al. (2004) *C Biomech,* **19**: 277-283.
[4] Ito et al. (1998) *J. A. Physiol*, **85**: 1230-1235.
[5] Reeves and Narici (2003) *J. A. Physiol*, **95**: 1090-1096.
[6] Ichinose et al. (1997) *A. Anatomica*, **159**: 78-83.
[7] Chen et al. (2019) *J. A. Physiol,* **126:** 1066-1073.

Temporal Relation between Muscle Growth and Contracture Development in Children with Cerebral Palsy: Implications for Early Intervention

[1]**Christian Svane**, [2]Maria Willerslev-Olsen
[1]Department of Neuroscience, University of Copenhagen, Copenhagen, Denmark
[2]Elsass foundation, Charlottenlund, Denmark
corresponding author: Christian Svane, email: christian.svane@sund.ku.dk

AIM

This study aimed to investigate the temporal relation between muscle growth and contracture development in children with cerebral palsy (CP) and the potential of early interventions directed at facilitating muscle growth to reduce the risk of contractures.

METHODS

First, we enrolled 52 infants younger than 17 weeks corrected age (CA) at high risk of CP. Of these, we obtained longitudinal data from 13 infants who were later diagnosed with CP. The children with CP were compared to a population of 95 typically developing children. At each assessment, medial gastrocnemius muscle volume was measured using freehand three-dimensional ultrasound, and ankle joint passive muscle torque, a measure of contracture development, was measured using hand-held dynamometry. Children were assessed from birth to the age of ~four.

In addition, we will enroll 25 infants at high risk of CP in an ongoing early intervention study directed at facilitating muscle growth compared to standard care. These infants will be assessed at baseline, post-intervention, and at 9-, 15-, 24-, 36-, and 48-months CA in the same manner as in the longitudinal part of the study.

RESULTS

Seven children with CP exhibited muscle growth comparable to typically developing children, whereas six showed impaired muscle growth, deviating from typically developing children around ~20 months of age. Three of the children with impaired muscle growth later developed increased passive muscle torque, while none of the children with comparable growth did.

Fifteen infants have been included and five infants have completed the early intervention. Early results indicate that the infants who received the intervention have increased muscle volume compared to children with CP who received standard care.

INTERPRETATION

Impaired muscle growth appears to contribute to the development of muscle contractures in children with CP. Early interventions with the aim of facilitating muscle growth are feasible and may be effective in reducing the risk of contractures in early childhood.

ACKNOWLEDGEMENTS

The study was funded by a grant from the Elsass Foundation. We want to express our gratitude to all the children and families who participated in this study.

Using EMG recordings to predict muscle forces through an artificial neural network approach

[1]**Amsal S. Rajan**, [2]Walter Herzog, [3]Azim Jinha
[1]Department of Kinesiology, University of Calgary, Calgary, AB, Canada
[2]Faculty of Kinesiology, The University of Calgary, Calgary, AB, Canada
amsal.rajan1@ucalgary.ca

INTRODUCTION

Electromyography (EMG) signals of dynamically contracting muscles have rarely been used to predict muscle forces obtained experimentally [1]. Being able to predict muscle forces accurately and reliably across muscles, subjects, and species would represent a major achievement in biomechanics research and has been the goal of many research groups over the past half century. The purpose of this project was to test the generalizability of using a pattern recognition algorithm to accurately predict muscle forces from corresponding EMG signals.

METHODS

We trained an artificial neural network to derive an EMG-force relationship based on experimentally measured EMG signals and muscle forces from the cat soleus muscle. From this relationship, muscle forces were then predicted and validated against the directly recorded forces. EMG and muscle forces were recorded in the soleus, gastrocnemius, tibialis anterior, and plantaris muscles from four adult cats. The cats were trained to walk and trot on a motor-treadmill at three speeds and three inclinations. Once testing was completed, voltage signals from an implanted tendon transducer were calibrated and converted to muscle forces. EMG and force signals were extracted from consecutive step cycles spanning two seconds per experimental condition. These data were then post-processed with filtering and resampling steps, and the EMG signals were then used to train an artificial neural network (ANN) to predict the measured muscle forces. The ANN was comprised of an input layer, two hidden layers, and an output layer. Once trained, forces were predicted from EMG signals for experimental conditions that were not used in the training of the network. The performance of the trained ANN was evaluated using root mean square errors and regression analysis to compare predicted and measured muscle forces.

RESULTS AND DISCUSSION

Here, we will show exemplar data from one trial with a cat walking at a speed of 0.8m/s on a level treadmill surface. The soleus forces for this cat were predicted using an ANN trained with the soleus EMG and forces measured form this same cat, but the predictions were for steps not used in the training of the ANN. The root mean square (RMS) error of the predicted vs. the experimentally measured forces was 1.31 N, with a coefficient of determination of $r^2 = 0.99$. Predictions of soleus forces for cats not used in the training of the ANN had a RMS error between 10-13% for the different walking conditions and correlation coefficients ranging from 0.94-0.96. These results suggest that muscle forces can be predicted extremely well from the corresponding EMGs using an artificial neural network approach. The original goal for this project was to use an ANN approach to predict muscle forces from EMG for the sheep medial gastrocnemius muscle. However, the EMG signals for these experiments had random baseline shifts which made accurate muscle force predictions impossible. We conclude from these studies that accurate muscle force predictions within a muscle and across subjects are excellent if the EMG signals are excellent, but become unfeasible if the EMG signals contain errors, such as random baseline shifts.

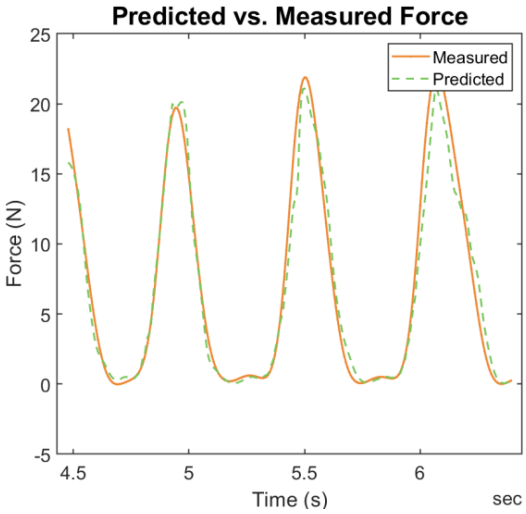

Figure 1: Measured vs. predicted soleus muscle force for three steps of a cat walking at a speed of 0.8m/s on a level treadmill.

CONCLUSIONS

The results of this study show that artificial neural networks can be promising in terms of capturing the essential elements of the EMG-force relationship of dynamically contracting muscles. The limitation of this approach is that force measurements need to be made at one point in the system of interest to train the artificial neural network. Further analyses will look at using this approach across different muscles in the cat hindlimb and in muscles of other animals.

ACKNOWLEDGEMENTS

I would like to thank Drs. T. Leonard, S. Bossuyt, and D. Stefanyshyn, for their help. Supported by NSERC of Canada, CIHR, and the Swiss National Science Foundation.

REFERENCES

[1] Liu MM et al. (1999). *J EMG & Kinesiol.*, *9*(6), 391–400.

3D WHOLE MUSCLE SHAPE CHANGES – EXPLORING A NOVEL APPROACH

[1,2]**Jeroen Aeles**, [1,3]Peter Aerts, Sam Van Wassenbergh[1]
[1] Department of Biology, University of Antwerp, Antwerp, Belgium
[2] Department of Movement and Sport Sciences, Vrije Universiteit Brussel, Brussels, Belgium
[3] Department of Movement and Sports Sciences, University of Ghent, Ghent, Belgium
corresponding author: Jeroen.aeles@vub.be

INTRODUCTION

When animals, including humans, move, their muscles contract, and by doing so change shape. While such shape changes are obvious and are inevitable for a muscle when generating force, we know little about its functional role in force production. Little is currently known about 3D whole muscle shape changes, which are evidently complex and non-linear in nature. The ability to ultimately measure shape changes during contraction would drastically improve our understanding of in vivo muscle biomechanics. Here we explore a novel approach for experimentally measuring 3D whole muscle shape changes using X-ray imaging. We present preliminary data on a validation experiment..

METHODS

Fresh cadaveric lower limbs of the domestic chicken (Gallus gallus domesticus) were used for this experiment. After surgically opening the skin over the posterior side of the lower leg, and removing most of the connective tissue surrounding the muscle, 35 opaque beads (⌀ = 0.35mm) were fixated all around the lateral gastrocnemius with a cyanoacrylate. The distal gastrocnemius tendon was severed distally as well as at the muscle-tendon junctions of the other gastrocnemius muscles. Two beads were implanted into the tendon, and three into the distal tibia (reference). Barium sulphate powder was applied to the entire muscle. High-speed stereo (3D) X-ray videos (750Hz) were recorded while the muscle was stretched cyclically by applying a force on the tendon. Ultrafast computed tomography (<2s) scans were reconstructed from images acquired while rotating the lower leg 360 degrees approximately along its longitudinal axis, with the muscle at resting length. 39 out of the 40 markers (beads) were successfully tracked during two shortening-lengthening cycles using XMALab [1]. The 3D Euclidean distance between each of the 35 muscle markers and the most distal reference marker was calculated for the entire cycle, and compared between the start and end of the cycle. CT slices were segmented in Matlab with Sashimi V1.1 [2].

RESULTS AND DISCUSSION

The distal tendon marker was used as a reference for the stretch-shortening cycles. This marker was displaced along the muscle-tendon line of action over 8.30 and 8.34 mm in cycle 1 and 2 respectively. One of the 34tracked muscle markers only had a displacement of 2.14 and 2.18 mm over cycle 1 and 2 respectively, which was considered too small given the amplitude of the displacement of the reference marker. On closer inspection, it appeared the marker got detached from the muscle and was therefore removed from further analyses. Of the remaining 33 muscle markers, the displacement ranged from 6.15 to 8.86 mm and from 6.11 to 9.05 mm for cycle 1 and 2 respectively.

Very small differences in the distance between the muscle markers and the distal reference marker were found when comparing the distance at the start and end of each cycle (mean: 0.07 ± 0.12 mm and 0.05 ± 0.05 mm for cycle 1 and 2 respectively), indicating no shifts in bead placement along the muscle surface.

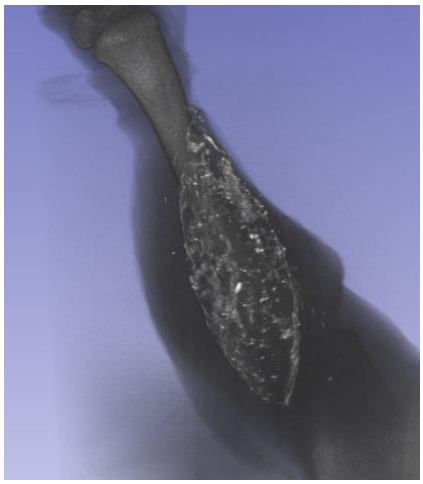

Figure 1: CT reconstruction of the gastrocnemius muscle.

These preliminary results suggest that the proposed approach can be used to track 3D whole muscle shape changes dynamically, at least during muscle stretching. Currently, we are working on comparing the 3D whole muscle shape between the CT reconstructed scans (Fig. 1) and reconstructed muscle shapes based on the marker data, as well as creating statistical shape models of these data. Ultimately, we aim to validate this technique for muscle shortening and in situ muscle contraction induced by electrical stimulation.

ACKNOWLEDGEMENTS

This research was funded by the European Commission through a Marie-Skłodowska Curie Actions Individual Fellowship to J Aeles. We thank Dr J Sanctorum of DynXLab for assistance in the CT reconstructions.

REFERENCES

[1] Knörlein BJ et al. J Exp Biol 219: 3701-3711, 2016.
[2] Bolsterlee B. https://github.com/bartbols/SASHIMI

HIP MUSCLE FUNCTION EXPLAINS A LARGER PROPORTION OF THE VARIANCE IN WALKING AND BALANCE PERFORMANCE AMONG TRANSTIBIAL THAN TRANSFEMORAL PROSTHESIS USERS

[1]**Andrew Sawers**, [2]Stefania Fatone
[1]Department of Kinesiology, University of Illinois Chicago, Chicago, IL, USA
[2]Department of Rehabilitation Medicine, University of Washington, Seattle, WA, USA
corresponding author: asawers@uic.edu

INTRODUCTION

Safe and efficient locomotion is a commonly stated goal of lower limb prosthesis (LLP) users, and thus a priority in rehabilitation [1]. There is growing evidence that hip strength may be a key determinant of LLP users' safety and mobility [2]. There is however no consensus regarding the association between hip strength and walking and balance performance that could guide clinical assessment and treatment of walking and balance deficits in LLP users [2]. The objective of this study was therefore to determine how much of the variance in unilateral transtibial (TT) and transfemoral (TF) prosthesis users' walking and balance performance could be explained by hip strength.

METHODS

Unilateral TT and TF prosthesis users were recruited from local prosthetic clinics. Maximum voluntary isometric hip extension and flexion, as well as abd- and adduction torque were measured with a motor-driven dynamometer in supine and side-lying positions, respectively. Participants performed 15 five-second trials per leg and muscle group combination, the order of which was randomized. Hip muscle function was characterized via peak torque, average torque, torque impulse, and torque steadiness, each of which were derived from the processed torque signal and scaled to body size [3]. Walking speed, endurance, and balance were measured by administering the 10-m walk test (10mWT), 2-min walk test (2MWT), and the narrowing beam walking test (NBWT), respectively. Forward stepwise multiple linear regression was used to determine the association between residual and intact limb isometric hip muscle function and walking and balance performance.

RESULTS AND DISCUSSION

13 TT (mean age: 53 yrs, 8 male, 10 due to trauma) and 13 TF (mean age: 52 yrs, 8 male, 9 due to trauma) prosthesis users were enrolled and completed the study protocol. Regression analyses revealed that isometric hip muscle function explained a larger proportion of the variance in TT than TF prosthesis users' walking speed (TT: 69%, TF: 33%), endurance (TT: 60%, TF: 46%), and balance (TT: 68%, TF: 48%) (Figure 1). Two metrics, residual limb peak hip extension torque, and residual limb hip abduction torque steadiness were consistently and significantly associated with TT prosthesis users' walking and balance performance. In contrast, intact hip abduction torque impulse was the lone metric of hip muscle function associated with TF prosthesis users' walking and balance performance. Different hip muscles and hip muscle functions may therefore serve as determinants of walking and balance performance in transtibial and transfemoral prosthesis users, suggesting amputation level specific targets for rehabilitation.

Compared to TT prosthesis users, isometric hip muscle function explained a smaller proportion of TF prosthesis users' walking and balance performance. Hip strength may therefore be unable to compensate for the loss of ankle and knee muscle function in TF prosthesis users, or simply play a smaller role in determining their balance and mobility. 30-40% of the variance in TT prosthesis users' and 52-67% of the variance in TF prosthesis users' walking and balance performance could not be explained by isometric hip muscle function. Other muscles, including the intact plantar flexors, different muscle functions, such as rate of torque development, as well as isokinetic muscle actions, lower limb muscle coordination [4], and variation in muscle structure and architecture should be considered in future research.

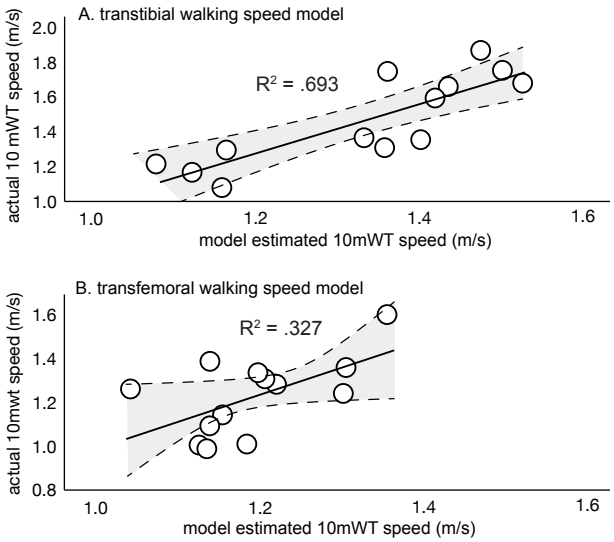

Figure 1: Isometric hip muscle function explained a larger proportion of the variance in transtibial (A) than transfemoral (B) prosthesis users' walking speed.

ACKNOWLEDGEMENTS

This work was supported by the Department of Defense under award number W81XWH-19-1-05476.

REFERENCES

[1] Manz et al. (2022). *JNER*, 19:119.
[2] Hewson et al. (2020). *POI*, **5**: 34-36.
[3] Sawers A & Fatone S (2022). *Clin Biomech,* **97**:105702.
[4] Wakeling JM et al. (2010). *J Exp Biol*, **25**: 374-386.

TORQUE LOSS DURING SIMULTANEOUS ACTIVATION OF AGONISTIC MUSCLES

[1]**Michael Baggaley**, [1]Andrew Sawatsky, [2]Heiliane de Brito Fontana, [1]Walter Herzog
[1]Faculty of Kinesiology, The University of Calgary, Calgary, AB, Canada
[2] Department of Morphological Sciences, Federal University of Santa Catarina, Florianopolis, Brazil.
corresponding author: michael.baggaley1@ucalgary.ca

INTRODUCTION

The quadriceps muscles of rabbits lose torque generating capacity when activated simultaneously [1]. In this study, we tested if this torque loss is unique to the quadriceps muscles or if it is a phenomenon also observed in other agonistic muscle groups. To achieve this, experiments were performed in New Zealand white rabbits. The torque generating capacity of the plantarflexor muscles (Plantaris (PL), medial/lateral Gastrocnemius (MG/LG), and Soleus) were measured during simultaneous and individual activation of the muscles via direct nerve stimulation of the branches of the tibial nerve. The data presented herein represents preliminary findings of an ongoing investigation.

METHODS

Plantarflexor muscles of four skeletally mature, New Zealand white rabbits were analysed. Maximum isometric torque was measured at 5 ° increments from 90 to 115 ° of plantarflexion. The nerve branches of LG, MG, and PL were isolated and individually activated via nerve cuffs. The soleus was activated via stimulation of the common LG/soleus nerve. Three activation frequencies (100, 60, and 30 Hz) were used at each joint angle. Peak torque was determined for each muscle individually and summed to determine the difference in torque between individual muscle activation and activation of all muscles simultaneously. Simultaneous activation of all nerve branches was performed using the same joint angles and activation levels as used for the individual muscle activations. Mean and standard deviation for each angle and condition were calculated, and differences between simultaneous vs. summed activations were quantified.

RESULTS AND DISCUSSION

Simultaneous activation of the plantarflexor muscles (SIM) resulted in a distinct change in torque generating capacity compared to the sum of the individual muscle torque capacity (SUM), and this change was dependent on the activation frequency (Figure 1A and B). SIM activation of the plantarflexor muscles resulted in a 31% (0.53 Nm) and 22% (0.31 Nm) loss of torque at 100 and 60 Hz compared to SUM, respectively. At 30 Hz SIM activation of the plantarflexor muscles resulted in a 27% (0.14 Nm) greater torque compared to the SUM condition. For all activation frequencies, the largest torque difference between SIM and SUM were observed at 90° (Figure 1B). The reduced torque generating capacity observed during SIM activation of the rabbit quadriceps muscles has been attributed to the inter-muscular pressure that develops in agonistic muscle activation as described by Siebert et al. [2]. These authors showed that controlled lateral compression of the isolated rabbit medial gastrocnemius impaired the force generating capacity of the muscle in a dose-dependent manner; more lateral force resulted in increased loss of force capacity [2].

The counterintuitive result observed at 30 Hz is difficult to interpret. It corroborates the dose-dependent effect of lateral compression observed previously [2]; however, if lateral compression was low at 30 Hz one would expect to see similar torque between SIM and SUM. Instead, the data presented herein suggests that there is a beneficial effect to SIM activation at low frequencies. It is possible that SIM activation results in a more optimal fascicle length and/or pennation angle, but further work is needed to test this hypothesis. Given the large variability in the data, further work is needed to determine whether this is a consistent effect observed in the rabbit plantarflexors.

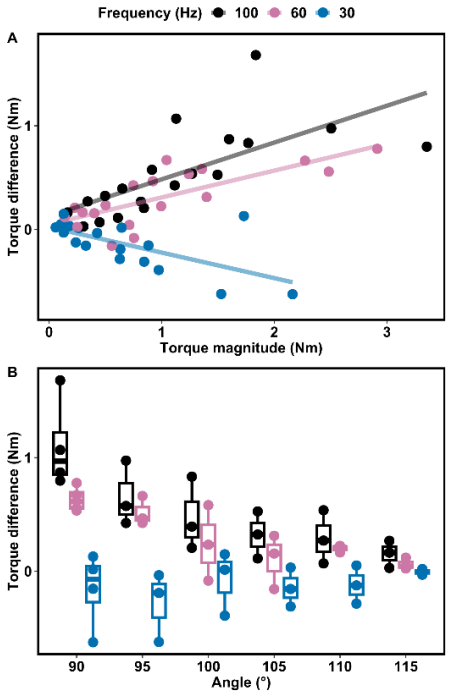

Figure 1: Torque magnitude in SIM vs. the difference in torque between SIM and SUM (A). Torque difference between SIM and SUM as a function of joint angle and activation frequency (B). Individual data points are for each rabbit in each condition. A positive difference indicates that the SUM was greater than SIM.

REFERENCES

[1] Fontana H et al. *J Exp Biol* **223**: jeb213843, 2020.
[2] Siebert T et al. *J Biomech* **74**:1822-1828, 2014.

Fascicle and muscle tendon unit shortening velocity in isokinetic contractions

[1]**Heiliane de Brito Fontana**, [2]Walter Herzog
[1] Department of Morphological Sciences, Federal University of Santa Catarina, Florianopolis, Brazil.
[2]Faculty of Kinesiology, The University of Calgary, Calgary, AB, Canada
corresponding author: heiliane.fontana@ufsc.br

INTRODUCTION

The well-known interdependence between velocity of shortening and maximal steady-state force generated by a muscle is described as a hyperbolic curve with muscle force progressively decreasing as fiber shortening velocity increases [1]. This property reflects the changes in cross-bridge dynamics that occur with changes in the rate of relative displacement between the myosin and the actin filaments. Mechanisms above the fiber level, such as muscle architecture and series elasticity, can potentially affect this property by changing the ratio between MTU and fascicle shortening velocities for a given level of force. In human testing, the force-velocity relationship of muscles is often estimated from torque-angular velocity tests using isokinetic dynamometers. In this study, we aimed to analyse the effect of joint angular speed on the ratio between vastus lateralis fascicle and muscle tendon unit shortening velocities during maximum isokinetic knee extensions.

METHODS

Knee extensor torque was measured on an isokinetic dynamometer (Biodex Multi-Joint System II, USA) in nine healthy young adults (25±3 yrs). During contractions, longitudinal plane images of the vastus lateralis (VL) muscle were obtained at 42–49 Hz using a 12.5-MHz linear array ultrasound probe. Maximum isometric contractions for the angular range between 85° and 180° of extension (15° increments) and maximum isokinetic contractions at eight different angular speeds (45, 90, 120, 180, 240, 300 and 500°/s) were performed with a 2 min interval between trials. Instantaneous muscle and fascicle shortening velocities were calculated by numerical differentiation of muscle [1] and fascicle lengths with respect to time. Average muscle and fascicle shortening velocities were calculated for the isokinetic range of joint movement, for the whole range of movement and for the ranges comprised from the onset of joint movement to the time of peak torque occurrence (pre-peak) and from the time of peak torque occurrence to the end of joint movement (post-peak). The ratio between MTU and fascicle shortening velocity (MTU/fascicle velocity) was calculated for the various ranges. A two factor repeated measures ANOVA with the main factors structural level (fascicle and MTU) and angular speeds (45, 90,. . .500/s) was used ($p<0.05$)

RESULTS AND DISCUSSION

Fascicle shortening velocities, either over the isokinetic or the entire movement range, were always substantially smaller than the corresponding MTU shortening velocity ($p<0.05$) (Figure 1). The ratio between MTU and fascicle shortening velocity increased non-linearly from 1.8 at 45°/s to 9.0 at 500°/s for the isokinetic range.

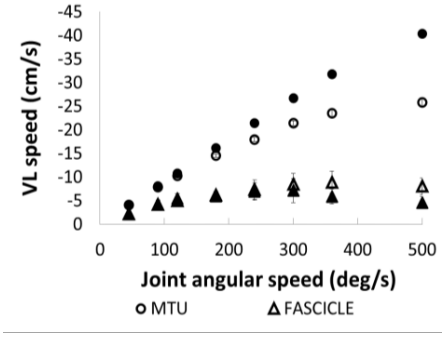

Figure 1: Mean (±SD) of vastus lateralis fascicle (triangle) and muscle tendon unit (MTU, circle) shortening velocities during the true isokinetic phase (filled symbols) and for the entire movement range (empty symbols).

Interestingly, the ratio MTU/fascicle velocity depended dramatically on whether force was increasing (pre-peak range) or decreasing (post peak range). In the pre-peak range, the ratio decreased from 1.4 to 0.6 with increasing joint angular speeds (45°/s to 500°/s). In contrast, in the post-peak range, the ratio MTU/fascicle velocity increased from 2.5 to 6.7 for increasing speeds. For the angular speeds tested, the ratio MTU/fascicle velocity at peak torque occurrence was always smaller than 2.

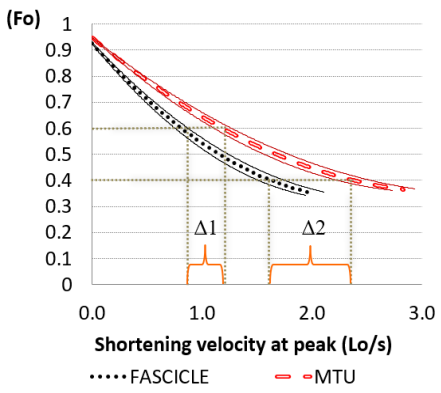

Figure 2: VL force–velocity at the fascicle and MTU levels. Force and velocities were normalized to maximum (Fo) and to optimal fascicle length (Lo). Δ1 and Δ2 is the difference in velocity at 0.6 and 0.4 of Fo respectively.

Assuming a close relationship between joint and fascicle dynamics results in an overestimation of the shortening velocity of the contractile component or of force production at peak torque [3]. The interactions between muscle architecture and series elasticity seem to partially counterbalance the reduction in force capacity of muscle fibers during fast contractions through an increase in MTU/fascicle velocity ratios with increasing speed. Force transmission across muscle structural levels, however, is still not well understood.

REFERENCES

[1] Hill. *Proc R Soc B Biol Sci* **1938**;126:136–95.
[2] Herzog and Read. *J Anat* **1993**;182:213–30.
[3] De Brito Fontana. *J. Electrom Kinesiol* **2014**;24:934-940
[4] Finni et al. *J. Biomech* **2023**;*in press*

Reliability of Countermovement Jump Force-Velocity vs. Velocity-Load Testing in Athletes

[1,2]**Landon W. J. Foley**, [1,2,3]Matthew H. Zukowski, [1,2]Matthew J. Jordan
[1]Integrative Neuromuscular Sport Performance Lab, University of Calgary, Calgary, Alberta, Canada
[2]Faculty of Kinesiology, The University of Calgary, Calgary, AB, Canada
[3]Canadian Sport Institute Calgary, Calgary, AB, Canada

corresponding author: landon.foley@ucalgary.ca

INTRODUCTION

The force-velocity (FV) relationship is a basic property of skeletal muscle that determines maximal muscle power capacity [1,2]. FV profiling (FVP) using the average force plotted against the average movement velocity during jumping is a common method to assess the functional lower body properties of athletes, and this is typically modelled as a linear relationship [3,4].

A.V. Hill found a hyperbolic muscle FV relationship in isolated muscle, whereas the FV relationship in functional tasks like jumping is thought to be linear when jumping force is plotted against the body centre of mass (BCM) velocity [3,5]. An alternative method in jumping is to plot jump performance (takeoff velocity -TOV) against the external load [6]. However, the reliability of these two methods in elite power athletes has not been described. Thus, given the importance of test reliability in determining a meaningful change during routine testing and monitoring of athletes [7], the aim of this study was to compare the reliability of the countermovement jump (CMJ) TOV-load profile compared to the standard FVP method that plots the average propulsive force as a function of the average BCM velocity.

METHODS

This study utilized an intraday test-retest design for the purposes of determining reliability. Elite athletes (mean age: 22 ± 2 yrs; 8 males, 6 females) from the University of Calgary with experience in plyometric training and Olympic lifting, and with no injury preventing full exertion at the time of testing, performed two trials (separated by 10 minutes of active recovery) of three loaded CMJs at 0%, 30% and 60% of body mass using a free weight trap bar on a dual force plate system (AMTI, Watertown, USA; frequency = 1000 Hz). Custom software (MATLAB, Natick, USA) was used to extract average force, average velocity, and TOV.

Intraclass correlation coefficients [ICC] using a 2-way mixed effects model, coefficient of variation, and Bland-Altman analysis was used to determine the 95% limits of agreement and compare the reliability between TOV-external load profile and FVP calculated as the average concentric velocity and average concentric force during the propulsive phase of the CMJ using a kinetic analysis.

RESULTS AND DISCUSSION

Linear profile methods showed TOV-load model parameters to be moderate-good, and FVP model parameters to be poor, whilst the reliability of TOV at each load condition was excellent.

Table 1: Test-retest reliability of takeoff velocity-load profile and force-velocity parameters

Jump Parameter	ICC (95% CI)	CV%
L_0	0.89 (0.68 - 0.98)	5.9
TOV_0	0.83 (0.54 - 0.94)	4.1
LV_{Slope}	0.57 (0.08 - 0.84)	10
F_0	0.66 (0.23 - 0.88)	11.3
V_0	0.00 (-0.51 - 0.51)	16.8
FV_{Slope}	0.00 (-0.51 - 0.51)	29.4

*95% CI = 95% confidence interval; CV% = within subject coefficient of variation; L_0 = theoretical maximal external load; TOV_0 = theoretical maximal take-off velocity; LV_{Slope} = slope of load-velocity profile; F_0 = theoretical maximal force production capability; V_0 = theoretical maximal velocity ; FV_{Slope} = slope of force-velocity profile

As supported by Bobbert et al. [6], our findings illustrate that the TOV-load profile appears to be a superior method to characterize functional force-velocity capacity in elite power athletes due to the relatively better reliability compared to FVP. Future research should assess the utility of the TOV-load method to predict sport performance capacity and to monitor performance changes in power athletes. Additionally, the possibility of examining the TOV-load relationship in injury contexts may help practitioners to individualize resistance training methods with elite power athletes.

REFERENCES

[1] Cormie P. et al. (2011). *Sports Medicine,* **41**: 17-38.
[2] Herzog, W. (2009). *Sport-Ortho-Trauma,* **25:** 286-293.
[3] Samozino et al. (2012). *Med. Sci. Sports Exerc.,* **44:** 313-322.
[4] Morin JB & Samozino P. (2015). *Int J Sports Physiol Perform.*, **11:** 267-272.
[5] Hill AV (1938). *Proc R Soc. Lond. B.,* **126:** 136-195.
[6] Bobbert M. et al. (2023). *Med. Sci. Sports Exerc.,* 10.1249/MSS.0000000000003147.
[7] Hopkins, WG. (2000). *Sports Med.,* **30:** 1-15.

ACUTE SKELETAL MUSCLE FATIGUE REDUCES CELLULAR PASSIVE AND ACTIVE STIFFNESS

[1]**Grace E. Privett**, [1]Austin W. Ricci, [1]Damien M. Callahan
[1]Department of Human Physiology, University of Oregon, Eugene, Oregon, USA
Corresponding author: damienc@uoregon.edu

INTRODUCTION

Skeletal muscle stiffness (index of relationship between loading and strain) is crucial to force transmission and joint stability. As a result, muscle stiffness may impact risk of soft tissue injury in athletes or falls risk in older adults. Whole muscle stiffness is reduced with exercise-induced fatigue **[1]** and fatigue is associated with enhanced injury risk **[2]**, suggesting a logical, but unproven mechanism linking acute modifications to muscle stiffness and subsequent injury. However, the means by which fatiguing exercise reduces muscle stiffness and the anatomical locus of these changes, are unknown. Intracellular mechanisms may be elucidated by assessing passive stiffness in single, permeabilized muscle fibers. Given the clinical relevance of mechanical assessment during active lengthening, the effect of fatigue on measures of active stiffness (i.e., residual force enhancement, RFE) may provide valuable insight into the causes of muscle strain injuries. Therefore, the purpose of this study was to assess measures of cellular passive and active stiffness in single fibers from fatigued and non-fatigued skeletal muscle of young adults.

METHODS

4 male and 4 female highly-trained volunteers performed one bout of unilateral repeated knee extensions until task failure. Immediately after fatigue, bilateral percutaneous needle biopsies were performed on the fatigued (F) and non-fatigued (NF) Vastus Lateralis muscles. After, single fibers were dissected and stiffness under active and passive conditions were evaluated. To measure passive stiffness, single fibers (89 NF, 82 F) were passively and incrementally stretched (8%/step) to 156% initial sarcomere length, reflecting an overall change in sarcomere length from 2.4μM to 3.7μM (Fig. 1A). Each length change was held for 2 min. Passive Young's Modulus was calculated as ΔStress/(Δ Strain). To measure RFE in a subset of fibers (5 NF, 5 F), isometric tension at standard reference length (sarcomere length = 3.2 μM) was compared to tension generated at the same length following active stretch (Fig. 1B). In the latter condition, residual force enhancement likely reflects the contribution of elastic elements to force generation under dynamic loading [3]. Effects of fatigue and biological sex on passive modulus and RFE were assessed via 2-way ANOVA.

Figure 1: Protocols used to measure passive (A) and active (B) mechanics at the cellular level.

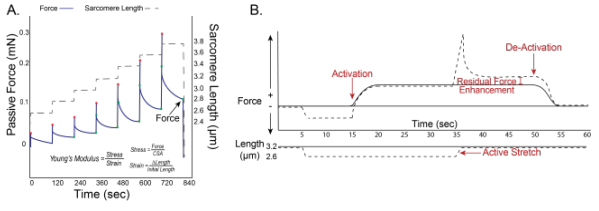

RESULTS AND DISCUSSION

Passive stiffness was higher at baseline in males versus females (32.8±17.6 vs. 25.9±9.6 kPa/%Lo, respectively, p=0.02, Fig. 2A), and was reduced by fatigue in both groups (NF: 29.3±14.4 vs. F: 18.7±8.6 kPa/%Lo, p<0.01). Passive stiffness reduction was greater in males versus females (p=0.021). RFE trended towards reduction with fatigue (p=0.1).

Figure 2: (A) Fatigue reduces passive Young's Modulus and (B) produces a trend towards reduced RFE. * Fatigue effect, # sex effect,ŧ interaction. α=0.05.

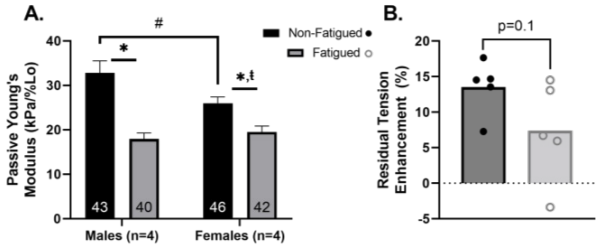

CONCLUSIONS

These results suggest acute fatigue reduces cellular passive stiffness, and the response differs by biological sex. The trend towards reduced RFE after fatiguing exercise may reflect altered contribution of non-contractile intracellular proteins, such as titin, to force generation under dynamic loading. Collectively, these findings suggest intracellular proteins contribute to fatigue-induced skeletal muscle compliance and may therefore be a target for interventions designed to disrupt the apparent associations between acute reductions in tissue stiffness and fatigue-induced injury risk.

ACKNOWLEDGEMENTS

This work was supported by funds from the Wu Tsai Human Performance Alliance. Many thanks are also due to the research volunteers, who make these studies possible.

REFERENCES

[1] E. Chalchat *et al.*, "Changes in the viscoelastic properties of the vastus lateralis muscle with fatigue," *Frontiers in Physiology*, vol. 11, p. 307, 2020.

[2] S. D. Mair, A. V. Seaber, R. R. Glisson, and W. E. Garrett, "The Role of Fatigue in Susceptibility to Acute Muscle Strain Injury," *Am J Sports Med*, vol. 24, no. 2, pp. 137–143, Mar. 1996, doi: 10.1177/036354659602400203.

[3] K. Nishikawa, "Titin: a tunable spring in active muscle," *Physiology*, vol. 35, no. 3, pp. 209–217, 2020.

Muscle length change associated with fascicle shortening and fascicle rotation in the sheep medial gastrocnemius

[1]**Esthevan Machado**, [1]Stephanie A. Ross, [1]Azim Jinha, [1,2]Fransiska M. Bossuyt, [1]Walter Herzog
[1]Faculty of Kinesiology, University of Calgary, Calgary, AB, Canada
[2]Neuro-musculoskeletal Functioning and Mobility Group, Swiss Paraplegic Research, Nottwil, Switzerland
corresponding author: esthevan.dossantos@ucalgary.ca

INTRODUCTION

Fascicle length changes and fascicle rotation are observed in pennate muscle function [1] and they produce a relative sliding of the proximal and distal aponeuroses, which in turn may cause length changes of the muscle. Fascicles tend to shorten when the entire muscle is shortening and when force is increasing [2]. Similarly, the angle of pennation in a uni-pennate muscle tends to increase when the entire muscle is shortening and when force is increasing [2]. In real life muscle function, shortening of a muscle might be associated with a decrease in force, and lengthening with an increase in force, making it difficult to know if the corresponding fascicles are shortening, elongating, or remain at about a constant length [3]. If we assume, maybe for simplicity rather than mechanical accuracy, that fascicle length changes and fascicle rotation can be directly related to the corresponding changes in muscle length, and we calculate the fascicle projection onto the line of action of the muscle, we can estimate the muscle belly length change associated with fascicle length changes and fascicle rotation. If such measurements and calculations were made in an in vivo muscle during unrestrained locomotion, one might gain insight into the function of a muscle. Of particular interest might be if fascicle shortening/lengthening is always associated with an increase/decrease in the angle of pennation causing simultaneous muscle shortening/lengthening, as one might expect. Or could fascicle shortening/lengthening occur at the same time as decreases/increases in angles of pennation, thus offsetting each other's contribution to the resultant length change of the muscle?

Measuring the force, fascicle lengths and angles of pennation continuously in the sheep medial gastrocnemius during locomotion, we hypothesized that at high gait speeds compared to slow speeds, muscle shortening associated with fascicle shortening is greater than muscle shortening associated with fascicle rotation. The aims of this study were to gain additional insight into the mechanical behavior of fascicles in a uni-pennate muscle (shortening vs. rotation) for different speeds of locomotion. Of particular interest was if shortening of fascicles was always associated with an increase in the angle of pennation and lengthening of fascicles with a decrease in the angle of pennation.

METHODS

We present exemplar data from one sheep that was trained to walk and trot on a motor-driven treadmill at different speeds (0.67 and 1.97 m/s). Medial gastrocnemius (MG) forces were measured using a buckle-type force transducer [4], and sonomicrometry crystals were used to measure fascicle lengths and fascicle angles of pennation [5]. Video recording was used to measure hindlimb kinematics (stance phase). All measurement systems were synchronized. Muscle length changes associated with changes in fascicle length and angle of pennation were determined. Data are presented as means.

RESULTS AND DISCUSSION

At the lower speed, the fascicle length change dominated the muscle length change for the first 60% of the stance phase. In the last 40%, decreases in the angle of pennation caused muscle lengthening offsetting the effects of the simultaneous fascicle shortening.

At the high speed, fascicle shortening dominated the muscle length changes while the relatively small changes in the angle of pennation had no significant effect on muscle length changes.

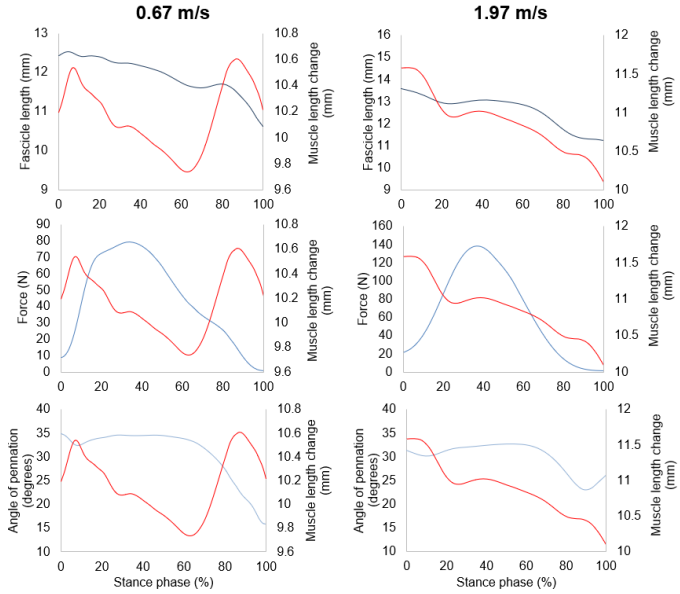

Figure 1. Average muscle length change (red line) and fascicle length, force, and angle of pennation (blue line) for 5 consecutive steps during the stance phase.

ACKNOWLEDGEMENTS

This work was supported by the Natural Sciences and Engineering Research Council (NSERC) of Canada.

REFERENCES

[1] Gans C et al. (1987). *J. Morphol.*, **192**: 63-85.
[2] Randhawa A et al. (2013). *Eur. J. Appl. Physiol.*, **113**: 437-447.
[3] Herzog W (2019). *BMC Biomed. Eng.*, **1**:28.
[4] Walmsley B et al. (1978). *J. Neurophysiol.*, **41**: 1203-1216.
[5] Griffiths RI (1991). *J. Physiol.*, **436**: 219-236.

Notes

CANMORE NORDIC CENTRE PROVINCIAL PARK

DAY LODGE – UPPER FLOOR

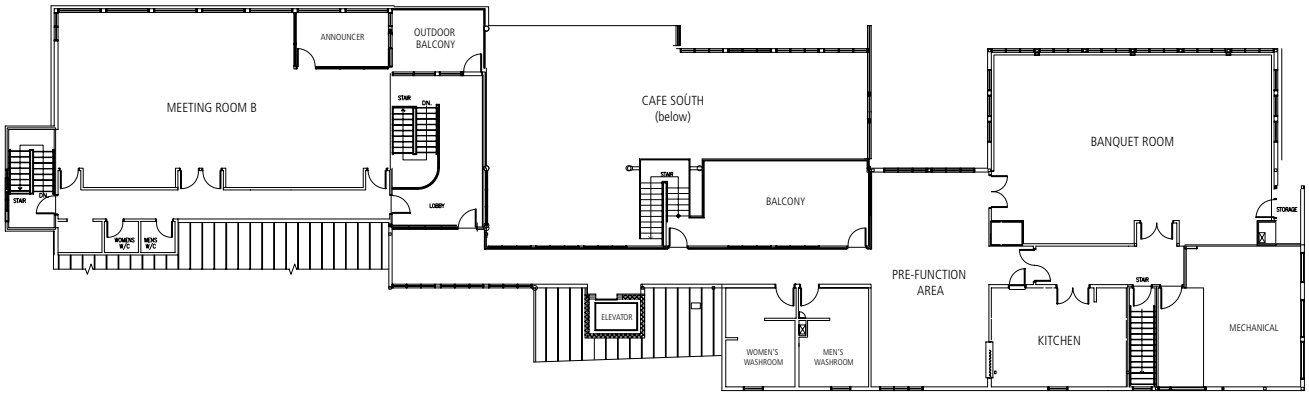

CANMORE NORDIC CENTRE PROVINCIAL PARK

DAY LODGE – MAIN FLOOR

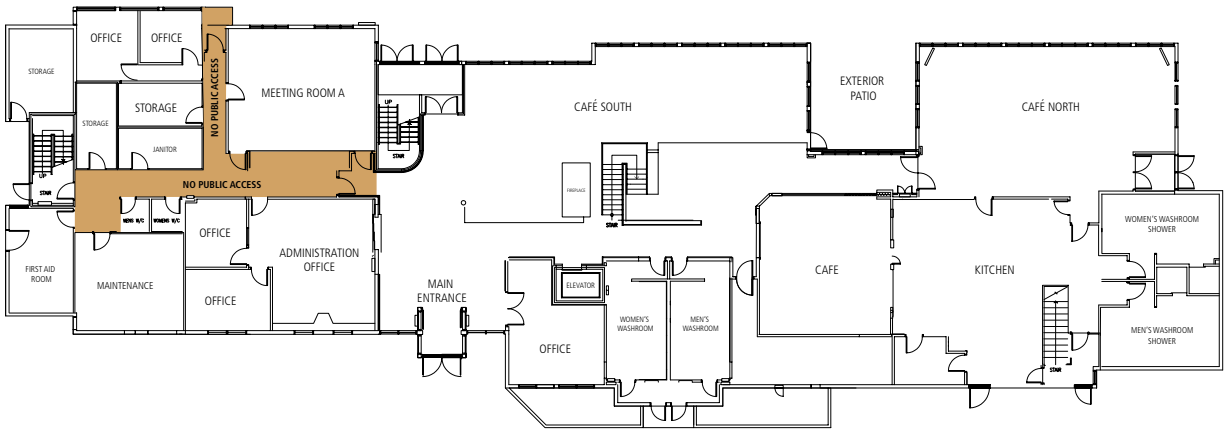

Schedule at a Glance

	Monday, June 19		Tuesday, June 20	Wednesday, June 21
09:30 - 09:50			Coffee	Coffee
09:50 - 11:30			Molecular Session	Session: Animal muscle function in vivo
11:30 - 12:15			Keynote Lecture	Keynote Lecture
12:15 - 01:15			Lunch	Lunch
01:15 - 2:30			Cellular Session	Session: Human muscle function in vivo
14:30 - 15:15	Registration starting at 14:00	Disc Golf at Canmore Nordic Centre / Free Time	Keynote Lecture	Keynote Lecture
15:15 - 16:30			Poster Session 1	Poster Session 2
16:30 - 17:00			Grassi Lakes Hike	Mountain Biking at Canmore Nordic Centre / Free Time
17:00 - 17:30		Reception		
17:30 - 18:30		Keynote Lecture		
18:30 - 19:00		Social		
19:00 - 19:30			Dinner for Keynote & Invited Presenters / Dinner on your own	Social
19:30 - 20:00				Banquet Dinner
20:00 - 21:00				